

**ACOUSTO-OPTIC SENSOR BASED ON
FIBRE LASER DYNAMICS**

PUA CHANG HONG

**THESIS SUBMITTED IN FULFILLMENT OF
THE REQUIREMENT FOR THE DEGREE
OF DOCTOR OF PHILOSOPHY**

**DEPARTMENT OF PHYSICS
FACULTY OF SCIENCE
UNIVERSITY OF MALAYA
KUALA LUMPUR**

2012

UNIVERSITI MALAYA

ORIGINAL LITERARY WORK DECLARATION

Name of Candidate: **Pua Chang Hong** (I.C/Passport No: **821025145491**)

Registration/Matric No: **SHC090005**

Name of Degree: **Doctor of Philosophy**

Title of Project Paper/Research Report/Dissertation/Thesis ("this Work"):

Acousto-Optic Sensor Based on Fibre Laser Dynamics

Field of Study: **Photonics, Physics.**

I do solemnly and sincerely declare that:

- (1) I am the sole author/writer of this Work;
- (2) This Work is original;
- (3) Any use of any work in which copyright exists was done by way of fair dealing and for permitted purposes and any excerpt or extract from, or reference to or reproduction of any copyright work has been disclosed expressly and sufficiently and the title of the Work and its authorship have been acknowledged in this Work;
- (4) I do not have any actual knowledge nor do I ought reasonably to know that the making of this work constitutes an infringement of any copyright work;
- (5) I hereby assign all and every rights in the copyright to this Work to the University of Malaya ("UM"), who henceforth shall be owner of the copyright in this Work and that any reproduction or use in any form or by any means whatsoever is prohibited without the written consent of UM having been first had and obtained;
- (6) I am fully aware that if in the course of making this Work I have infringed any copyright whether intentionally or otherwise, I may be subject to legal action or any other action as may be determined by UM.

Candidate's Signature

Date

Subscribed and solemnly declared before,

Witness's Signature

Date

Name: Prof. Dr. Harith bin Ahmad

Designation: Professor

Abstract

All these years, a lot of attempts to build an unassisted optical microphone have failed due to the poor acoustic impedances matching of air and fibre. Although there are theoretical works support that unassisted optical microphones is possible, however not much experimental work has been published to support the argument. This thesis presents an unassisted fibre optic acoustic sensor operate based on the fibre laser dynamic behaviours that overcomes the problem of the acoustic impedance mismatch between air and fibre.

Fibre laser dynamic behaviours which are sensitive to acoustic waves are chosen to work as the basic principle of the acousto-optic sensor setup. The behaviours of the fibre laser dynamic are studied on both theoretical and experimental. The experimental results show that the fibre laser is sensitive to the acoustic waves where the incident acoustic waves will cause the fluctuation of the optical output power. The fluctuation amplitude and frequency of the fibre laser is dependent on the acoustic waves amplitude, frequency, and the fibre laser parameters such as pump power, gain, and cavity length. Those relations are studied intensively to understand the operation of the optical microphone.

As for sensitivity enhancement and noise reduction, dual wavelength fibre laser is proposed to sense the acoustic waves intensity which below the triggering level of laser dynamics. Mode competition between two difference wavelengths has further enhanced the sensitivity level of the design optical microphone. Besides that, the mode hopping effect due to the mode competition has reduced the high frequency spiking and noise significantly producing better acoustic signal measurement in low frequency domain.

Abstrak

Selama ini, banyak usaha dilakukan untuk membina mikrofon optik tanpa bantuan diafragma telah menemui jalan buntu disebabkan oleh impedans akustik sepadan antara udara dengan gentian optic adalah sangat lemah. Meskipun ada hasil teori yang menyokongkan operasi bagi mikrofon optik tanpa bantuan diafragma, tetapi tidak banyak karya diterbitkan dalam bentuk eksperimen yang dapat menyokong pernyataan itu. Tesis ini membentangkan sensor akustik gentian optik tanpa bantuan diafragma yang beroperasi berdasarkan perilaku dinamik gentian optik yang boleh mengatasi masalah ketidasepadan impedansi akustik antara udara dengan gentian optik.

Dinamik laser gentian optik yang peka pada gelombang akustik dipilih untuk beroperasi sebagai prinsip asas sensor akusto-optik ini. Tingkah laku dinamik laser gentian optik dikaji dari segi teori and eksperimen. Keputusan eksperimen menunjukkan bahawa laser gentian adalah peka kepada gelombang akustik dimana ia akan menyebabkan perubahan pada jumlah kuasa keluaran optik. Amplitud dan frekuensi kuasa laser gentian optik adalah bergantung kepada amplitud dan frekuensi gelombang akustik serta parameter-parameter laser gentian optik seperti pam kuasa, gandaan kuasa, and panjang rongga. Hubungan antara parameter-parameter ini dikaji secara mendalam untuk memahami cara optik mikrofon ini beroperasi.

Untuk meningkatkan kepekaan and mengurangkan hingaran, laser gentian optik dengan dua panjang gelombang telah dicadangkan untuk mengesan kehadiran keamatan gelombang akustik dibawah tahap pengesanan dinamik laser. Persaingan antara mod bagi dua panjang gelombang yang berlainan dalam laser telah meningkatkan kepekaan mikrofon optik. Disamping itu, kelompatan mode juga mengurangkan hingaran berfrekuensi tinggi apabila pengukuran gelombang akustik berfrekuensi rendah dilakukan.

Acknowledgement

I would like to express my deepest gratitude to my supervisor, Professor Harith Ahmad and Professor Richard M. De La Rue for the invaluable guidance and advice he has given to me, both in research and the way of life. I would also like to express my appreciation to University Malaya for offering such a complete environment and funding for my Ph.D. research.

A Ph.D. work cannot be achieved with the effort of a mere individual but requires a group of personnel working towards the same objectives. I would like to take this opportunity to thank those who have assisted me in the course of my Ph.D. study. Among others, Siti Fatimah Norizan who actually assisted me in discovering the solution for the unassisted optical microphone discussed in this thesis, Dr. Chong Wu Yi for advising and assistance given on the experiments, and Dr. Jason Lim for all assistance on the modelling and simulation part in my thesis.

Last but not least, I would like to thanks my family members for their patience and understanding I the years of my post-graduate study.

Contents

	Page
Front Page	i
Declaration	ii
Abstract	iii
Abstrak	iv
Acknowledgement	v
Contents	vi
List of Figures	ix
List of Tables	xvi
List of Symbols and Abbreviations	xvii
List of Related Publications	xviii
Chapter 1 Introduction	1
1.1 Acoustic sensors	2
1.2 Acousto-Optic Sensors (AOS)	4
1.2.1 Fibre Laser	5
1.2.2 AOS operating methods	6
1.2.3 Advantages and disadvantages of AOS	7
1.2.4 Limitation and difficulty in current AOS	8
1.3 Research Objectives	9
1.3.1 Proposed method	10
1.4 Thesis Outline	11
References	13

Chapter 2 Theory	15
2.1 Erbium Doped Fibre Laser (EDFL)	16
2.2 Introduction to Laser Dynamics	20
2.3 Basic Rate Equations	21
2.3.1 Steady states	23
2.3.2 Linear stability	24
2.3.3 Damped relaxation oscillations	26
2.4 Erbium Doped Fibre Laser	27
2.5 Modulated Laser	32
2.6 Summary	35
References	36
 Chapter 3 Experimental Setup, Basic Characterization, and Modeling	 39
3.1 Experimental Setup	40
3.2 Noise and Resonance Frequency	43
3.3 Turn on Transient	47
3.3.1 Experimental results	48
3.3.2 Modeling	54
3.4 Pump Modulation	57
3.5 Loss Modulation	60
3.6 Summary	62
References	64

Chapter 4 Optical Microphone	66
4.1 Optical Microphone	67
4.2 Conventional SMF as Sensing Medium	69
4.3 Special SMF (SSMF) as Sensing Medium	78
4.4 EDF Length	89
4.5 Design and Prototype	91
4.6 Summary	94
 Chapter 5 Enhancement and Other Applications	 97
5.1 System Enhancement	98
5.2 Arrayed Waveguide Grating (AWG)	99
5.3 Experiment Setup	101
5.4 Mode Competition	102
5.5 Summary	115
References	117
 Chapter 6 Conclusions	 119
6.1 Conclusions	120
6.2 Future Works	126
6.3 Other Applications	127
References	127
 Appendix	 128

List of Figures

Chapter 1:

Figure 1.1: Optical microphone classification [9].	6
--	---

Chapter 2:

Figure 2.1: Fibre lasers design in (a) linear cavity and (b) ring cavity.	16
---	----

Figure 2.2: Energy level structure of Erbium ion with the optical transitions when pumped under 980 nm or 1480 nm.	18
--	----

Figure 2.3: (a) Spontaneous and (b) stimulate emission process diagram.	19
---	----

Figure 2.4: Two level laser system. R_p denotes the pumping rate, N_2/T_1 and N_1/T_1 are the decay rate of the populations, $G(N_2 - N_1)n$ is the gain for stimulated emission, and n is the number of laser photons.	22
---	----

Figure 2.5: Simple three level system for EDFL model.	28
---	----

Figure 2.6: Complete 3 level system for EDFL.	28
---	----

Chapter 3:

Figure 3.1: Diagram of (a) experiment setup and (b) light beam propagation and interaction.	40
---	----

Figure 3.2: ASE spectrum of EDFL pumped with 980 nm laser at 12 mW without feedback from reflection.	41
--	----

Figure 3.3: ASE spectrum and random lasing of EDFL under free running condition at different pump power.	42
--	----

Figure 3.4: Screen capture of optical power pumping at 15.7 mW together with the FFT calculation performs by digital oscilloscope.....	44
Figure 3.5: FFT frequency spectrum of optical output power fluctuation under different pump power conditions.....	46
Figure 3.6: Graphs of (a) resonance frequency, ω against pump power, P and (b) ω^2 against P	46
Figure 3.7: Typical turn-on transient of a laser [4].....	48
Figure 3.8: Screen capture from digital oscilloscope of fibre laser turn-on transient effect with pumping at 44.5 mW.....	49
Figure 3.9: Turn-on transient effect with pumping at different pump power levels: (a) 66.9 mW, (b) 61.3 mW, (c) 55.7 mW, (d) 50.1 mW, (e) 44.5 mW, (f) 38.9 mW, (g) 33.3 mW, and (h) 27.7 mW.....	50
Figure 3.10: Relation between latency period or turn-on time and pump power.....	52
Figure 3.11: First spiking peak amplitude and frequency under different pump power levels.....	52
Figure 3.12: Comparisons of both resonance frequency and RO frequency parameters in graphs of (a) frequency against pump power and (b) frequency ² against pump power.....	53
Figure 3.13: Numerical simulation result using Matlab Software with parameters value of $k = 10000$, $g = 90000$, and $I_p = 130$	56

Figure 3.14: Numerical modelling of spiking and RO happen in turn on transient with pump power at (a) 60 mW, (b) 70 mW, (c) 80 mW, (d) 90 mW, (e) 100 mW, (f) 110 mW, (g) 120 mW, (h) 130 mW, and (i) 140 mW.....	57
---	----

Figure 3.15: Fibre laser optical output waveforms under a continuous pump power level of 15.0 mW - with modulated oscillation by a 500 Hz sinusoidal function at different modulation amplitudes at (a) 35.2 mW, (b) 42.6 mW, (c) 49.6 mW, (d) 57.8 mW, (e) 64.0 mW, and (f) 71.5 mW.....	59
---	----

Figure 3.16: Fibre laser optical power fluctuation under the impact of strong acoustic wave.....	60
--	----

Chapter 4:

Figure 4.1: Optical microphone setup with SMF as sensing medium.....	68
--	----

Figure 4.2: Optical spectrum of the ASE generated with and without the present of sound waves at (a) 16 mW and (b) 27mW 980 nm pump power.....	69
--	----

Figure 4.3: Optical output fluctuation under modulation of 500 Hz sound wave at different sound pressure level.....	71
---	----

Figure 4.4: Average voltage output from photodetector as refer to the incident sound level.....	72
---	----

Figure 4.5: Comparison of (a) background noise without acoustic signal and (b) with a 2 kHz of acoustic signal between the electrical and the optical microphones captured using a digital oscilloscope.....	73
--	----

Figure 4.6: The FFT positive output for sound generated at (a) 200 Hz, (b) 1 kHz, (c) 10 kHz and (d) 20 kHz.....	75
--	----

Figure 4.7: Optical spectrum output with different SMF length as sensing medium pumping at 30.8 mW.....	76
Figure 4.8: Average output voltage from photo-detector at different pump power when connected to different length of SMF as sensing medium (a) without present of sound wave and (b) with the present of 10 kHz sound wave.....	77
Figure 4.9: Standard deviation of the photo-detector output voltage for (a) background noise and (b) modulated signal at different pump power.....	78
Figure 4.10: Comparison between 25 km of SMF sensing medium and 10 m of SSMF sensing medium in the foreground. The SSMF fibre spool is placed in a mini-CD cassette.....	80
Figure 4.11: Comparison of the resonance frequency distribution with the optical power fluctuation under acoustic modulation at different frequency.....	81
Figure 4.12: Optical output pattern under modulation of different frequency of acoustic wave.....	82
Figure 4.13: Optical output pattern under the sinusoidal acoustic wave modulation at different frequency.....	83
Figure 4.14: Different regions from the resonance frequency distribution categorize based on the output pattern.....	84
Figure 4.15: Resonance frequency of the OM noise at different pump power.....	85

Figure 4.16: Relation between resonance frequency, ω and pump power above lasing threshold, P_T with 80 μm SSMF sensing medium at length 1 m, 10 m, 20 m and 1 km.	86
Figure 4.17: The linear relation between parameter ω^2 and pump power above lasing threshold, P_T with different SSMF length.	86
Figure 4.18: The relation between the constant, k and the SSMF fibre length in logarithm scale.	87
Figure 4.19: Modulated optical amplitude as compared with the intensity noise frequency distribution for a 5 s record of the detected laser output.	88
Figure 4.20: The resonance frequency of different EDF length under different pump power.	89
Figure 4.21: Interior part of the OM module.	91
Figure 4.22: The sensor prototype with a 20 m SSMF sensing medium in cylindrical shape spool on a plastic bottle with 3.5 cm outer diameter.	92
Figure 4.23: Schematic drawing of the fibre laser cavity connected to an angle patch-cord.	93
Chapter 5:	
Figure 5.1: Structure of AWG	99
Figure 5.2: Divergent of multiplexed wavelength to arrayed waveguides in first FPZ.	100
Figure 5.3: Optical ray path of different wavelength at second FPZ.	100
Figure 5.4: AWG enhancement OM.	101

Figure 5.5: Optical spectrum of dual wavelength fibre laser pumped at 23.2 mW.....	102
Figure 5.6: Optical output from (a) output A and (b) B ₁ and B ₂ with FFT frequency distributions that measured and calculated using build in MATH function of the digital oscilloscope.....	103
Figure 5.7: Optical output from both output B ₁ and B ₂ with calculated FFT frequency distribution for (a) output B ₁ and (b) output B ₂	104
Figure 5.8: Random spiking due to the transient effect from outputs (a) B ₁ and B ₂ and (b) summation from both of them.....	105
Figure 5.9: Optical output from B ₁ and B ₂ under the modulation of 500 Hz acoustic waves at amplitude of (a) 65 dBA and (b) 88.3 dBA SPL.....	106
Figure 5.10: Optical output from both output B ₁ and B ₂ at frequencies 1530.516 nm and 1532.068 nm with calculated FFT frequency distribution pumping at 15.6 mW.....	108
Figure 5.11: Relation between first and second resonance frequency with pump power.....	109
Figure 5.12: Screen capture of optical output power from B ₁ and B ₂ simultaneously under the modulation of sound wave at 500 Hz with a digital oscilloscope.....	109

Figure 5.13: Dual wavelength fibre laser generated using 1x16 AWG with different channels combination at wavelengths: (a) 1530.52 nm and 1531.32 nm, (b) 1530.52 nm and 1532.07 nm, (c) 1530.52 nm and 1532.88 nm, (d) 1530.52 nm and 1533.65 nm, (e) 1530.52 nm and 1534.40 nm, and (f) 1530.52 nm and 1535.22 nm pumped at 15.7 mW.....111

Figure 5.14: The relation between SRF with the peak power from output B_2112

Figure 5.15: Digital oscilloscope readings from output B_1 and B_2 at wavelengths 1530.52 nm and 1533.65 nm with average peak power at -21.25 dBm and -27.39 dBm. (a) and (b) are noise readings with the frequency domain analysis for (a) 1530.52 nm and (b) 1533.65 nm. (b) is the chaos condition with a small acoustic disturbance incident on the OM while (d) is the chaos condition with a strong acoustic disturbance.....113

List of Tables

Table 1.1 Applications of acoustic sensors in various research field.

List of Symbols and Abbreviations

AOS	Acousto-Optic Sensors	LED	Light Emitting Diode
ASE	Amplified Spontaneous Emission	MRI	Magnetic-Resonance Imaging
AWG	Arrayed Waveguide Grating	Nd	Neodymium
C band	Conventional band	OM	Optical Microphone
EDF	Erbium-Doped Fibre	OSA	Optical Spectrum Analyser
EDFL	Erbium-Doped Fibre Laser	RIN	Relative Intensity Noise
Er	Erbium	RO	Relaxation Oscillation
FBG	Fibre Bragg Grating	SAW	Second Resonance Frequency
FFT	Fast Fourier Transform	SMF	Single Mode Fibre
FPZ	Free Propagation Zone	SPL	Sound Pressure Level
FRF	First Resonance Frequency	SRF	Second Resonance Frequency
LASER	Light Amplified by Spontaneous Emission of Radiation	SSMF	Special Single Mode Fibre
LD	Laser Diode	Th	Thulium
		WDM	Wavelength Division Multiplexing
		Yb	Ytterbium

List of Related Publications

- [1] C. H. Pua, S. F. Norizan, S. W. Harun, and H. Ahmad, "Non-membrane optical microphone based on longitudinal modes competition," *Sensors and Actuators A: Physical*, vol. 168, pages: 281-285, 2011.
- [2] C. H. Pua, H. Ahmad, S. W. Harun, and R. M. D. L. Rue, "Direct Airborne Acoustic Wave Modulation of Fabry-Perot Fiber Laser (FPFL) over 100 kHz of Operating Bandwidth," *Applied Optics*, vol. 51(15), pages: 2772-2777, 2012.
- [3] C. H. Pua, H. Ahmad, S. W. Harun, and R. M. D. L. Rue, "Study of Dual-Wavelength Mode Competition in an Erbium-Doped Fiber Laser (EDFL) Produced by Acoustic Waves." *IEEE Journal of Quantum Electronics*, vol. 48(12), pages: 1499-1504, 2012.

Chapter 1

Introduction

1.1 Acoustic Sensors

1.2 Acousto-Optic Sensors (AOS)

1.2.1 Fibre laser

1.2.2 AOS operating methods

1.2.3 Advantages and disadvantages of AOS

1.2.4 Limitation and difficulty in current AOS

1.3 Research Objective

1.3.1 Proposed method

1.4 Thesis Outline

References

1.1 Acoustic Sensor

Sensors are devices that are used to measure environmental input parameters and then convert this information into digital or analogue signals that can be read by observers - or stored in computers for further processing. Therefore, acoustic sensors can be defined as devices with the capability to detect acoustic waves or mechanical waves. Acoustic wave sensors have been in commercial use for more than 70 years [1]. The most common application of acoustic sensors is in the telecommunications industry. Common telecommunication devices like the telephone, the cell phone, and the microphone all contain sound sensors, which is a category of acoustic sensor that converts sound waves into electrical signals before transmitting them to their destination. Certainly, acoustic sensors are not only used for audible sound detection but also cover a wide frequency spectrum of acoustic wave sensing - from low frequency mechanical vibration to ultrasound. Recently, the advantages of acoustic wave sensors such as price competitiveness, inherently rugged design, high sensitivity, and intrinsic reliability have encouraged applications in other fields - including but not limited to:- automotive (torque [2] and tire pressure [3] sensors), medical (chemical sensors [4]), and industrial and commercial (vapour sensors [5], humidity sensors [6], temperature sensors [7], and mass sensors [8]).

Research in acoustic wave sensing is still active even though the discipline is almost a century old. As can be seen, the emergence of acoustic sensor applications in other fields becomes possible through studies of the relationship between environmental changes and acoustic wave motion, velocity, frequency, or phase characterization. Table 1.1 shows how acoustic sensors can be used in various applications. All these advantages and potential and actual applications of acoustic wave sensors have made them into an important player in sensing research and industry.

Table 1. 1 Applications of acoustic sensors in various research fields.

Applications	Measurement method	Relation
Temperature	Surface Acoustic Wave (SAW) velocity	The SAW velocity is temperature dependent and is determined by the orientation and type of crystalline material used to fabricate the sensor.
Pressure	SAW velocity	SAW velocities are strongly affected by stresses applied to a piezoelectric substrate on which the wave is propagating.
Torque	SAW resonant frequency	Torque causes deformation of the single crystal substrate of a SAW device - which in turn causes a change in its resonant frequency.
Mass (Thickness and Biosensor)	SAW resonant centre frequency	The mass sensitivity is related to the structure geometry and resonant centre frequency. Applications can also be found in areas such as film thickness monitoring, liquid media chemical sensing, and bio sensing.
Humidity	SAW resonant centre frequency	The mass loading effect in mass sensors and the elasticity changes due to swelling caused by humidity absorption (i.e. changes in the viscoelastic properties of a thin film)

1.2 Acousto-Optic Sensors (AOS)

Research interest in the field of optics can be traced back to at least as early as 300BCE in the works of Euclid, Heron and Claudius Ptolemy in Alexandria on the behaviour of light, the laws of reflection, refraction, and optical aberrations. Since then research work in optics has been evolving - and optical devices have become more and more important, slowly replacing some electrical devices - especially in telecommunication and sensors. Replacement of copper wires with optical fibre in telecommunications networks is one of the successful examples of optical technology development - while AOS is one of the active research fields into which optical technology has emerged.

The first known AOS that involved interaction between acoustic waves and optics was invented by Alexander Graham Bell in 1880 and patented as the “photophone” [9]. The “photophone” converted sound waves or acoustic waves into a vibrating light beam by vibrating a mirror that was used to reflect the light beam. The vibrating light beam was then transmitted to the receiver which converted the vibrating light beam back to sound waves. However, A.G. Bell stopped further research on this invention due to the strong interference from atmospheric conditions. More precisely, it was due to the lack of two important optical technologies at that time. These are the LASER (Light Amplification by Stimulated Emission of Radiation) and the optical fibre or optical waveguide.

The successful implementation of many modern optical devices relies on the laser, which was first demonstrated experimentally by Theodore Maiman [10] on 16 May 1960 at Hughes Research Laboratories in Malibu, California. The intense light beam generated by a laser allows it to interact with other mediums or energy and be transmitted without losing the information which is being carried. The invention of

optical fibres further boosted the use of the laser, by providing a low loss transmission medium with the ability to guide the light beam, which meant that the light could now be “bent” easily using guidance in the optical fibre. The combination of both technologies has also led to the realization of fibre lasers, which are an important area of current research and development activity.

1.2.1 Fibre lasers

A fibre laser uses optical fibre doped with active ions as the gain medium. Typical active gain media are generally doped with rare-earth elements such as erbium, ytterbium, neodymium, dysprosium, praseodymium, and thulium. Depending on the laser wavelength, different rare-earth elements will be doped into the optical fibre. Combinations of different rare-earth dopants are also useful. The use of fibre lasers carries advantages that include:

- The laser beam is generated in a physically flexible fibre, which means that the laser beam can easily be delivered in any direction, anywhere.
- High output power can be obtained by using multiple kilometre-long rare-earth doped fibres. The efficient cooling that is possible because of the high surface-to-volume ratio of the fibre allows it to deliver continuous high power output.
- High optical quality can be obtained due to the guiding properties of optical fibres that reduce the thermal distortions in the optical path.
- Compact size and reliability.
- Efficient pump-signal overlap, due to the guiding nature of optical fibre - ensuring high pump conversion efficiency.

In fact, fibre lasers have become the premier choice of light source for many applications.

1.2.2 AOS operating methods

All this while, conventional acoustic sensors or electrical microphones have been utilizing the membrane displacement caused by the acoustic vibration to generate an electrical signal. In contrast to electrical microphones, optical microphones utilize the displacement of the membrane to modulate the optical signal in the fibre. Hence, a laser source or suitable LED (Light Emitting Diode) is always needed in AOS. There are at least three properties of the light from a laser that can be modulated: the intensity, the phase, and the polarization. However, it is quite typical that phase and polarization are eventually reduced or converted into intensity modulation. This is due to the limitation of photodiodes which only respond to changes in optical intensity. To perform the reduction or conversion to varying intensity, phase modulations require an interferometer while polarization modulations need a polarizer or bire-fringent element.

Figure 1.1 shows a classification of optical microphones according to different modulation approaches and techniques.

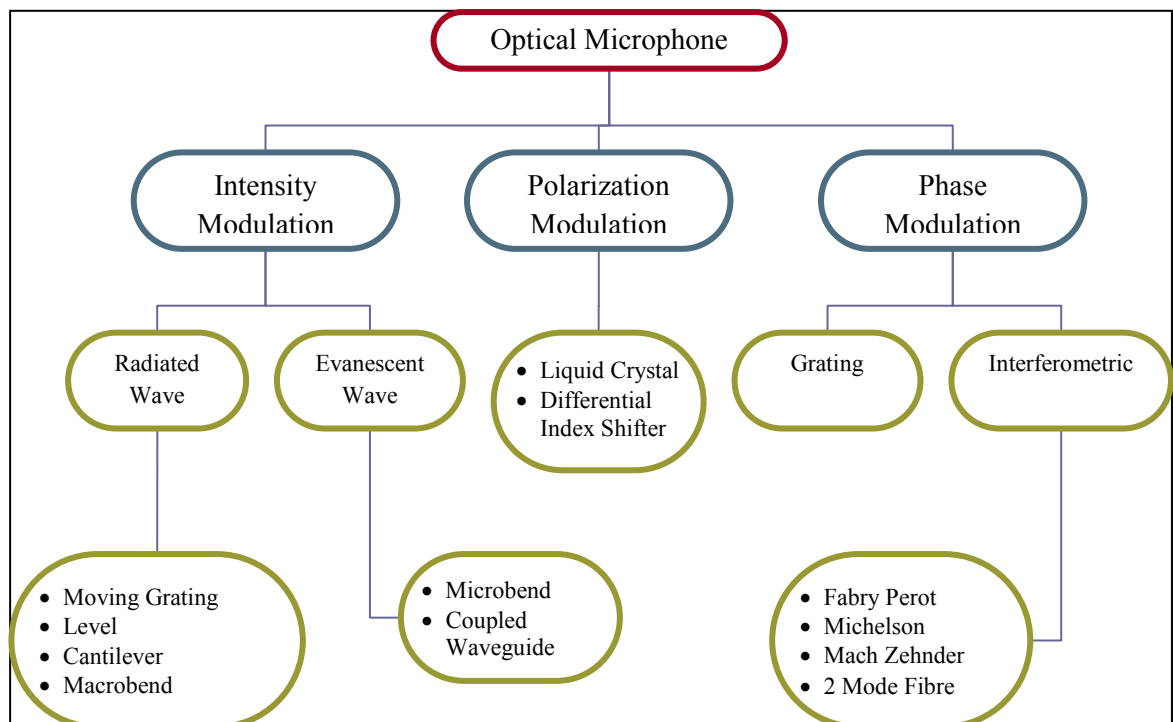


Figure 1.1: Optical microphone classification [9].

1.2.3 Advantages and disadvantages of AOS

Optical fibre sensor technology has matured to the point where there are more than 60 different types of sensor that have been developed over the past few years [11].

Generally, fibre sensors offer advantages such as:

- (a) higher sensitivity over existing techniques,
- (b) geometric versatility - where the sensor can be configured into many different shapes according to requirements,
- (c) a common technology base for sensing of different physical perturbations,
- (d) dielectric construction that allows it to be used in high voltage, electrically noisy, high temperature, and corrosive environments, and
- (e) inherent compatibility with the fibre based telecommunication network.

These advantages have allowed the access of optical acoustic sensors to application in harsh environments filled with explosive gases or materials or within medical tools such as equipment for magnetic-resonance imaging (MRI).

However, when compared with conventional acoustic sensors or microphones, AOS is more complicated in its transduction [9]. Conventional microphones consist of two stage transducers: (1) acoustic pressure to membrane displacement which describes the mechanical behaviour of the microphone and (2) membrane displacement to electrical signal conversion, which depends on the electrical properties. On the other hand, AOS involves at least three transduction stages: (1) acoustic pressure to membrane displacement, which describes the mechanical behaviour - as in a conventional microphone, (2) membrane displacement to modulate the optical intensity that describes the mechanic-optical transduction process, and (3) optical intensity to

electrical signal transduction, which describes the opto-electrical signal conversion process. Phase and polarization modulating transducers are more complicated, because an extra step is needed within the second step, splitting it into (2a) and (2b): (2a) being the membrane displacement that generates phase shift or polarization state changes and (2b) being the phase shift or polarization state changing the modulated optical intensity. The more transducer steps there are, the more is the potential for noise and uncontrolled fluctuation to be present, increasing the difficulties of the optimization of the devices.

1.2.4 Limitations and difficulties in current AOS

In 1977, Culshaw et al. had proposed an optical microphones that used unassisted optical fibre as the sensing element [12] and carried out theoretical work on the idea. The basic sensing mechanism was based on the change in refractive index, n of optical fibre when interacting with incident acoustic waves that will cause a certain amount of phase shift in the optical signal. However, it is known that the fibre sensitivity to airborne sound is poor, due to the acoustic impedance mismatch between air, fibre-jacket and fibre [9]. Thus, a transducer in the form of a membrane or other low mass structure is needed in optical microphones to mediate the differences in impedance. In the end, optical fibres have been found to be a better conduit for sound-modulated light, rather than being used as a sensing medium.

Adding a membrane to the optical setup not only increases the number of transducer stages involved in the set-up but also adds difficulty in the fabrication process - and limits the sensing points in a single set-up. As an example, the interferometric hydrophone requires that the sensor heads are located in a very small dimension holder, together with a rather complex readout system when multiplexed [13]. In most optical microphone set-ups, stringent alignment conditions and limited sensing points have caused the fabrication cost to be very high. To overcome the limited sensing

point issue, research in distributed optical microphones has been actively carried out, in the past few years [13-15].

1.3 Research Objective

As the idea of using unassisted fibre as a sensing element proposed by Culshaw et al. 35 years ago has not been successful realize, it has become a great motivation in the present research work. Hence, the objectives of this research work are to develop an optical acoustic sensor design with:

- (a) the capability to sense airborne acoustic waves or sound waves using an unassisted optical fibre as sensing element, without involving any stringent alignment or complicated set-ups,
- (b) “unlimited” sensing points that are able to perform large area sensing with sensor that can distribute out for more than 10 m length and point sensing with sensing head which is not larger than 6 cm of diameter, and
- (c) different sensing application capabilities such as vibration sensors, optical microphones which have frequency band from 100 Hz to 20 kHz, and ultrasound sensors which cover frequency band from 20 kHz up to 100 kHz under a common base principle with sensing threshold of 65 dBA.

The achievement of these objectives can be divided into four stages. The first stage is to find a suitable optical set-up that is sensitive to acoustic waves and can be modulated by the weakly coupled acoustic waves. The second stage involves basic characterization of the set-up to study the sensitivity, operating bandwidth, and response to the acoustic wave modulation. This work is to be followed by enhancement and optimization of the AOS set-up. Finally, the results obtained above are used to design a universal set-up for different sensor application purposes.

1.3.1 Proposed method

The method proposed in this research is the utilization of fibre laser dynamics as the basic configuration, as well as utilizing a dual wavelength fibre laser in order to enhance the sensitivity. Laser dynamics is one of the laser behaviour discovered in the early days of laser (1960) [16]. The dynamic behaviour of a laser may become extremely sensitive to acoustic waves, which generate erratic intensity fluctuations in the laser beam under small perturbations. Hence, the fibre-laser dynamic behaviour has been chosen for use as the basic structure of the AOS setup. The proposed method can be considered currently as the most sensitive unassisted fibre-based acoustic sensor; i.e. a fibre-based acoustic sensor without a diaphragm or an intermediate coupling structure. However, the sensitivity is still low when compared to an assisted fibre-based acoustic sensor. The acoustic wave intensity threshold to trigger the dynamic fluctuation in the fibre laser is still considered to be high, as compared with currently achievable diaphragm sensitivity.

To increase the sensitivity of the set-up, an AWG (Arrayed Waveguide Grating) was implemented into the setup to generate a dual wavelength fibre laser by feedback the optical power from two selected channels. Dual-wavelength Erbium Doped Fibre Lasers (EDFLs) are liable to mode-competition due to the homogeneous broadening effect[17] and consequent gain competition. This mode-competition is also sensitive to acoustic waves that interact with the set-up and can further increase its sensitivity.

1.4 Thesis Outline

This thesis is divided into six chapters. Chapter 2 gives a brief introduction to the laser dynamics which provide the basic principle for the proposed acoustic sensor. In this chapter, an analytical analysis on the fibre laser dynamics is provided, starting from the most basic laser rate equations. Chapter 2 also develops and implements rate equation analysis for the Erbium Doped Fibre Laser (EDFL), followed by a simple analysis of the modulation behaviour.

The experimental set-up is presented in Chapter 3 - and is followed by the basic characterization of the setup that concentrates on the noise, resonance frequency, and the dynamic behaviour of the setup. The discussion will be concentrated on the relationship between the noise, the resonance frequency and the relaxation oscillation frequency. The turn-on transient will also be studied, in order to understand the output pattern produced during modulation. The differences between pump modulation and loss modulation are also discussed. In this chapter, presentation of an unassisted optical acoustic sensor has been presented which delivered the first objective of the research.

In Chapter 4, a simple unassisted fibre optical microphone with the flexibility in changing the sensing medium is presented. The optical microphone is first connected to a conventional single mode fibre (SMF) for airborne sound sensing purposes. The response of the optical output intensity to the acoustic wave will be discussed. The sensing medium is also replaced with a special SMF to increase the sensitivity, which simultaneously reduces the sensor size significantly. The relationship between the operating bandwidth and the sensitivity to the resonant frequency is studied intensively. At the end of this chapter, a detailed description of the prototype of the eventual portable and customizable optical microphone required is mentioned. This chapter also delivered the second objective of this thesis.

Further enhancement of the optical microphone is performed by implementing a 1x16 Arrayed Waveguide Gratings (AWG) - and will be discussed in Chapter 5. The creation of a dual wavelength laser more clears conditions. The natural behaviour of one mode, which compensates for the loss or gain of the other mode in a laser cavity, will be demonstrated. This behaviour, which limits the modulation sensitivity above the dynamic threshold, will be discussed. The possibility of acoustic sensing below the threshold of dynamic laser behaviour, which utilizes dual wavelength mode competition generated by the AWG, is discussed. The advantages of the dual wavelength fibre laser optical microphone are presented. At the end of this chapter, the setup has successfully delivered the third objective which is the last objective of this research.

In Chapter 6, the last chapter, all of the work presented in this thesis is summarized. Future work and other potential applications of the acoustic sensor are also suggested.

References

1. Drafts, B. *Acoustic wave technology sensors*. Sensors Weekly, 2000.
2. Chih-Jer, L., H. Chih-Wei, and L. Hai-Ping. *A study of wireless torque sensing based on SAW sensors*. in *Computer Communication Control and Automation (3CA), 2010 International Symposium on*. 2010.
3. Wen, W., et al. *Optimized Surface Acoustic Wave-based Pressure Sensor Using Equivalent Circuit Model*. in *Nano/Micro Engineered and Molecular Systems, 2006. NEMS '06. 1st IEEE International Conference on*. 2006.
4. Hossenlopp, J.M., *Applications of Acoustic Wave Devices for Sensing in Liquid Environments*. Applied Spectroscopy Reviews, 2006. **41**(2): p. 151-164.
5. Nomura, T., A. Saitoh, and S. Furukawa. *Surface acoustic wave vapor sensor using ultrathin multilayer films*. in *Frequency and Time Forum, 1999 and the IEEE International Frequency Control Symposium, 1999., Proceedings of the 1999 Joint Meeting of the European*. 1999.
6. Rimeika, R., et al. *Humidity sensor using leaky surface acoustic waves in YX-LiTaO₃ with nanostructured porphyrin film*. in *Sensors, 2009 IEEE*. 2009.
7. Sternhagen, J.D., et al., *A novel integrated acoustic gas and temperature sensor*. Sensors Journal, IEEE, 2002. **2**(4): p. 301-306.
8. Hsu-Cheng, O. and M. Zaghloul, *Synchronous One-Pole LiNbO₃ Surface Acoustic Wave Mass Sensors*. Electron Device Letters, IEEE, 2010. **31**(5): p. 518-520.
9. Bilaniuk, N., *Optical microphone transduction techniques*. Applied Acoustics, 1997. **50**(1): p. 35-63.

10. Theodore Maiman, in *Wikipedia*.
11. Giallorenzi, T., et al., *Optical fiber sensor technology*. Quantum Electronics, IEEE Journal of, 1982. **18**(4): p. 626-665.
12. Culshaw, B., D.E.N. Davies, and S.A. Kingsley, *Acoustic sensitivity of optical-fibre waveguides*. Electronics Letters, 1977. **13**(25): p. 760-761.
13. Løvseth, S.W., et al., *Fiber Distributed-Feedback Lasers Used as Acoustic Sensors in Air*. Appl. Opt., 1999. **38**(22): p. 4821-4830.
14. Iida, T., K. Nakamura, and S. Ueha. *A microphone array using fiber Bragg gratings*. in *Optical Fiber Sensors Conference Technical Digest, 2002. OFS 2002, 15th*. 2002.
15. Hang, L., C. He, and B. Wu, *Novel distributed optical fiber acoustic sensor array for leak detection*. Optical Engineering, 2008. **47**(5): p. 054401-6.
16. Erneux, T. and P. Glorieux, *Laser Dynamics* 2010, New York: Cambridge University Press.
17. Becker, P.C., N.A. Olsson, and J.R. Simpson, *Erbium-Doped Fiber Amplifiers - Fundamentals and Technology* 1999, San Diego: Academic Press.

Chapter 2

Theory

2.1 Erbium Doped Fibre Laser (EDFL)

2.2 Introduction to Laser Dynamics

2.3 Rate Equations

2.3.1 Steady states

2.3.2 Linear stability

2.3.3 Damped relaxation oscillations

2.4 Erbium Doped Fibre Laser

2.5 Modulated Laser

2.6 Summary

References

2.1 Erbium Doped Fibre Lasers (EDFL)

Fibre lasers are usually understood to be lasers based on optical fibres that have an active gain medium that is doped with rare-earth atoms. The fibre gain media dopants that are typically used are erbium (Er)[1], neodymium (Nd)[2], ytterbium (Yb)[3], or thulium (Th)[4]. Each doped medium has an emission spectrum that is suitable for different lasing wavelengths in the range from 0.4 μm up to 4 μm . Among these rare-earth ions, Er is the most common choice for building a fibre laser, because of its demonstrated capability to support the generation and amplification of short optical pulses in the 1550 nm spectral region that is useful for both optical communication applications and for sensors[5].

Fibre lasers are typically realised in either Fabry-Perot (linear) cavity[6] or ring cavity[7] configurations. There are three basic elements in the set-up for a fibre laser – and these are the gain medium, the pump source, and the oscillation cavity, as shown schematically in Figure 2.1.

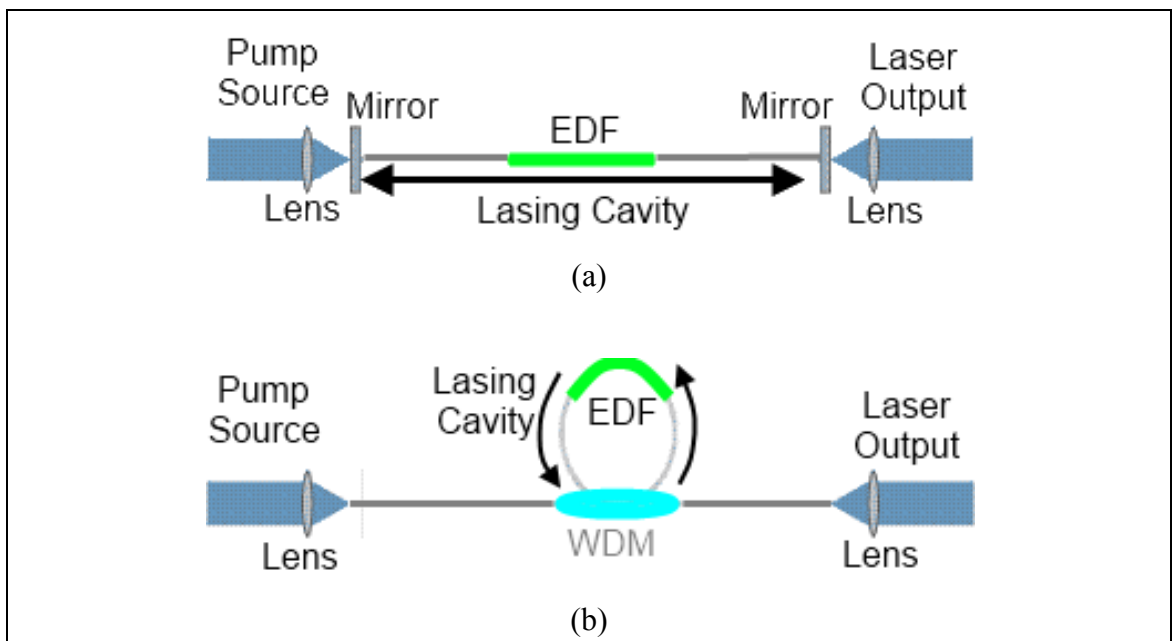


Figure 2.1: Fibre lasers realised in (a) linear cavity and (b) ring cavity configurations.

The linear, or Fabry-Perot, cavity is basically formed by a doped-fibre gain-medium between two reflector mirrors at the fibre ends, as shown in Figure 2.1(a). The reflective mirrors can be replaced by Fibre Bragg Gratings (FBG) or circulator that forms a fibre loops. The optical signal oscillates forwards and backwards within the linear cavity. The ring cavity laser, is assembled from the components of gain fibre, Wavelength Division Multiplexing (WDM) de-multiplexer and isolator, as shown in Figure 2.1(b). A ring that includes a fibre gain medium is formed between the fibre outputs. In the ring cavity, pump power is coupled into the ring and absorbed by the gain medium, while the emitted laser power can be directed out of the ring through the WDM demultiplexer to the fibre output. An isolator is normally place in the ring cavity to ensure operation in a single direction around the ring.

Among all the rare-earth doped materials, erbium-doped fibre (EDF) is the most commonly used, due to its applications in the telecommunications field. The emission of the EDF in the 1550 nm spectral region gains the advantage of operating in the low loss region in silica fibre in the third telecommunications window[8]. Besides that, the ability to provide high output power, low threshold pump power, and narrow line-width are reasons that EDF is chosen for many other applications.

EDFL operates as a three level laser system that involves the atomic energy levels ${}^4I_{15/2}$, ${}^4I_{13/2}$, and ${}^4I_{11/2}$, as shown in Figure 2.2. Two common pump sources that are used to pump EDF gain media are 980 nm and 1480 nm semiconductor lasers, because of their photon energy match with the energy difference between the ground level ${}^4I_{15/2}$, for E_1 , and the excited levels, ${}^4I_{13/2}$, and ${}^4I_{11/2}$ respectively, for E_2 that can produce gain in the 1550 nm region. The energy gap, ΔE , between the pump and emission frequencies, can be related by $\Delta E = E_2 - E_1 = h\nu$, to the frequency ν , where h is Planck's constant.

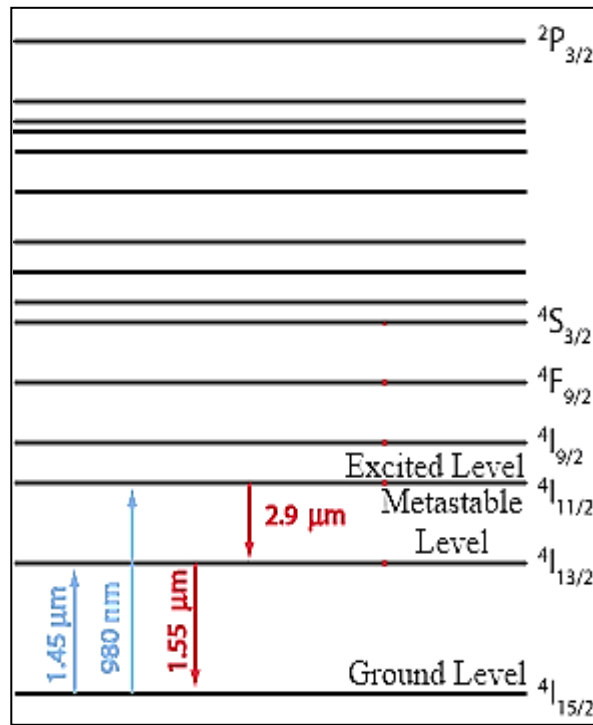


Figure 2.2: Energy level structure of Erbium ion with the optical transitions when pumped under 980 nm or 1480 nm.

Amplification in the lasing process for an EDFL is achieved by continuous emission of stimulated radiation by the excited Er ions of the EDF. To generate stimulated emission, a 980 nm pump laser is coupled into the EDF to interact with the Er ions. The pump laser will be absorbed by the Er ions at the ground level, $4i_{15/2}$ and the ions will be excited to the level, $4i_{11/2}$. The excited ions at this level are unstable and have a very short lifetime of approximately 10 μs , before they decay to a lower level called the metastable level, $4i_{13/2}$, in non-radiative form. Hence, the atomic population in level $4i_{11/2}$ can be assumed to be zero. In contrast to the excited level, excited ions at the metastable level are much more stable and have a longer lifetime of 10 ms. The long lifetime of the metastable level allows the ions to remain excited for longer, which also encourages the generation of stimulates emission.

In the metastable state, the excited ions will de-excite back to the ground state and release energy either as radiative emission (photons) or non-radiative emission (phonons). There are two possible types of radiative emission - which are spontaneous

emission and stimulated emission, as shown in Figure 2.3. Spontaneous emission is generated when there is no incident photon that triggers the de-excitation, as shown in Figure 2.3(a). The photons emitted spontaneously produce light with a characteristically broad spectral width when the emitting ions are de-excited to the ground state. The photons emitted are incoherent and they are emitted randomly in all directions. On the other hand, stimulated emission is generated when there is an incident photon that has a wavelength that corresponds to the transition energy gaps, as shown in Figure 2.3(b). The emitted photon will be coherent with the incident photon that triggers the emission.

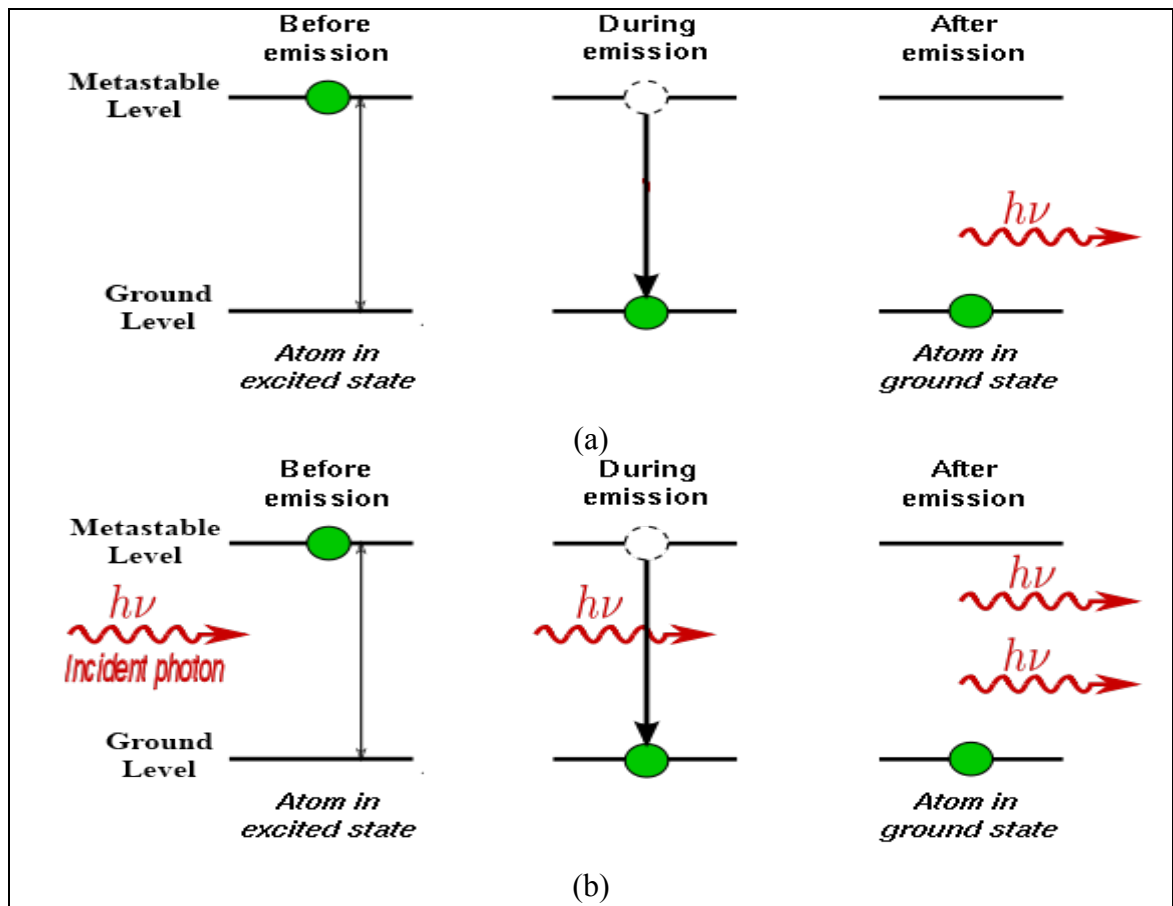


Figure 2.3: (a) Spontaneous and (b) stimulate emission process diagram.

Stimulated emission is important in fibre lasers, since it allows incident light source to be amplified and built up coherently in the laser cavity. However, spontaneous emission also plays an important role when it comes to free running fibre lasers without the input of photons at a specific frequency - or feedback into the laser system. In free running fibre lasers, broad spectrum spontaneous emission is firstly generated in the fibre cavity. This emission will then be amplified further due to stimulated emission, when it propagates throughout the whole length of the EDF - and the output is called amplified spontaneous emission (ASE).

With a feedback mechanism incorporated into a fibre laser, part of the output will be reflected back to the laser cavity. This input then again goes through the stimulation process and increases the amount of coherent emission. This process will continue until the emission wavelength with highest gain reaches the lasing threshold. From this point onwards, the highest gain wavelength, with lowest loss, will dominate the stimulated emission process and cause the gain at all other wavelengths to be clamped[9].

2.2 Introduction of laser dynamics

In the early days of laser research in the 1960s, many of the physicists working in the field observed erratic intensity fluctuations in the laser beams that they were producing. This kind of erratic intensity fluctuation led to the generation of irregular spiking in the laser output. Various explanations have been produced to explain the fluctuation behaviour, including environmental fluctuations, passive modulation, etc [10]. However, the cause of this behaviour was only properly understood in the early 1980s (except for the work of isolated pioneers such as L.W. Casperson) and widely accepted in the early 1990s, with the basic idea that the pulsating output originated from the interaction between the radiation field and matter [11]. This interaction, together

with the population redistribution of the energy levels of the medium, is proof of the intrinsic nonlinearity of laser systems. The lasing process is also affected by other nonlinear effects attributable to the properties of the media inside the laser cavity. The pulsing behaviour is affected by external disturbances and variations of the laser parameters with time.

The erratic intensity fluctuations and irregular pulsing are categorized under the heading of laser dynamical instabilities. A substantial amount of research has been carried out to understand the causes of the laser dynamics, especially the erbium ion concentration [12, 13] and ion-ion interaction due to quenching effects [14]. In the framework of dynamical systems, many of the observed instabilities can be investigated using simple classical equations based on material properties to simplify the simulation or modelling process. To understand the backbone of physics underlying this research, a simple model of acoustic modulation was formulated using the rate equations of a laser system as the starting point.

2.3 Basic rate equations

There are various ways to model lasers, which include both the full quantum mechanical treatment, employing a semi-classical approach, and purely classical models. The purely classical approach provides the simplest form with which to construct the rate equations. Although the equations provide less information in numerical terms compared to other models, useful information can still be extracted analytically from these purely classical equations[11]. For simplicity, a two level laser system, as shown in Figure 2.4 is used. N_1 and N_2 represent the number of atoms in the ground and excited levels respectively, G is the gain coefficient that can be related to the absorption and emission coefficients and cavity length [15], n is the number of laser photons, R_p is the pumping rate, and T_1^{-1} is the decay rate of the population.

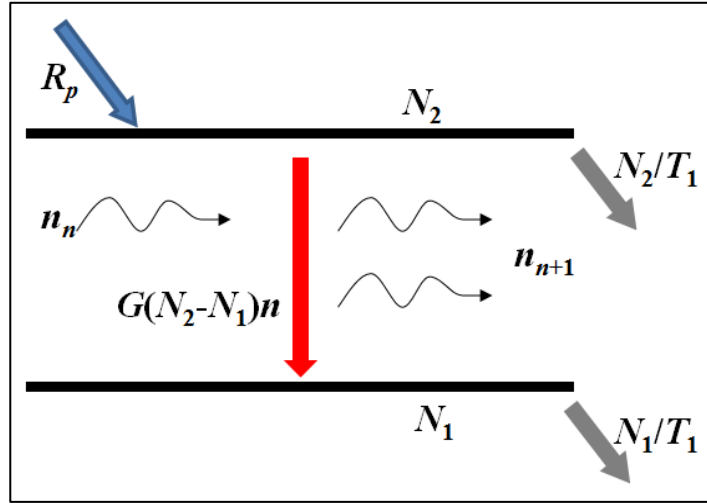


Figure 2.4: Two level laser system. R_p denotes the pumping rate, N_2/T_1 and N_1/T_1 are the decay rates of the populations, $G(N_2 - N_1)n$ is the gain for stimulated emission, and n is the number of laser photons.

Since the light-matter interaction is restricted to stimulated emission and absorption only, the rate equations can be written as[11]:

$$\frac{dn}{dT} = G(N_2 - N_1)n - \frac{n}{T_c}, \quad (2.1)$$

$$\frac{dN_2}{dT} = R_p - \frac{N_2}{T_1} - G(N_2 - N_1)n, \quad (2.2)$$

$$\frac{dN_1}{dT} = -\frac{N_1}{T_1} + G(N_2 - N_1)n, \quad (2.3)$$

where T_c^{-1} is the decay rate due to loss of photons by mirror transmission. These equations can be simplified by substituting the expression for population inversion, $N = N_2 - N_1$ and then further reduced to only two equations by combining Eqs. (2.2) and (2.3):

$$\frac{dn}{dT} = GNn - \frac{n}{T_c}, \quad (2.4)$$

$$(2.3) - (2.2) \quad \frac{dN}{dT} = -\frac{1}{T_1}(N - N_0) - 2GNn, \quad (2.5)$$

where $N_0 = R_p T_1$ is the population difference in the absence of laser light. To convert the equations into a simpler form that can be solved easily, units are removed from the equations to form dimensionless equations. This can be done by introducing new variables I , D , and t defined as:

$$I = 2GT_1 n, \quad D = GT_c N, \quad \text{and} \quad t = T/T_c. \quad (2.6)$$

Differentiating Eqs. (2.6) with respect to T gives:

$$\frac{dI}{dT} = \frac{I}{T_c} (D - 1), \quad \frac{dD}{dT} = \frac{\gamma}{T_c} [A - D(1 + I)], \quad \text{and} \quad \frac{dt}{dT} = \frac{I}{T_c}. \quad (2.7)$$

Multiplying dI/dT and dD/dT with dT/dt , gives:

$$\frac{dI}{dt} = I(D - 1), \quad (2.8)$$

$$\frac{dD}{dt} = \gamma[A - D(1 + I)] \quad (2.9)$$

where $A = GT_c N_0$ and $\gamma = T_c/T_1$. At this point, the rate equations have been successfully simplified to contain only two independent parameters - which then allow easier analysis, as well as a reduced number of numerical solutions when compared with the four independent parameters in Eqs. (2.4) and (2.5).

2.3.1 Steady states

Analysis of steady states can use to predict bifurcations and anticipate interesting transient regimes. In the steady state, there are two conditions to be satisfied, that is there are no changes in the photon intensity, $dI/dt = 0$ and the inverted population, $dD/dt = 0$. Hence, Eqs. (2.8) and (2.9) can be written as:

$$I(D - 1) = 0, \quad (2.10)$$

$$A - D(1 + I) = 0, \quad (2.11)$$

There are two solutions for Eqs. (2.10) and (2.11), which are the zero intensity solution:

$$I = 0 \quad \text{and} \quad D = A, \quad (2.12)$$

and the non-zero intensity solution:

$$I = A - 1 \geq 0 \quad \text{and} \quad D = 1. \quad (2.13)$$

The inequality in Eq. (2.13) is important because the intensity, I , can only have a positive value. Eq. (2.13) also means that lasing action is possible only if $A > 1$. The critical point at which $(I, D, A) = (0, 1, 1)$ is called the laser first threshold [11]. The critical point in this case is also the bifurcation point, as it connects two steady state solutions. There are several useful points of information that we can gather from Eqs. (2.12) and (2.13). When the laser is in the OFF state, it does not emit any radiation (zero intensity solution) - and hence the population difference is determined by the value of the pump ($D = A$). As the pump power exceeds the lasing threshold value ($A = 1$), the laser is turned ON and starts to emit radiation (non-zero intensity solution), for which the energy is proportional to the pump and cavity gain in excess of the threshold: ($I = A - 1$).

2.3.2 Linear stability

The stability of the steady state can be studied by adding in small deviations u and v , which are defined by:

$$u = I - I_s \quad \text{and} \quad v = D - D_s. \quad (2.14)$$

where $(I, D) = (I_s, D_s)$ denotes either the OFF or ON solutions. Differentiating Eq. (2.14) gives:

$$du/dt = dI/dt \quad \text{and} \quad dv/dt = dD/dt \quad (2.15)$$

Replacing Eqs. (2.14) and (2.15) into (2.8) and (2.9) gives:

$$\frac{du}{dt} = u(D_S - 1) + I_S v + I_S(D_S - 1) + uv \quad (2.16)$$

$$\frac{dv}{dt} = \gamma[-D_S u - (1 + I_S)v + A - D_S(1 + I_S) - uv] \quad (2.17)$$

and simplifying these expressions using the steady state Eqs. (2.10) and (2.11) with condition $(I, D) = (I_S, D_S)$ - and neglecting the quadratic terms in u and v to obtain the linearized equations for u and v - gives:

$$\frac{du}{dt} = u(D_S - 1) + I_S v \quad (2.18)$$

$$\frac{dv}{dt} = \gamma[-D_S u - (1 + I_S)v] \quad (2.19)$$

Combining Eqs. (2.18) and (2.19) by introducing $u = c_1 \exp(\sigma t)$ and $v = c_2 \exp(\sigma t)$, where σ represents the growth rate, leads to:

$$\sigma^2 + \sigma[\gamma(1 + I_S) - D_S + 1] + \gamma(1 + I_S - D_S) = 0 \quad (2.20)$$

Examining the solutions for u and v , it is noteworthy that when $\text{Re}(\sigma_j) < 0$ ($j = 1, 2$), small deviations u and v will decay to zero - which leads to a stable steady-state situation. If, however, $\text{Re}(\sigma_j) > 0$, then u and v will grow exponentially - which leads to an unstable situation. Hence, for the zero intensity steady state (2.12):

$$\sigma_1 = A - 1 \quad \text{and} \quad \sigma_2 = -\gamma, \quad (2.21)$$

which also means that it is stable if $A < 1$ and unstable if $A > 1$ in the zero-intensity steady-state. While, for the non-zero intensity steady state (2.13):

$$\sigma_2 + \gamma A \sigma + \gamma(A - 1) = 0 \quad (2.22)$$

It can be seen that, from Eq. (2.22), the sum of the roots is always negative ($\sigma_1 + \sigma_2 = -\gamma A < 0$) and the product of the roots is always positive ($\sigma_1 \sigma_2 = \gamma(A - 1) > 0$) -

which means that σ_1 and σ_2 both have negative values, which also implies that $\text{Re}(\sigma_j) < 0$ ($j = 1, 2$). Hence, this solution is always stable.

2.3.3 Damped relaxation oscillations

In lasers, it is common to observe lightly damped intensity oscillation after a sudden excitation change, either in the loss or the gain in the cavity. To understand this behaviour, Eq. (2.22) is solved using the ‘completing the square’ method to obtain:

$$\sigma_{1,2} = -\gamma \frac{A}{2} \pm i\sqrt{\gamma(A-1) - \gamma^2 A^2/4} \quad (2.23)$$

Provided that $\gamma(A-1) - \gamma^2 A^2/4 \geq 0$, expanding the two roots for small γ will produce:

$$\begin{aligned} \sigma_{1,2} &= -\gamma \frac{A}{2} \pm i \left\{ \sqrt{\gamma(A-1)} + \frac{1}{2} [\gamma(A-1)]^{-\frac{1}{2}} \left(-\frac{\gamma^2 A^2}{4} \right) + \dots \right\} \\ \sigma_{1,2} &= -\gamma \frac{A}{2} \pm i\sqrt{\gamma(A-1)} + O(\gamma^{\frac{3}{2}}), \end{aligned} \quad (2.24)$$

where the notation $O(\gamma^{3/2})$ is the correction term that is proportional to $\gamma^{3/2}$.

By applying a general solution for u , where $u = I - (A-1) = ce^{(\sigma_1 t)} + \bar{c}e^{(\sigma_2 t)}$ and \bar{c} is the complex conjugate of c , u can be rewritten as:

$$u \approx Ce^{(-\gamma \frac{A}{2} t)} \sin(\sqrt{\gamma(A-1)}t + \phi), \quad (2.25)$$

where C and ϕ are arbitrary constants determined by the initial conditions. Since I is proportional to u (through $I = A - 1 + u$), the laser intensity will oscillate at a frequency proportional to $\sqrt{\gamma}$ and decay slowly with a rate that is proportional to γ . The oscillation frequency [16]:

$$\omega \equiv \sqrt{\gamma(A-1)}, \quad (2.26)$$

is called the relaxation oscillation (RO) frequency of the laser and is a reference frequency for all lasers that exhibit intensity oscillations - and the damping rate of the laser RO is,

$$\Gamma \equiv \gamma \frac{A}{2}. \quad (2.27)$$

2.4 Erbium doped fibre laser

The simplest model of the EDFL can be constructed using a purely three level atomic system, with emission between the intermediate and the ground state. Although there are four level atomic systems that enable more precise modelling of the EDFL, most of the important characteristics of EDFLs can be obtained from this simple 3-level model[17].

Figure 2.5 shows the possible erbium atom transitions between the ground state, denoted by 1, intermediate state, denoted by 3, and metastable state, denoted by 2. N_1 , N_2 and N_3 represent the populations of each level. The operation of these three levels can be described by three simple processes. The process starts with pumping by a short wavelength pump laser (normally 980 nm), which is used to excite the Er^{3+} ions to a higher energy level, represented by level 3. Er ions at level 3 are unstable and quickly decay to level 2 (a mostly radiationless transition). The lifetime of Er ions at level 2 is longer (~ 10 ms) which allows them to stay at level 2 while waiting for stimulated emission to happen, accompanied by decay back to the ground level. ϕ_p and ϕ_s represent the incident light intensity flux of the pump and signal respectively, σ_p and σ_s are either the absorption or emission cross-sections of the pump and signal - and Γ_{xy} represent the transition probability from level x to y . Generally $\phi_p \sigma_p$ represents the pumping rate, while $\phi_s \sigma_s$ represents the stimulated emission rate.

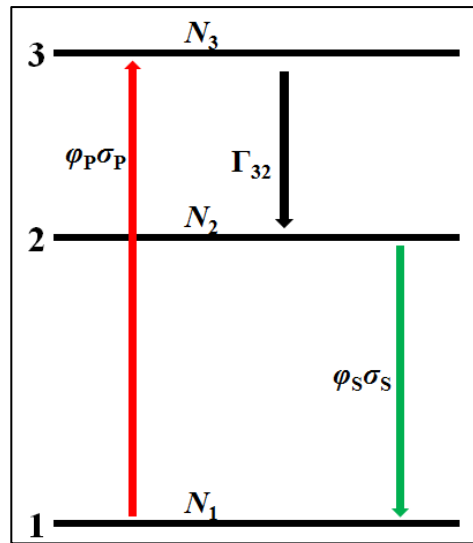


Figure 2.5: Simple three level system for EDFL model.

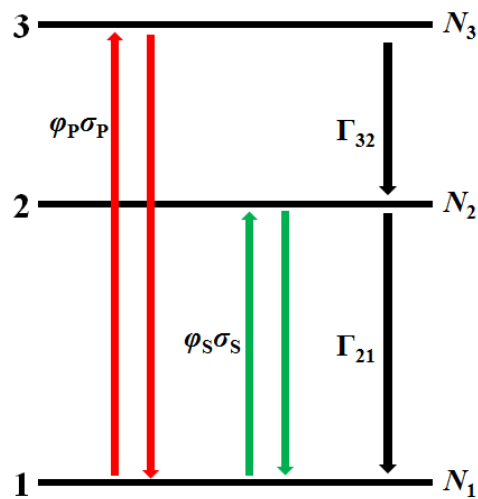


Figure 2.6: Complete 3 level system for EDFL.

However, the three-level system is normally presented in a slightly more complete way. The processes include: (a) the re-emission of pump laser photons that causes the Er ions to de-excite from level 3 to level 1 after absorption, (b) re-absorption of the signal, which causes the excitation of Er ions from level 1 to level 2, and (c) spontaneous emission, which causes the de-excitation of Er ions from level 2 to level 1. These transition processes are presented schematically in Figure 2.6. In this case, the absorption and emission cross-sections are assumed to be the same.

Due to the unstable condition of level 3, Er ions that have been excited to level 3 will decay to level 2 or level 1, almost instantaneously. Hence, N_3 will always remain small in comparison with N_1 - and dN_3/dT will be small in comparison with $N_1\varphi_p\sigma_p$. Eq. (2.28) to Eq. (2.30) simplify to:

$$\frac{dN_1}{dT} \approx \Gamma_{21}N_2 - \varphi_P\sigma_P N_1 + (N_2 - N_1)\varphi_S\sigma_S \quad (2.31)$$

$$\frac{dN_2}{dT} \approx -\Gamma_{21}N_2 + \Gamma_{32}N_3 - (N_2 - N_1)\varphi_S\sigma_S \quad (2.32)$$

$$0 \approx -\Gamma_{32}N_3 + \varphi_P\sigma_P N_1 \quad (2.33)$$

Substituting Eq. (2.33) into Eq. (2.32) produces:

$$\frac{dN_2}{dT} \approx -\Gamma_{21}N_2 + \varphi_P\sigma_P N_1 - (N_2 - N_1)\varphi_S\sigma_S \quad (2.34)$$

To obtain amplification or lasing, population inversion between levels 1 and 2, for which at least half of the total population of erbium ions needs is excited to level 2, will need to be achieved. Here, the inversion population $N \equiv N_2 - N_1$, was introduced to further simplify Eqs. (2.31) and (2.34) to give:

$$\frac{dN_1}{dT} \approx \Gamma_{21}N_2 - \varphi_P\sigma_P N_1 + N\varphi_S\sigma_S \quad (2.35)$$

$$\frac{dN_2}{dT} \approx -\Gamma_{21}N_2 + \varphi_P\sigma_P N_1 - N\varphi_S\sigma_S \quad (2.36)$$

Then, from $N \equiv N_2 - N_1$:

$$\begin{aligned} \frac{dN}{dT} &= \frac{dN_2}{dT} - \frac{dN_1}{dT} \\ &= -2\Gamma_{21}N_2 + 2\varphi_P\sigma_P N_1 - 2N\varphi_S\sigma_S \end{aligned} \quad (2.37)$$

The total population can be represented by, $N_T = N_1 + N_2 + N_3 \approx N_1 + N_2$, since N_3 is small, in comparison with N_2 and N_3 . Thus $2N_2 = N + N_T$, and $-2N_1 = N - N_T$, were obtained. Substitution into Eq. (2.37) produces:

$$\frac{dN}{dT} = -\Gamma_{21}(N + N_T) - \varphi_P\sigma_P(N - N_T) - 2N\varphi_S\sigma_S \quad (2.38)$$

The rate changes of the population inversion in Eq. (2.38) include the three main processes in a laser. The first term describes the relaxation of excited Er ions to their equilibrium position, also called spontaneous emission. The second term is the pumping process, which generates population inversion. The third term is the nonlinear coupling between population inversion and signal intensity, which is also known as the stimulated emission.

As in section 2.3, the analytical equation that describes the number of photons in the laser cavity can be written as,

$$\frac{d\varphi_S}{dT} = -\varphi_S\gamma_c + \varphi_S\sigma_S N = \varphi_S(-\gamma_c + \sigma_S N) \quad (2.39)$$

where γ_c is the decay rate due to the loss of photons due to mirror transmission. To convert Eq. (2.39) into a dimensionless equation, the following new variables are introduced:

$$t \equiv \gamma_c T, I \equiv \frac{2\varphi_s \sigma_s}{\Gamma_{21} + \varphi_P \sigma_P}, \text{ and } D \equiv \frac{\sigma_s}{\gamma_c} N \quad (2.40)$$

These are then substituted into Eq. (2.39):

$$\begin{aligned} \frac{dI}{dt} &= \frac{2\sigma_s}{\Gamma_{21} + \varphi_P \sigma_P} \cdot \frac{d\varphi_s}{dT} \cdot \frac{dT}{dt} \\ &= \left(\frac{2\sigma_s}{\Gamma_{21} + \varphi_P \sigma_P} \right) [\varphi_s (-\gamma_c + \sigma_s N)] \left(\frac{1}{\gamma_c} \right) \\ &= \left(\frac{2\varphi_s \sigma_s}{\Gamma_{21} + \varphi_P \sigma_P} \right) \left(-1 + \frac{\sigma_s N}{\gamma_c} \right) \\ \therefore \frac{dI}{dt} &= I(-1 + D) \end{aligned} \quad (2.41)$$

and then into Eq. (2.38):

$$\begin{aligned} \frac{dD}{dt} &= \frac{\sigma_s}{\gamma_c} \cdot \frac{dN}{dT} \cdot \frac{dT}{dt} \\ &= \frac{\sigma_s}{\gamma_c} [-\Gamma_{21}(N + N_T) - \varphi_P \sigma_P(N - N_T) - 2N\varphi_s \sigma_s] \left(\frac{1}{\gamma_c} \right) \\ &= \frac{\sigma_s}{\gamma_c^2} [(\varphi_P \sigma_P - \Gamma_{21})N_T - (2\varphi_s \sigma_s + \varphi_P \sigma_P + \Gamma_{21})N] \\ &= \frac{\Gamma_{21} + \varphi_P \sigma_P}{\gamma_c} \left[\frac{(\varphi_P \sigma_P - \Gamma_{21})\sigma_s N_T}{(\Gamma_{21} + \varphi_P \sigma_P)\gamma_c} - \frac{\sigma_s N}{\gamma_c} \left(1 + \frac{2\varphi_s \sigma_s}{\Gamma_{21} + \varphi_P \sigma_P} \right) \right] \\ \therefore \frac{dD}{dt} &= \gamma[A - D(1 + I)] \end{aligned} \quad (2.42)$$

where:

$$\gamma = \frac{\Gamma_{21} + \varphi_P \sigma_P}{\gamma_c} \quad \text{and} \quad A = \frac{(\varphi_P \sigma_P - \Gamma_{21})\sigma_s N_T}{(\Gamma_{21} + \varphi_P \sigma_P)\gamma_c} \quad (2.43)$$

It should be noted that Eqs. (2.41) and (2.42) are identical to Eqs. (2.8) and (2.9), but with different definitions for γ and A - which also means that the analysis presented in section 2.3 can be applied to EDFL systems by using the definitions of γ and A in Eq. (2.43).

2.5 Modulated laser

In order to analyse the behaviour of the laser under modulation, the initial operating conditions for the fibre laser are introduced,

$$I(0) = I_i \quad \text{and} \quad D(0) = D_i. \quad (2.44)$$

Under a small modulation level, an asymptotic solution of Eq. (2.41) and (2.42) can be obtained by setting $\gamma = 0$, which then leads to:

$$\frac{dI}{dt} = I(1 - D_i) \quad \text{and} \quad \frac{dD}{dt} = 0 \quad (2.45)$$

Solving Eq. (2.45) gives $D = D_i$ and $I = I_i \exp[(D_i - 1)t]$, which means that the intensity either decays to zero exponentially or grows exponentially, depending on the value of D_i . However neither result leads to the stable non-zero intensity steady-state that can be found in real experimental results. To obtain the solution for this singular limit ($\gamma = 0$), γ has to be separated out from the multiplication of the parameters on the right hand side of Eq. (2.42).

To separate the γ from the multiplication equation, a new time parameter is introduced:

$$s \equiv \omega_R t \quad (2.46)$$

where ω_R is the Relaxation Oscillation (RO) frequency.

New dependent variables x and y are introduced as:

$$x \equiv \frac{D-1}{\omega_R} \quad \text{and} \quad y \equiv \frac{I-(A-1)}{A-1} \quad (2.47)$$

Both variables x and y are deviations of D and I from steady state values under $I(0) = I_i$.

Substituting Eqs. (2.46) and (2.47) into Eq. (2.41) leads to:

$$\begin{aligned} \frac{dy}{ds} &= \frac{dy}{dI} \cdot \frac{dI}{dt} \cdot \frac{dt}{ds} \\ \frac{dy}{ds} &= (1+y)x \end{aligned} \quad (2.48)$$

and Eq. (2.42):

$$\begin{aligned} \frac{dx}{ds} &= \frac{dx}{dD} \cdot \frac{dD}{dt} \cdot \frac{dt}{ds} \\ \frac{dx}{ds} &= -y - \varepsilon^2 x [1 + (A-1)(1+y)] \end{aligned} \quad (2.49)$$

where ε^2 is defined as:

$$\varepsilon^2 \equiv \sqrt{\frac{\gamma}{A-1}} \ll 1. \quad (2.50)$$

Coming back to the above condition, when $\gamma = 0$ or $\varepsilon = 0$, now leads to:

$$x' = -y \quad \text{and} \quad y' = (1+y)x \quad (2.51)$$

which allows bounded periodic solutions.

Laser modulation can be carried in two different ways; that is, either through pump modulation or through loss modulation. Pump modulation will affect the evolution equation of the population inversion, while loss modulation changes the evolution equation of the intensity. Pump modulation is straightforwardly carried out by

changing the pump intensity according to different specified input wave patterns. The modulated pump intensity can be represented by:

$$A_m = A(1 + mF(t)) \quad (2.52)$$

where A is the pump mean value, m is the modulation amplitude, and $F(t)$ is the modulation wave function - which can be sinusoidal, square, triangular or pulsating wave. Eq. (2.52) can be replaced directly into Eq. (2.49), in order to analyse the laser intensity under pump modulation.

Loss modulation is not a straightforward process - and always refers to changes in the total losses within the laser cavity. In this case, the cavity decay rate, T_c^{-1} becomes an important parameter in the equation, since T_c^{-1} is now a variable instead of being constant. A time-dependent cavity decay rate, $T_c^{-1}(T) = T_c^{-1}(1+mF(T))$ is then introduced into Eq. (2.4), leading to:

$$\frac{dn}{dT} = GNn - \frac{n(1+mF(T))}{T_c}. \quad (2.53)$$

where m is the modulation amplitude and $F(T)$ is the modulation wave function. Replacing the same dimensionless parameters in Eq. (2.6) to Eq. (2.53) produces:

$$\frac{dI}{dt} = I(D - 1 - mG(t)) \quad (2.54)$$

where $F(T) \equiv G(t)$.

Although both methods just described are able to modulate the laser output intensity, they play different roles in the work of this thesis. Pump modulation is a simpler and more direct way to modulate the laser output intensity, and therefore it implies lower noise and less uncertainty. Controlling the pump power is also relatively simple, e.g. by just using a signal generator and a laser diode. Thus pump modulation is

used to study the behaviour and for characterization of the laser system. On the other hand, acoustic sensing is totally reliant on loss modulation, since acoustic waves can only generate loss in the laser cavity instead of modulating the pump intensity. Hence study of loss modulation becomes important in acoustic wave sensing, although it carries more noise and uncertainty.

2.6 Summary

In this chapter, simple models of standard two-level laser and three-level laser operation for EDF-based lasers were developed on the basis of a rate equation approach. Analysis has been carried out on the processes involved, in order to understand the optical intensity changes with respect to related parameters such as pump power, Er ion life time, absorption coefficient and emission coefficient. EDFL behaviour during steady-state and dynamic condition has also been studied. Lastly, pump and loss modulation of fibre lasers has been demonstrated to support the possibility of applying the dynamic behaviour of the laser as the operating mechanism in acoustic sensors.

References

- [1] B. J. Ainslie, "A review of the fabrication and properties of erbium-doped fibers for optical amplifiers," *Lightwave Technology, Journal of*, vol. 9, pp. 220-227, 1991.
- [2] T. M. Kwok, A. A. Pau, R. A. Betts, F. F. Ruhl, and G. F. Zheng, "Fabrication and characterisation of rare earth doped optical fibres," in *TENCON 90. 1990 IEEE Region 10 Conference on Computer and Communication Systems*, 1990, pp. 104-108 vol.1.
- [3] J. Wang, J. Li, P. Liu, X. Mao, L. Wang, L. Liu, J. Peng, C. Zhang, K. Zheng, H. Wei, J. Fu Yong, F. Yan, T. Ning, and W. Jian, "Fabrication and characteristics of Yb³⁺ doped silica optical fibers," in *Optical Fiber Communication & Optoelectronic Exposition & Conference, 2008. AOE 2008. Asia*, 2008, pp. 1-3.
- [4] Z. Zhang, A. J. Boyland, J. K. Sahu, W. A. Clarkson, and M. Ibsen, "High-Power Single-Frequency Thulium-Doped Fiber DBR Laser at 1943 nm," *Photonics Technology Letters, IEEE*, vol. 23, pp. 417-419, 2011.
- [5] M. J. F. Digonnet, *Rare-Earth-Doped Fiber Lasers and Amplifiers*: Marcel Dekker, 2001.
- [6] C. Jianfeng, L. Yunqi, C. Tongjian, and W. Tingyun, "Fiber laser sensor based on fiber-Bragg-grating Fabry-Perot cavity," in *Communications and Photonics Conference and Exhibition (ACP), 2010 Asia*, 2010, pp. 238-239.
- [7] R. Ibrahim, Y. Gottesman, B.-E. Benkelfat, and Q. Zou, "Erbium-Doped-Fiber Characterization: Dynamic Study of Laser Ring Cavity Based on a General Model," *J. Lightwave Technol.*, vol. 25, pp. 1819-1825, 2007.

- [8] M. N. Zervas and G. Hoven, "Optical Amplifiers - Fibre Optic Communication Devices." vol. 4, N. Grote and H. Venghaus, Eds., ed: Springer Berlin Heidelberg, 2001, pp. 151-196.
- [9] P. W. France, *Optical Fibre Lasers and Amplifiers*: CRC PR. I. Llc., 1991.
- [10] Y. I. Khanin, *Fundamentals of Laser Dynamics*. Cambridge: Cambridge International Science Publishing Ltd., 2006.
- [11] T. Erneux and P. Glorieux, *Laser Dynamics*. New York: Cambridge University Press, 2010.
- [12] H. L. An, E. Y. B. Pun, X. Z. Lin, and H. D. Liu, "Effects of ion-clusters on the intensity noise of heavily erbium-doped fiber lasers," *Photonics Technology Letters, IEEE*, vol. 11, pp. 803-805, 1999.
- [13] F. Sanchez, P. Le Boudec, P.-L. François, and G. Stephan, "Effects of ion pairs on the dynamics of erbium-doped fiber lasers," *Physical Review A*, vol. 48, pp. 2220-2229, 1993.
- [14] F. Sanchez and G. Stephan, "General analysis of instabilities in erbium-doped fiber lasers," *Physical Review E*, vol. 53, pp. 2110-2122, 1996.
- [15] G. Stewart, V. Karthik, and G. Whitenett, "Optical fibre sensors based on the dynamic response of fibre lasers," in *17th International Conference on Optical Fibre Sensors (OFS 2005)*, Belgium, 2005, pp. 916-919.
- [16] C. Yuh-Jen, P. L. Mussche, and A. E. Siegman, "Cavity decay rate and relaxation oscillation frequency in unconventional laser cavities," *Quantum Electronics, IEEE Journal of*, vol. 31, pp. 391-398, 1995.

- [17] P. C. Becker, N. A. Olsson, and J. R. Simpson, *Erbium-Doped Fiber Amplifiers - Fundamentals and Technology*. San Diego: Academic Press, 1999.

Chapter 3

Experimental Set-up, Characterization, and Modelling

3.1 Experimental Setup

3.2 Noise and Resonance Frequency

3.3 Turn on Transient

3.3.1 Experimental results

3.3.2 Modelling

3.4 Pump Modulation

3.5 Loss Modulation

3.6 Summary

References

3.1 Experimental setup

The experimental set-up used for the work of this thesis was a simple free running linear cavity fibre laser that consisted of 3 m of erbium-doped fibre (EDF), a 980 nm pump laser, and a Wavelength Division Multiplexer (WDM) coupler, as shown in Figure 3.1(a). A fibre laser linear cavity was formed in between point A and point B, with a branch at the 980 nm/1550 nm WDM coupler to guide the 980 nm pump into the cavity as shown Figure 3.1(b). The total length of the cavity was about 10 m from point A to B including EDF, WDM coupler, and connectors at both fibre ends A and B. During the experiments, the 980 nm laser acted as a pump source and was directed into the laser cavity using a WDM coupler. Pump photons which pass through the active medium will be absorbed by Erbium (Er) ions, exciting them and generating population inversion. These excited Er ions will then relax to the ground state either by releasing spontaneous emission or stimulated emission. Emission released by Er ions is labelled as signal in Figure 3.1.

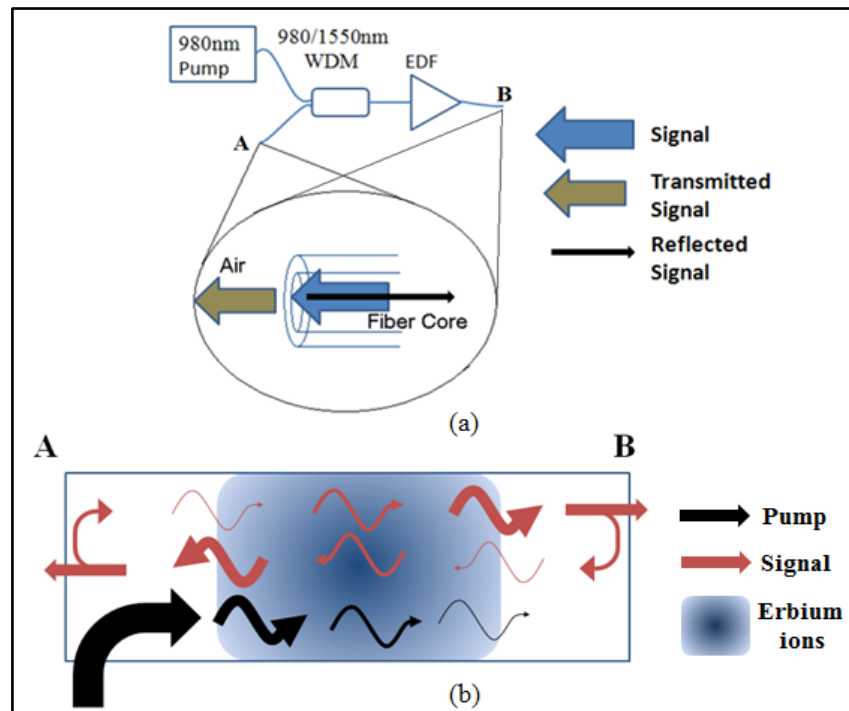


Figure 3.1: Diagram of (a) experiment setup and (b) light beam propagation and interaction.

The direction of spontaneous emission is arbitrary. Some portion of the emitted signals will be guided along the fibre axis and propagate in both directions towards the fibre ends (A and B). When the signal arrives at a fibre end, A or B, that is flat and orthogonal to the signal propagation direction, it will experience both transmission and reflection. Both fibre ends were flatly cleaved (90 degree to the waveguide channel) to obtain maximum reflection from the fibre ends without using other optical reflective devices. The fibre end reflection has a similar function as the reflection created by the mirrors in a solid-state laser cavity - but with a much lower reflectivity, which is the ~4%, that corresponds to the plane-wave Fresnel reflection, according to the equation shown below:

$$R = \frac{n_2 - n_1}{n_2 + n_1} \times 100\% \quad (3.1)$$

The reflected signals from both fibre ends, A and B, will pass through the Er gain medium and experience amplification. The output signal from the system, before any lasing occurs, is called Amplified Spontaneous emission (ASE). The ASE spectrum of the EDF used in these experiments falls within the conventional band (C band) - ranging from 1530 nm to 1565 nm, which is well within the fibre optic transmission band from 1260 nm - 1675 nm, as shown in Figure 3.2.

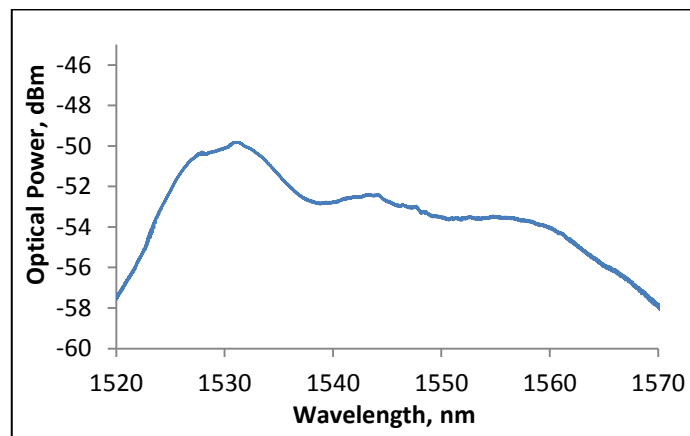


Figure 3.2: ASE spectrum of EDFL pumped with 980 nm laser at 12 mW without feedback from reflection.

In any laser cavity, either bulk or fibre based lasers, there will be quite a large number of longitudinal modes oscillating at the same time when the gain of the amplifying medium exceeds the loss of the cavity [1]. This can be interpreted as to when the ASE overcoming the loss of the cavity or reaching the lasing threshold. The longitudinal modes falling within the maximum gain region will have a high probability of lasing compared to those modes at both ends of the gain curve. The lasing probability of the EDF can be represented by the ASE as shown in Figure 3.2. Modes within the 1530 nm region will have a higher lasing probability as they experienced higher gain when passing through the gain medium. As the pump power increases, the ASE level will increase as the cavity gain increases. Once the ASE level increases above the lasing threshold, multiple sharp and narrow lasing peaks can be observed at the 1530 nm region as shown in Figure 3.3.

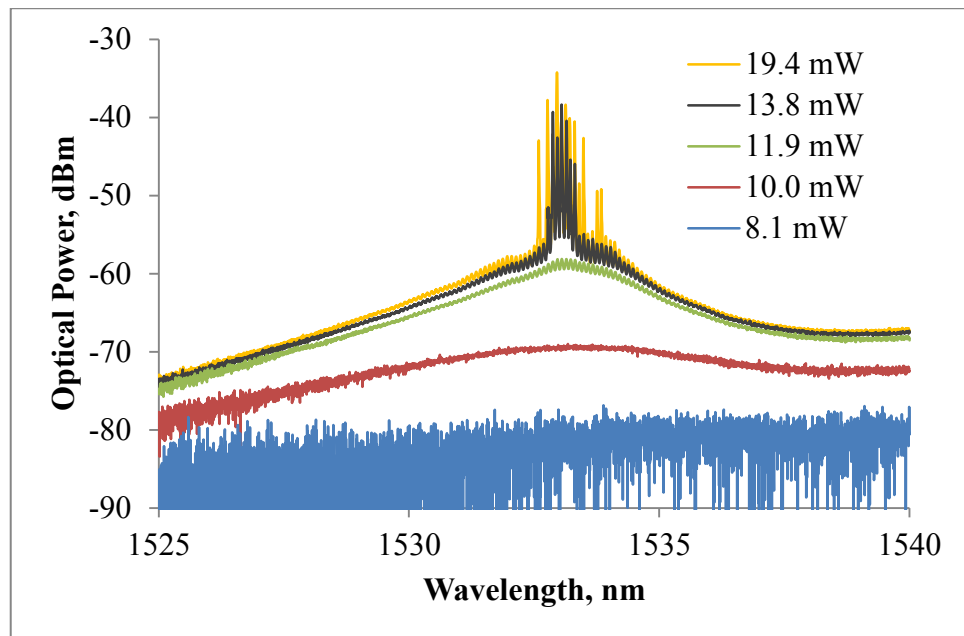


Figure 3.3: ASE spectrum and random lasing of EDFL under free running condition at different pump power.

The multiple lasing peaks are caused by the broad ASE spectrum of the EDF emission - and the long cavity set-up, which has a length of approximately 10 m that allows a large number of longitudinal modes to oscillate, as described above. The modes that survive are those that satisfy the specific conditions of the resonator geometry, which determine the standing wave patterns in the cavity, the reflectivity of the mirrors and the gain spectrum of the medium. The lasing wavelengths are governed by Eq. (3.2):

$$\Delta\lambda_{res} = \frac{\lambda_0^2}{n_r L} \quad (3.2)$$

where L is the length of the cavity, λ_0 is the centre wavelength, and n_r is the effective refractive index of the fibre. Several longitudinal modes in the 1530 nm spectral region can oscillate simultaneously and therefore undergo mode competition as a result of the homogeneous gain nature of the EDF. This competition causes the unstable behaviour of the lasing frequency and lasing power that leads to the detected optical power fluctuation. Further increases of pump power above the lasing threshold mainly contribute to the generation of a higher lasing power level and broader lasing bandwidth, with a slightly increased ASE level. This behaviour results from the domination of stimulated emission in the gain medium, when sufficient optical power is fed back into it.

3.2 Noise and Resonance Frequency

In order to understand the behaviour of the set-up, the noise was studied by measuring the time-domain fluctuation of the total optical power. The optical power fluctuations in the fibre laser were obtained using a photo-detector to convert the optical power into a voltage that was subsequently displayed on a digital oscilloscope. The optical output power was quite stable, although there were noticeable fluctuations at

high frequencies in few tens of kHz, as shown in the top part of Figure 3.4. An analysis was performed on the output optical-power fluctuation-frequency by performing a Fast Fourier Transform (FFT) on a 1 s period of recorded optical power. Figure 3.4 also shows the results for the direct FFT calculation obtained using the built-in function of the digital oscilloscope that was used to display the optical power.

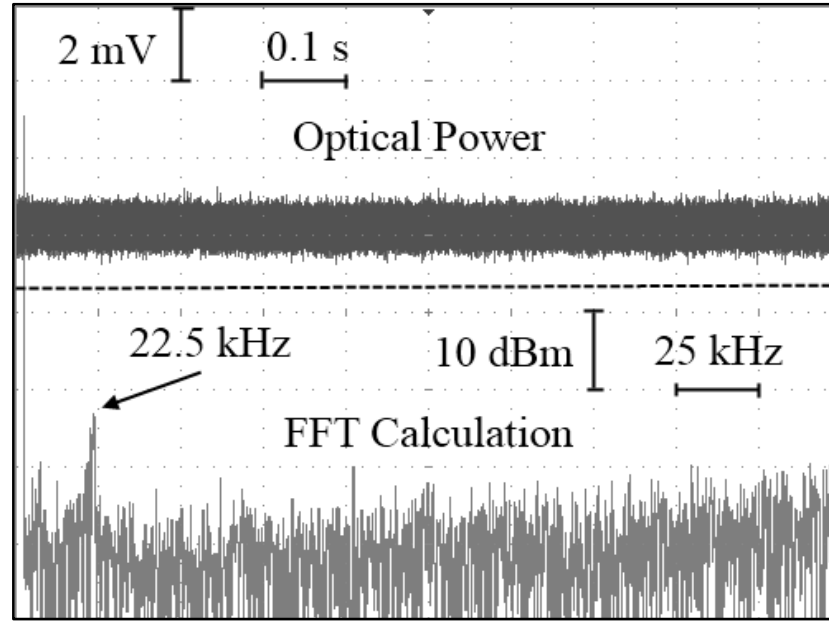


Figure 3.4: Screen capture of optical power pumping at 15.7 mW together with the FFT calculation performs by digital oscilloscope.

The FFT spectrum, with a peak at 22.5 kHz, indicates that the optical power fluctuates over a specific frequency band. Fluctuation of the optical power in this range of frequencies is dependent on several factors, such as cavity length, that determine the round-trip period of optical propagation in the cavity, the gain - which is determined by the gain medium and pump power - and the cavity loss, which determined by the propagation loss in the cavity and the reflectivity of the cavity mirrors. The relation between all these parameters is given indirectly in Section 2.3 by the parameter γ . From Eq. (2.43), it can be seen that γ is directly proportional to the pumping rate, $\phi_p \sigma_p$, and inversely proportional to the cavity decay rate, γ_c . $\phi_p \sigma_p$ is also proportional to the gain, while γ_c is proportional to the cavity loss and inversely proportional to the cavity length

or the round trip period. The peak of the FFT frequency spectrum is at the frequency determined by resonance effects when light in the laser interacts with the acoustic waves. In certain cases, the resonance frequency also called relative intensity noise (RIN)[2]. The resonance frequency can also be calculated theoretically from Eq. (2.26).

Among the three main parameters affecting the resonance frequency, the pump power is the easiest parameter to change, since it can be varied without any modification of the set-up. Optical pumping at different power levels, ranging from 10.8 mW to 68.5 mW, was carried out for periods of 1 s, in order to study the changes of the resonance frequency. FFT calculations were performed on each data point to obtain the frequency spectrum of the output power fluctuation. These results were then plotted in a graph, as shown in Figure 3.5. The most obvious behaviour that can be observed is the shifting of the resonance frequency to higher frequencies when the pump power is increased.

As mentioned above, γ which represent the ratio of pumping rate to the cavity decay rate is directly proportional to the pump power, P . Thus, from Eq. (2.26), the resonance frequency can be stated as [3]

$$\omega \propto \sqrt{P}, \omega = k \sqrt{P}, \text{ or } \omega^2 = kP. \quad (3.3)$$

Further analysis was carried out on the resonance frequency data by plotting the resonance frequency, ω , against pump power, P , and ω^2 against P - in graphs as in Figure 3.6. Both graphs shown in Figure 3.6 fit the predictions of Eq. (3.3). By using curve fitting methods, the linear equation that fits the graph in Figure 3.6(b) can be represented by:

$$\omega^2 = 120 P - 1400 \quad (3.4)$$

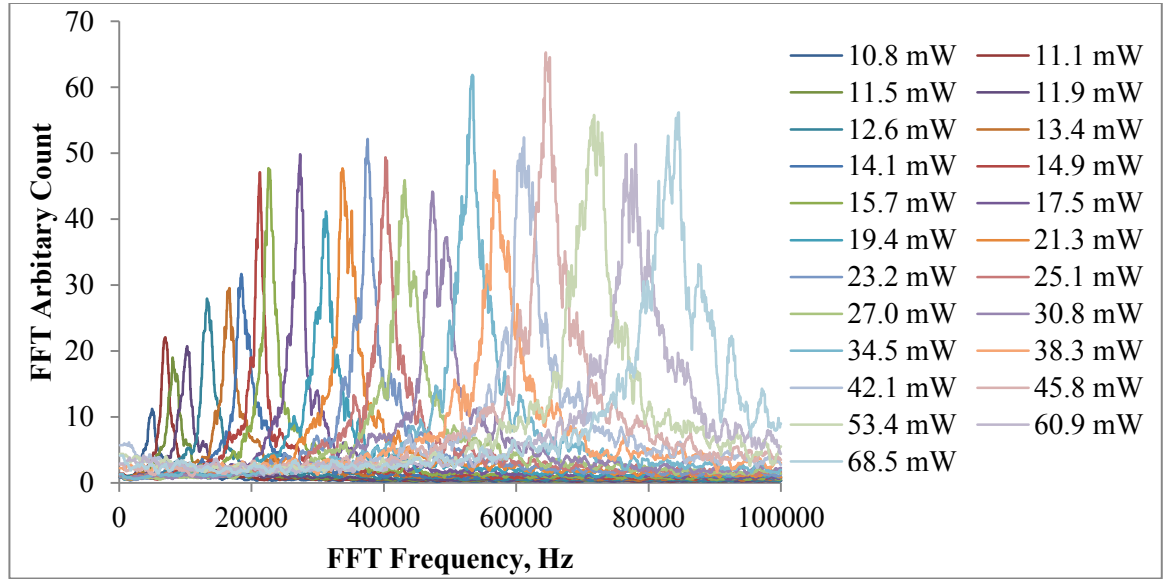


Figure 3.5: FFT frequency spectrum of optical output power fluctuation under different pump power conditions.

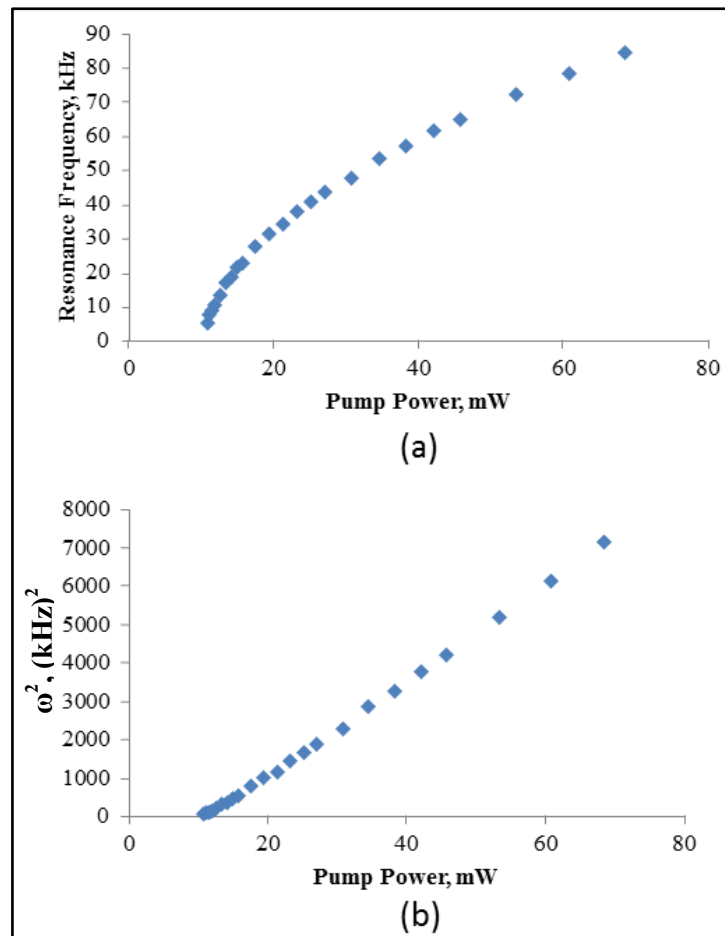


Figure 3.6: Graphs of (a) resonance frequency, ω against pump power, P and (b) ω^2 against P .

Besides the relationship between the resonance frequency and the pump power, Eq. (3.4) also carries information on the lasing threshold of pump power. The lasing threshold of the pump power can be obtained by substituting $\omega = 0$, - which gives a value of 11.7 mW that is near to the experimental value of 12.1 mW.

3.3 Turn-on transient behaviour

The turn-on transient [4], the laser transience [5], or the so-call ‘onset dynamics’ [6] is the time evolution of the laser intensity when the pump laser is switched from a level below the lasing threshold to a level above the lasing threshold value. This dynamic effect can be observed in most of the lasers used today [4]. The study of the laser turn-on transient behaviour is important, as it carries information on several laser parameters that are useful in understanding the properties of a particular laser [7]. There are three distinct regimes in the turn-on transient effect, as shown in Figure 3.7 [4]:

- (a) Latency regime:- is the regime between the time when the pump power is switched on, until the observation of first spike - where the laser output power remains low. It is also called the “lethargy” or “turn-on” regime
- (b) Spiking regime:- is the regime where strong pulsations happen, generating sharp spikes that are separated by periods of very low emission.
- (c) Relaxation oscillation (RO) regime – The regime where damped oscillations occur as the laser approaches its steady state, due to exponentially damped sinusoidal oscillations.

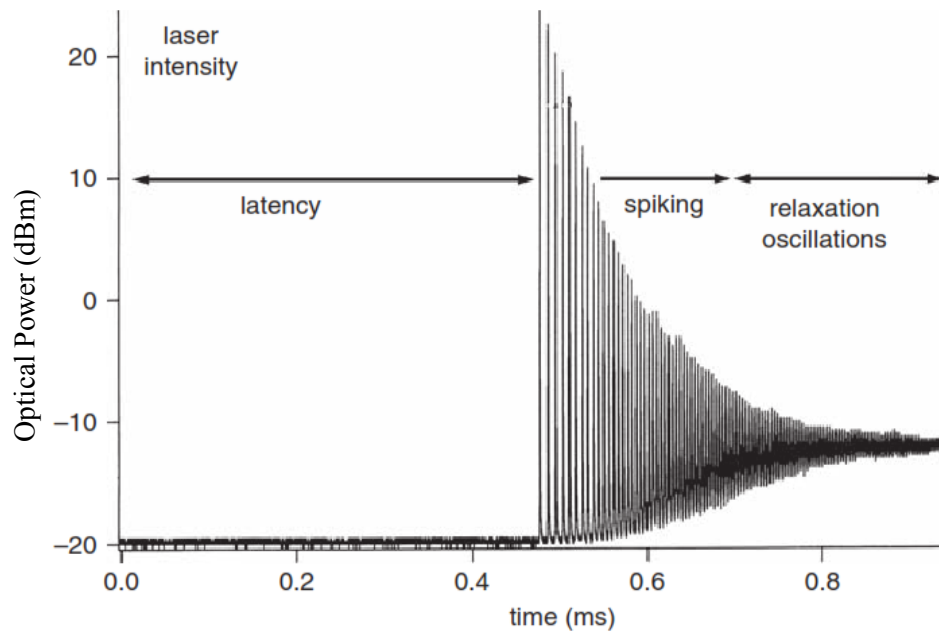


Figure 3.7: Typical turn-on transient of a laser [4].

3.3.1 Experimental results

In the experiments, a step input of pump power was directed into the fibre laser system to generate the turn-on transient effect in the fibre laser. Figure 3.8 shows graphs of the digital oscilloscope with fibre laser output power levels (black colour line) and pump power levels (grey colour line) under the transient conditions. As discussed in the previous section, the turn-on transient behaviour can be observed when the pump power is switched from below the threshold to above the threshold, as shown by the grey line in Figure 3.8(a). Switching the pump power from 0 mW to above the threshold power at 44.5 mW does not cause the laser output power to increase immediately – and output remains at a minimum level for a period of 3.58 ms that is labelled as the latency regime. The latency regime is followed by a series of spiking oscillations and RO. A clearer diagram focussed on the spiking and RO regimes is shown in Figure 3.8(b). The first two sharp spikes in the spiking regime were separated by low intensity emissions for a period of about 23.0 μ s. These separation periods between spikes reduce slowly and the spike intensities decay exponentially when moving towards the RO regime. In the RO

regime, the intensity fluctuation is smooth, but oscillates in a damped sinusoidal wave form. A series of turn-on transients with different pump powers has been captured, in order to understand the relation of pump power to the latency, spiking, and RO. The captured traces are shown in Figure 3.9.

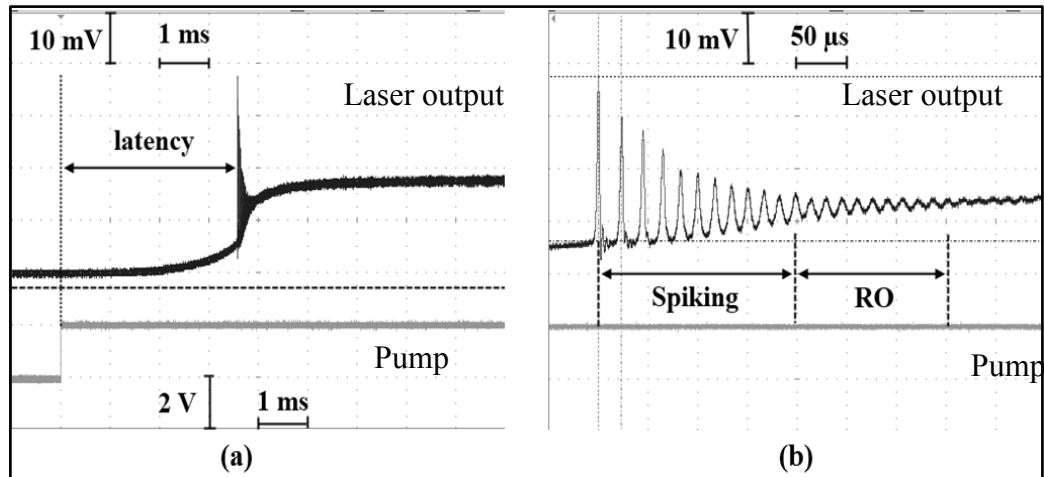


Figure 3.8: Screen capture from digital oscilloscope of fibre laser turn-on transient effect with pumping at 44.5 mW.

There are several changes that are observable in the sub-figures in Figure 3.9, as the pump power is decreased:

- (a) the turn-on time increases,
- (b) the spiking power reduces, and
- (c) the damping effect increases.

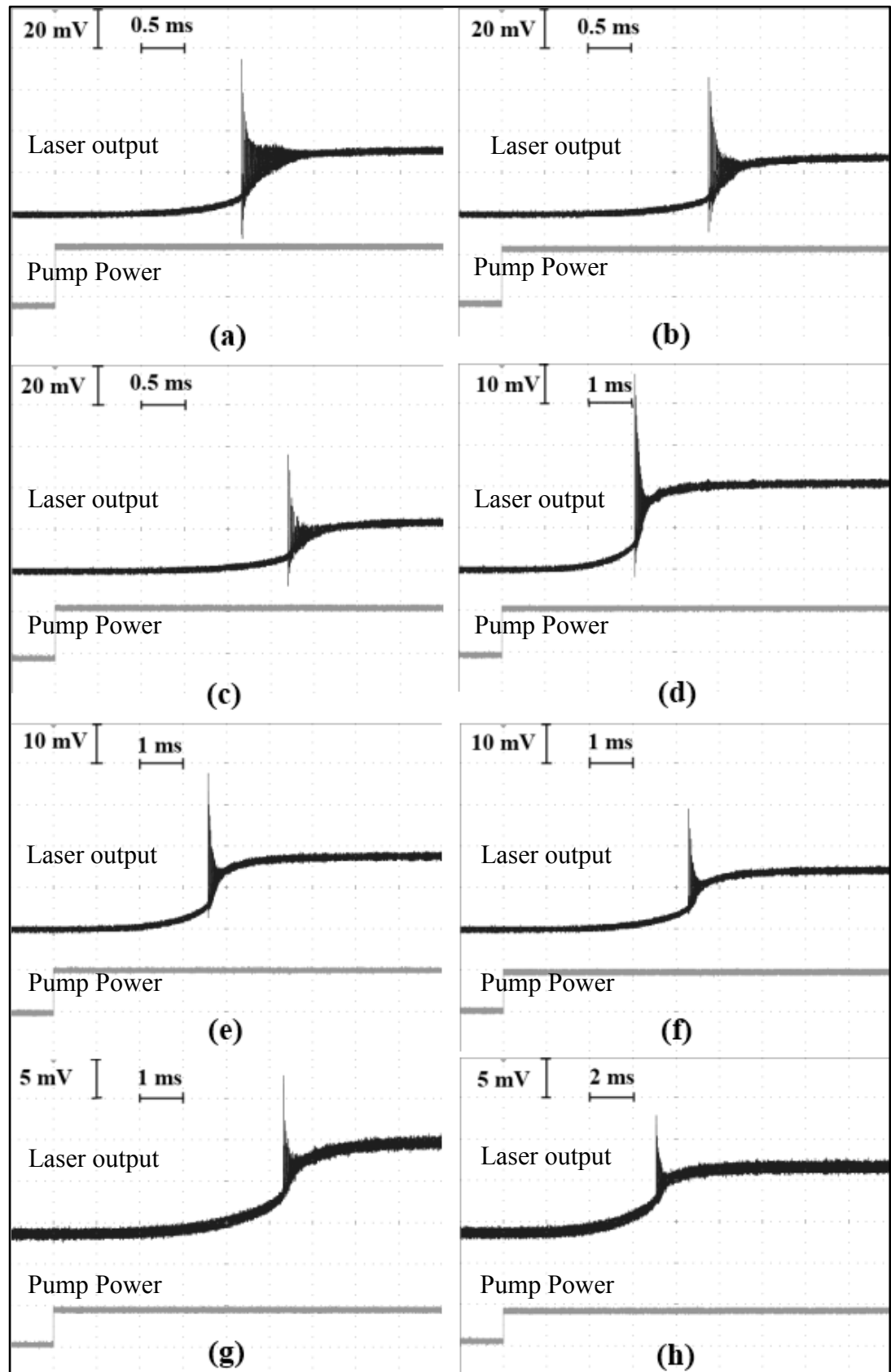


Figure 3.9: Turn-on transient effect with pumping at different pump power levels: (a) 66.9 mW, (b) 61.3 mW, (c) 55.7 mW, (d) 50.1 mW, (e) 44.5 mW, (f) 38.9 mW, (g) 33.3 mW, and (h) 27.7 mW.

The relationship between these parameters can be represented in a more direct manner. Figure 3.10 shows the relationship between the latency period and pump power. The plot of the latency regime period does not show a linear graph, and this means that it cannot be described by the linearized theory presented in Chapter 2. The nonlinearity is caused by the high inversion of population, which does not remain close to the laser OFF state [4]. However, an analytical investigation of the latency regime period can be carried out to obtain the value of the latency regime period by using Eqs. (2.8) and (2.9) to obtain [4]:

$$t_{on} \cong \gamma^{-1} \left(\frac{1-A_-}{A_+-1} \right) \quad (3.5)$$

where t_{on} is the turn on time, A_+ denotes the value of the pump power level above threshold, which is larger than 1 - and A represents the value of the pump power level below threshold, which is less than 1.

Since the initial pump power is zero in our case, Eq. (3.5) can be further simplified to:

$$t_{on} \cong \gamma^{-1} \left(\frac{1}{A_+-1} \right) \quad (3.6)$$

The results will show a straight line graph for plots of t_{on} against $1/(A_+ - 1)$ according to Eq. (3.6), which matches the experimental results given in Figure 3.10.

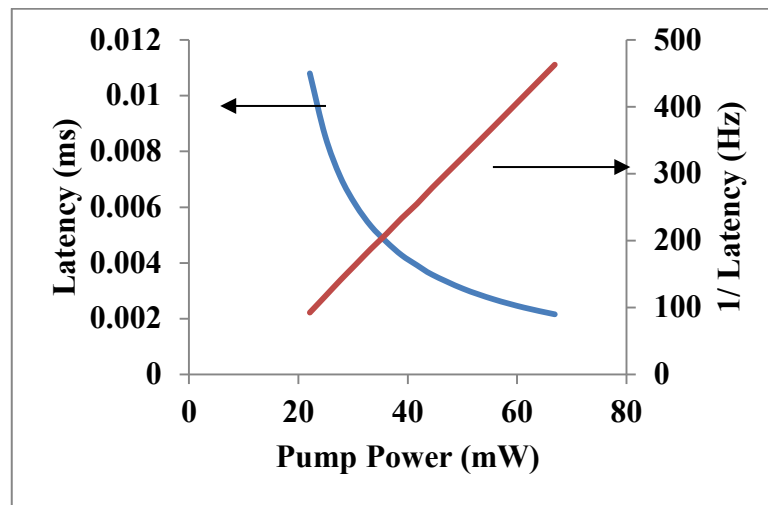


Figure 3.10: Relation between latency period or turn-on time and pump power.

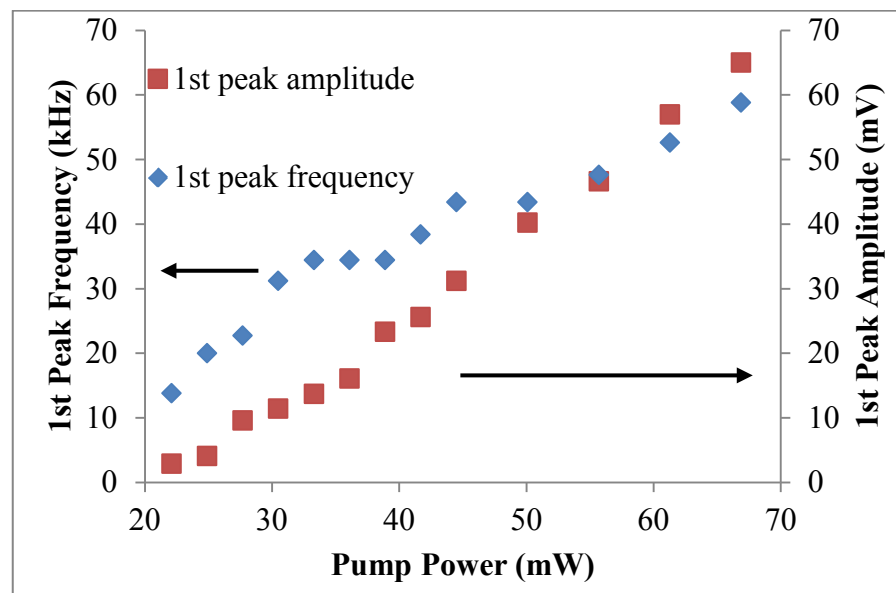


Figure 3.11: First spiking peak amplitude and frequency under different pump power levels.

The relationships between the pump power of the first spiking peak amplitude and the frequencies of the first and second spiking peaks are plotted in Figure 3.11. As can be observed, both the amplitude and the frequency of the first spiking peak are increased when the pump power increases. The RO of the transient effect directly follows these peaks. There is no clear boundary between the spiking regime and the RO regime - which implies possible inaccuracy in their separate characterisation. To avoid this problem, measurements were made in the centre of the RO regime. The measured RO frequencies at different pump power levels were then compared with the resonance peak frequency of the fibre laser noise spectrum in the same pump power range. Comparisons between both parameters are plotted in Figure 3.12, which contains graphs of both: (a) frequency, ω against pump power and (b) ω^2 against pump power.

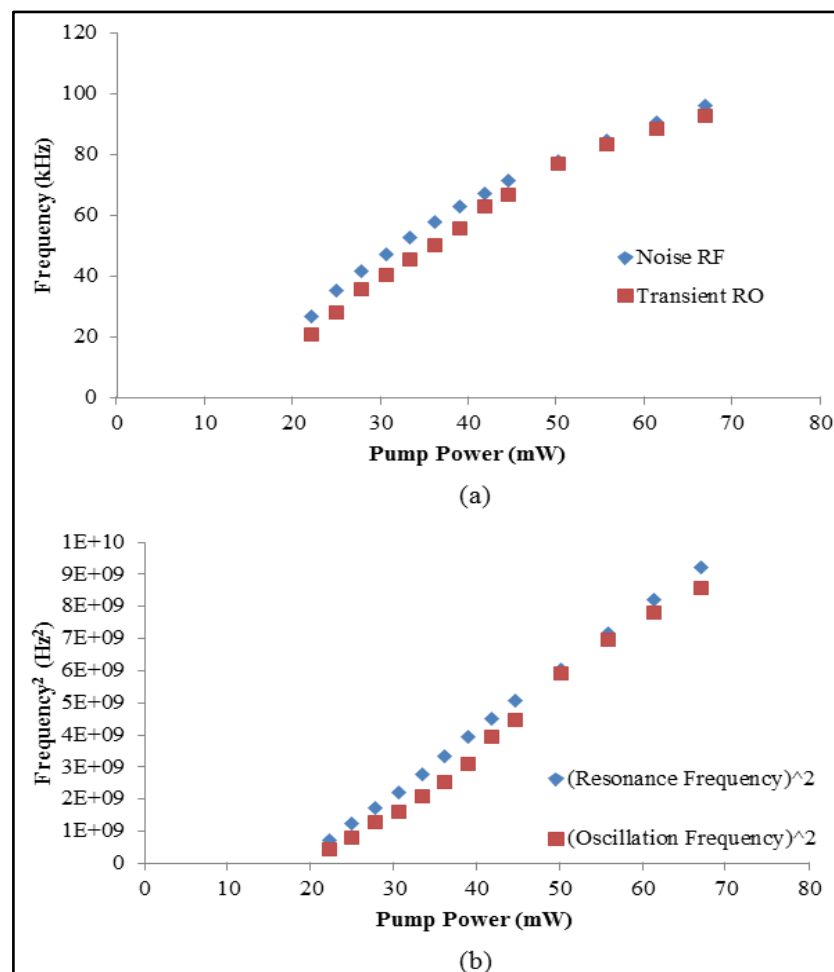


Figure 3.12: Comparisons of both resonance frequency and RO frequency parameters in graphs of (a) frequency against pump power and (b) frequency² against pump power.

From Figure 3.12(a) & (b), both the resonance peak frequency and the RO frequency show similar trends according to the changes of pump power level, with slight differences in frequencies, especially at low pump powers. However, it is possible to predict the value of one parameter if the other parameter is known. In other words, the RO occurs at a nearly or slightly lower frequency than the resonance frequency peak of the fibre laser noise. From Figure 3.8(b), it is clear that during the pulsing regime, the frequencies between pulses are lower at lower frequencies. The power fluctuation of the noise spectrum increases toward the RO regime and oscillates in an almost sinusoidal form. This power fluctuation frequency will continue increases in the RO regime, before it reaches a steady state where it will actually oscillate at the resonance frequency.

3.3.2 Modelling

Spiking and relaxation oscillation have been observed for the switch-on transient effect, in experimental results. A simulation was carried out to demonstrate that the switch-on transient follows the prediction of the laser dynamic model. The simulation was based on the simple rate equations from Eqs. (2.38) and (2.39). Eqs. (2.41) and (2.42), which are already normalized, are not used – because the embedded pump intensity parameter is separated into two parameters, namely γ and A . An independent pump intensity parameter is needed, as the pump power plays a major role in experimental results. Hence the new parameters:

$$k = \frac{\gamma_c}{\Gamma_{21}}, g = \frac{\sigma_s N_T}{\Gamma_{21}}, D = \frac{N}{N_T}, I_P = \frac{\sigma_P \varphi_P}{\Gamma_{21}}, I = \frac{\sigma_s \varphi_s}{\Gamma_{21}} \text{ and } t = T\Gamma_{21} \quad (3.7)$$

are introduced into Eq. (2.39)

$$\frac{d\varphi_s}{dT} = \varphi_s(-\gamma_c + \sigma_s N)$$

$$\frac{d\varphi_s}{d(T\Gamma_{21})} = \varphi_s \left[-\frac{\gamma_c}{\Gamma_{21}} + \frac{\sigma_s N_T}{\Gamma_{21}} \left(\frac{N}{N_T} \right) \right]$$

$$\frac{dI}{dt} = I(-k + gD) \quad (3.8)$$

and Eq. (2.38)

$$\frac{dN}{dT} = -\Gamma_{21}(N + N_T) - \varphi_P \sigma_P (N - N_T) - 2N\varphi_s \sigma_s$$

$$= -(\Gamma_{21} + \varphi_P \sigma_P + 2\varphi_s \sigma_s)N + \varphi_P \sigma_P N_T - \Gamma_{21} N_T$$

$$\frac{d\left(\frac{N}{N_T}\right)}{d(T\Gamma_{21})} = -\left(1 + \frac{\sigma_P \varphi_P}{\Gamma_{21}} + 2\frac{\sigma_s \varphi_s}{\Gamma_{21}}\right) \frac{N}{N_T} + \frac{\sigma_P \varphi_P}{\Gamma_{21}} - 1$$

$$\frac{dD}{dt} = -(1 + I_P + 2I)D + I_P - 1$$

$$\frac{dD}{dt} = -(1 + I_P + 2I)D + I_P - 1 \quad (3.9)$$

Both Eqs. (3.8) and (3.9) are similar to simulation equations in [6] and [8]. k and g are the decay rate and the unsaturated gain of the lasing light intensity, respectively. I and I_P are, respectively, the fibre laser intensity and the pump laser intensity - while D represents the population inversion.

To perform a numerical simulation using the Matlab software, Eqs. (3.8) and (3.9) were written in a linear form as:

$$I(n) = I(n-1) \cdot \{1 + [-k + gD(n)] \cdot \Delta t\} \quad (3.10)$$

$$D(n) = D(n-1) + \{-[1 + I_p + 2I(n-1)] \cdot D + I_p - 1\} \Delta t \quad (3.11)$$

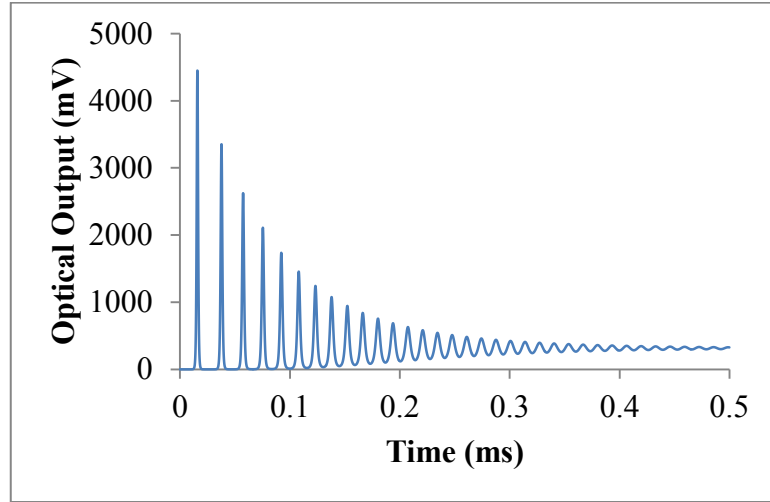


Figure 3.13: Numerical simulation result using Matlab Software with parameters value of $k = 10000$, $g = 90000$, and $I_p = 130$.

Figure 3.13 shows one of the numerical simulation results from using both Eqs. (3.10) and (3.11). The simulation result shows the spiking and the RO regime. Although the simulation does show the transient effect in the spiking and RO regimes, the simulation output still differs significantly from experimental results. The reason for this difference is that the equations used form a simplified and linearized model. There are some important parameters that are not considered in this model, in order to simplify the equations. As mentioned in the previous section, this model cannot be used to estimate the latency regime period due to the linearization of the equations. However, the spiking and RO parts of the transient behaviour are predictable using these equations. There has been some work on simulating transient effects in fibre lasers by [3, 9], using more detailed and complicated models. Figure 3.14 shows a series of turn-on transient simulation results at different pump power levels, from 60 mW to 140 mW.

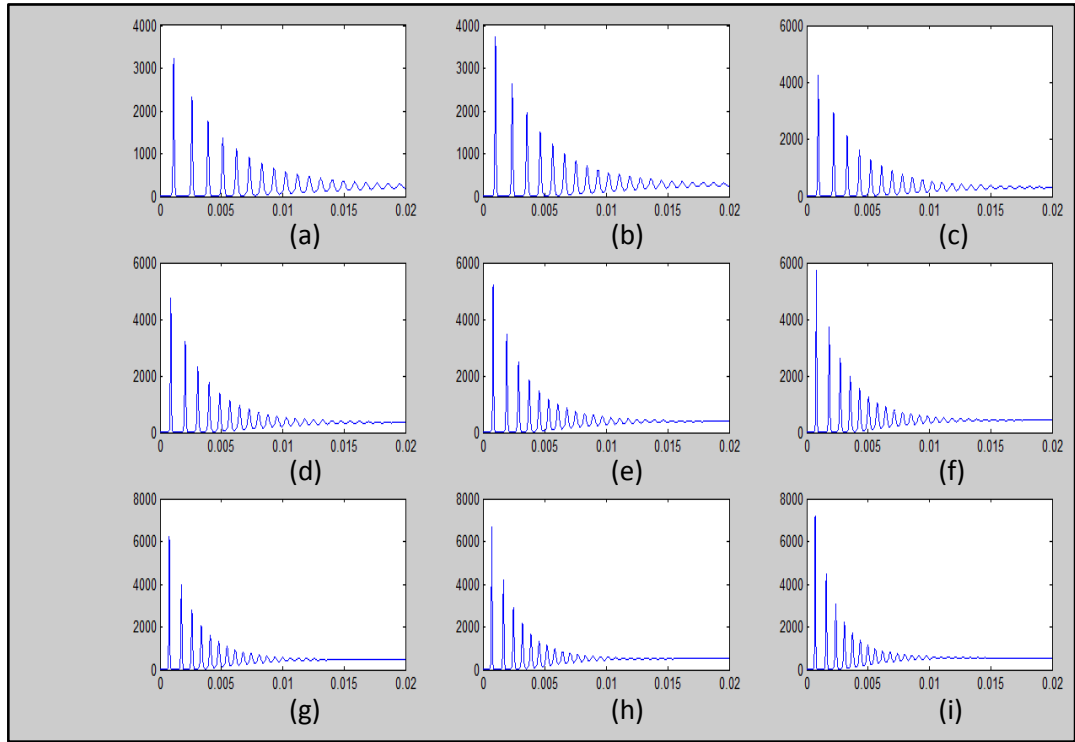


Figure 3.14: Numerical modelling of spiking and RO happen in turn on transient with pump power at (a) 60 mW, (b) 70 mW, (c) 80 mW, (d) 90 mW, (e) 100 mW, (f) 110 mW, (g) 120 mW, (h) 130 mW, and (i) 140 mW.

3.4 Pump Modulation

For an optical system to work as a sensor, its amplitude, phase, or polarization must be capable of being modulated. In this system, the modulation is expected to come from the environment and the system intensity is either directly or indirectly modulated. The changes of the intensity will carry information about the incident acoustic wave. However, before studying the incident acoustic wave modulation in which the output will carry noise from the environment and the optical system itself, the optical modulation of the system was studied via the pump modulation model[10].

Pump modulation is a direct way to modulate the intensity of the optical fibre laser, due to its direct relation to the gain of the fibre laser. In a controlled environment, noise can be reduced to a lower level, in comparison with acoustic wave modulation. The turn-on transient experimental results in Section 3.3.1 are one example of pump

modulation in the form of a step function. In this section, the pump laser diode is driven using a HP8116A function generator to modulate the pump power sinusoidally.

Figure 3.15 shows a series of fibre laser outputs under modulation, by a 500 Hz sinusoidal waveform, of the pump power - at different amplitudes captured by a digital oscilloscope. The pump power is offset to a level of 15.0 mW to sustain a certain percentage of inversion population in the gain medium. From Figure 3.15, it is obvious that only in Figure 3.15(a) is the output in a sinusoidal form - and all of the other outputs are generating spiking effects at the peak of the modulation pattern. The generation of spikes in the fibre laser output only happens when the pump power is above the lasing threshold. This spiking behaviour follows the same principles as for the turn-on transient generation.

From the series of screen captures shown in Figure 3.15, together with the insets that show magnification of the spiking regions, it is observed that when the modulation amplitude increases:

- (a) the peak power increases,
- (b) the number of spikes increases, and
- (c) the spiking frequency increases.

As the modulation amplitude increases, more pump power was pumped into the system (due to the low offset of pump power up to only 15 mW, modulation more than 15 mW that suppose fall in the negative region will remain as 0 mW), increasing the population inversion. The different spiking effects behaviour generated under pump modulation are similar to the transient effect mentioned in Section 3.3.

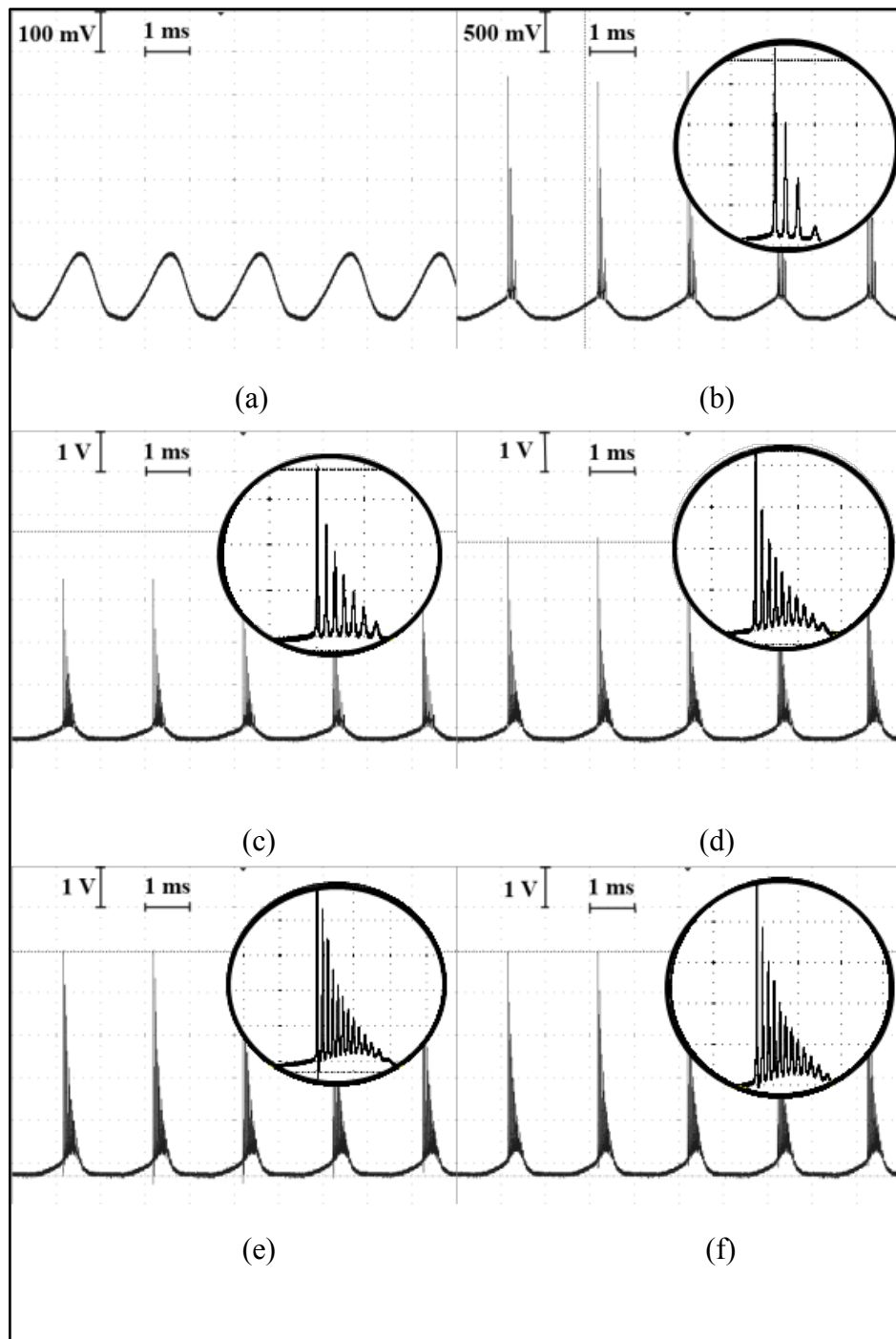


Figure 3.15: Fibre laser optical output waveforms under a continuous pump power level of 15.0 mW - with modulated oscillation by a 500 Hz sinusoidal function at different modulation amplitudes at (a) 35.2 mW, (b) 42.6 mW, (c) 49.6 mW, (d) 57.8 mW, (e) 64.0 mW, and (f) 71.5 mW.

3.5 Loss Modulation

Loss modulation is the other main modulation method in laser systems. Loss modulation can easily be achieved by implementing an acousto-optic or electro-optic modulator inside the laser cavity [4]. In this thesis, the loss modulation was performed directly using acoustic waves in the form of either mechanical vibration in a solid medium or as sound waves propagating in air. The interaction of acoustic waves with fibre optics causes time-dependent changes in geometry - such as changes in the fibre length or the refractive index, due to compression and expansion of the fibre material. These effects will cause phase-shifts and collapses in the existing modes that sustain in the laser cavity - these effects will contribute to modulation of the cavity loss. Figure 3.16 shows one example of loss modulation produced by ‘knocking’ of the fibre laser system.

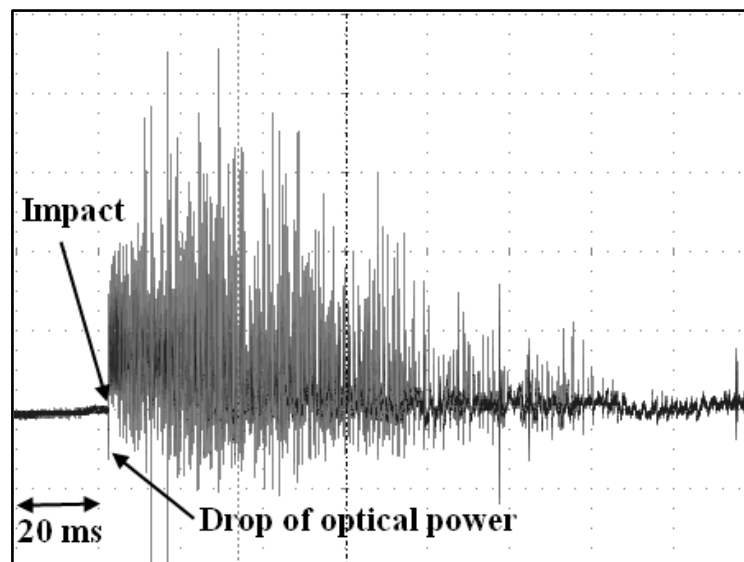


Figure 3.16: Fibre laser optical power fluctuation under the impact of strong acoustic wave.

Increase of the cavity loss has been observed when a strong airborne acoustic wave is incident on the fibre laser system, the cavity losses are increased, causing the output power to drop, as labelled in Figure 3.16. This drop is due to the fact that the incident acoustic wave transfers part of its energy into the fibre and causes the silica molecules to vibrate more strongly (effectively raising the local temperature), eventually contributing to cavity losses. The increase of cavity loss reduces the optical power feedback to the gain medium, which allows population inversion to build up in the gain medium. As the vibration of silica molecules becomes weaker and weaker with time, the cavity loss reduces as well. Laser feedback increases at the same time, until it is above the threshold for stimulated emission or lasing to take place. The sudden increase in the optical feedback power will generate random spiking for a short period. The turn-on transient spiking observed in Figure 3.16 is more chaotic and does not follow exactly the damping pattern, as in the case at the RO regime. This discrepancy arises is suspected to be cause the energy of the acoustic vibration does not disappear as rapidly as does the pump modulation. The slow decay of the acoustic energy in the fibre causes the instability of the spiking intensity and frequency.

For the same reason, the acoustic wave modulation can be expected to be far more complicated than is the case for pump modulation. Further investigation of the effects of acoustic wave modulation will be described in the next two chapters, which are concentrated on airborne acoustic wave or sound sensing. Hence, till current level, an unassisted acoustic sensor has been demonstrated to sense the vibration of surrounding environment. The similar setup has been improved and enhanced in the sensitivity by adding single mode fibre (SMF) as sensing medium so that the sensor can sense the weak acoustic waves that travel in the air.

3.6 Summary

In this chapter, a free running linear cavity fibre laser with an EDF as the gain medium has been presented. This fibre laser generates an emission spectrum that falls within the so called “C-band” (C for ‘Conventional’), which spans from 1520 nm to 1570 nm - with the highest emission level occurring in the region of 1530 nm region. Multiple lasing peaks are observed when the pump power is level is sufficiently far above the threshold. The number of lasing peaks will increase - and cover a broader spectrum - when the pump power is increased.

The noise in the fibre laser set-up has become a specific concern in the present study, as it was found to be related the RO frequency - an important parameter for the laser system. Noise in the output from the experimental laser set-up fluctuates at the RO frequency and its characterisation is obtained by performing an FFT operation on the period of the optical output. The resonance frequency is related to the pump power and can be represented by:

$$\omega^2 = 120 P - 1400 \quad (3.12)$$

where P is the pump power in mW.

The turn-on transient behaviour of the fibre laser was studied by providing a step input in the pump-power level. The latency measured experimentally agreed closely with the theoretical relationship developed from the rate equations. Furthermore, it also agreed with the results of numerical simulation that was carried out to simulate the turn on transient behaviour of the fibre laser. However, due to the over-simplification of the rate equations that was used, only spiking and RO could be simulated without the latency in the transient behaviour becoming apparent.

At the end of the chapter, pump modulation and loss modulation have been performed, in order to observe the modulation behaviour. The pump modulation can be considered as the modulation applied in a controlled environment where a damped spiking effect is exhibited that is similar to the turn-on transient. It also been observed that the peak power level of the spikes, the number of spikes - and the spiking frequency - all depend on the modulation frequency. It is further understood that the nature of the interaction of the externally incident acoustic waves with the fibre core is much more complicated than the above formulation and could include energy dissipation in the fibre. Hence, chaotic conditions with random spiking are observed in loss modulation. This carries the meaning that the unassisted acoustic sensor has been demonstrated on vibration sensing.

References

- [1] C. H. Pua, S. F. Norizan, S. W. Harun, and H. Ahmad, "Non-membrane optical microphone based on longitudinal modes competition," *Sensors and Actuators A: Physical*, vol. 168, pp. 281-285, 2011.
- [2] X. Jin and S. L. Chuang, "Relative intensity noise characteristics of injection-locked semiconductor lasers," *Applied Physics Letters*, vol. 77, pp. 1250-1252, 2000.
- [3] G. Stewart, V. Karthik, and G. Whitenett, "Optical fibre sensors based on the dynamic response of fibre lasers," in *17th International Conference on Optical Fibre Sensors (OFS 2005)*, Belgium, 2005, pp. 916-919.
- [4] T. Erneux and P. Glorieux, *Laser Dynamics*. New York: Cambridge University Press, 2010.
- [5] I. J. Sola, J. C. Martín, J. M. Álvarez, and S. Jarabo, "Erbium doped fibre characterisation by laser transient behaviour analysis," *Optics Communications*, vol. 193, pp. 133-140, 2001.
- [6] L. Luo and P. L. Chu, "Onset dynamics in erbium doped fiber lasers with applications to parameters measurement," *Optics Communications*, vol. 149, pp. 307-311, 1998.
- [7] G. Stewart, G. Whitenett, K. Vijayraghavan, and S. Sridaran, "Investigation of the Dynamic Response of Erbium Fiber Lasers With Potential Application for Sensors," *Lightwave Technology, Journal of*, vol. 25, pp. 1786-1796, 2007.
- [8] L. Luo, T. J. Tee, and P. L. Chu, "Chaotic behavior in erbium-doped fiber-ring lasers," *J. Opt. Soc. Am. B*, vol. 15, pp. 972-978, 1998.

- [9] V. K. a. G. Stewart, "Theoretical and experimental investigation of fiber ring laser dynamics and transient analysis," presented at the 7th International conference on Optoelectronics, Fiber Optics and Photonics, Cochin, India, 2004.
- [10] A. N. Pisarchik, A. V. Kir'yanov, Y. O. Barmenkov, and R. Jaimes-Reátegui, "Dynamics of an erbium-doped fiber laser with pump modulation: theory and experiment," *J. Opt. Soc. Am. B*, vol. 22, pp. 2107-2114, 2005.

Chapter 4

Optical Microphones

4.1 Optical Microphone

4.2 Conventional SMF as Sensing Medium

4.3 Special SMF (SSMF) as Sensing Medium

4.4 EDF Length

4.5 Design and Prototype

4.6 Summary

References

4.1 Optical Microphone (OM)

Similar to conventional microphones, optical microphones (OMs) are generally used to detect airborne acoustic waves or sound. OMs are devices which are able to convert airborne sound signals to lightwave signals without intermediary electronics[1]. As mentioned in Chapter 1, even though most of the optical microphones described in the literature have use diaphragms like those in electrical microphones, the operating principle can be totally different. Electrical microphones are generally signal sources, while OMs typically modulating existing signal sources[1]. In fibre based OMs, sound modulation can be done only with the assistance of a diaphragm or some other low mass structure. Unassisted fibre based OMs or optical fibre microphones without diaphragms have been considered to be impossible, due to the poor acoustic impedance matching between air and fibre[1]. The acoustic impedance can be calculated from

$$Z = \frac{P}{vS} \quad (4.1)$$

where P is sound pressure, v is particle velocity, and S is surface area. The acoustic impedance of air (Z_{air}) is 40 g/(cm²s) and silica glass (Z_{silica}) is 1.3 x 10⁶ g/(cm²s). Due to the large difference of acoustic impedance, most of the incident acoustic waves will be reflected instead of transmitted into the fibre. The reflection of the acoustic wave can be calculated by

$$R = \left(\frac{Z_{\text{air}} - Z_{\text{silica}}}{Z_{\text{air}} + Z_{\text{silica}}} \right)^2 \times 100\% \quad (4.2)$$

which leads to a value of 99.98%.

Due to the low transmission percentage, most proposed OMs were not unassisted optical microphones, even though many optical hydrophones are unassisted [2]. However there have still been some rare cases of attempts to build unassisted OMs.

One of the earliest examples to be found is the work proposed by B. Culshaw, et al[3], which made use of the changes of refractive index, n , under the pressure of sound waves, eventually leading to a phase shift of the optical signal. Nevertheless, this work is largely theoretical and did not provide any demodulation scheme.

The set-up proposed is sensitive to vibration, as presented in Chapter 3. However the sensitivity of the set-up was too low for sensing of low intensity sound waves, and it only responded to strong acoustic vibrations. This is due to the small surface area that is able to interact with the sound with only 10 m of cavity length. To increase the sensitivity of the setup, a long single mode fibre (SMF) is attached to point B of the set-up and is labelled as the sensing medium, shown in Figure 4.1. The implementation of this extra fibre length increases the interaction surface of the fibre with the sound waves. A larger interaction surface means that more energy from the acoustic waves is transmitted into the fibre and hence there is a stronger modulation of the fibre laser. With this simple setup, an unassisted fibre based acoustic sensor was successfully built.

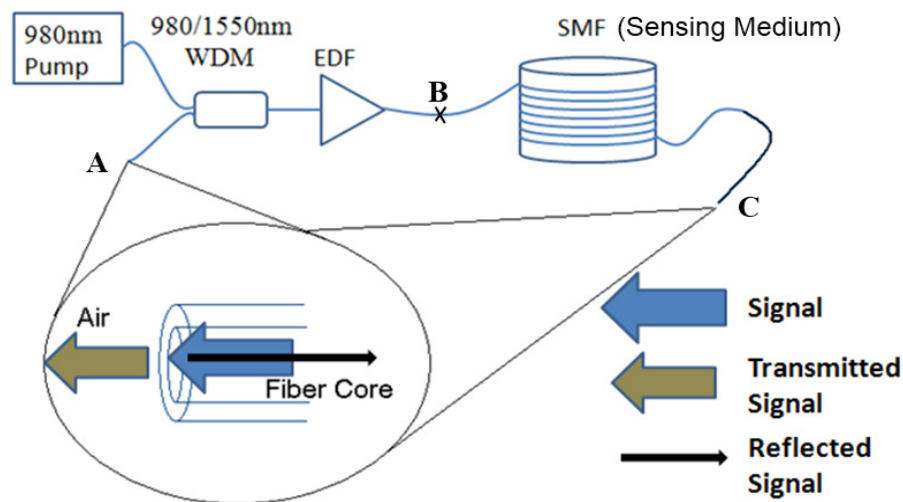


Figure 4.1: Optical microphone set-up with SMF as sensing medium.

4.2 Conventional SMF as Sensing Medium

The earliest report of this work used 25 km of conventional SMF fibre (SMF-28) on a drum with an inner diameter of 15.0 cm, an outer diameter of 20.0 cm, and height of 9.5 cm as the sensing medium as described in ref. [4]. A 25 km fibre drum was chosen due to its sensitivity to normal vocal sound pressure level (SPL). To study the response of this OM to sound waves, a 500 Hz sound wave at 100 dBA SPL was generated using a multimedia speaker that faced the fibre drum. Figure 4.2(a) and (b) show the optical spectra of the OM outputs measured using an Optical Spectrum Analyser (OSA) from Yokogawa (AQ6370) under normal conditions and when it was under modulation by sound waves at different pump powers. Under normal conditions without sound waves, a broad Amplified Spontaneous Emission (ASE) with multiple lasing peaks was observed at around 1530 nm. These lasing peaks are the longitudinal modes which fulfil the conditions to form standing wave patterns in laser cavity, as mentioned in Chapter 3. These peaks are unstable, due to the mode competition that is caused by the homogenous broadening effect in EDF [5, 6].

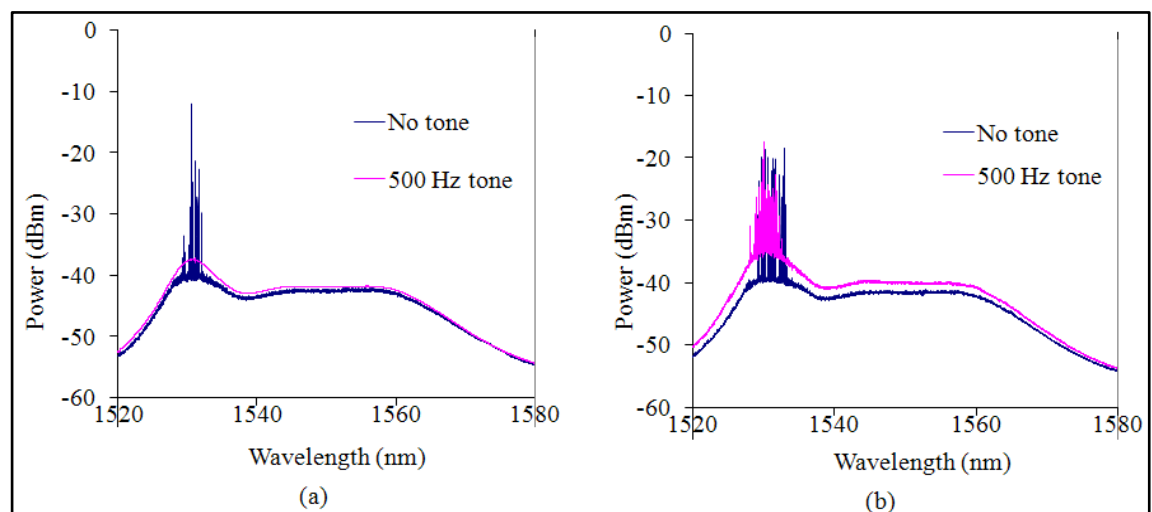


Figure 4.2: Optical spectrum of the ASE generated with and without the present of sound waves at (a) 16 mW and (b) 27mW 980 nm pump power.

When the OM pumped at 16 mW was exposed to the 500 Hz sound wave, it was observed that the ASE spectrum level increased while all the lasing peaks disappear as shown in Figure 4.2(a). In most cases, many longitudinal modes can oscillate simultaneously. However, different modes have different gain, loss and saturation parameters due to the spectral emission probability of the EDF. These different modes will then compete each other to stimulate the population inversion in the laser gain medium [7] and the oscillation of one mode will reduce the gain available for the other modes, thus making the lasing wavelengths unstable. Under such unstable lasing conditions, the lasing effect will be suppressed when there are any external disturbances such as an acoustic wave. In this case, part of the energy of the incident sound wave will be transferred into the fibre causing the fibre particles to vibrate in the fibre. Compression and rarefaction of the fibre will lead to the changes of refractive index, n , of the fibre and causes a phase shift to the current survival modes in the laser system[3]. Under this condition, the required phase shift of 2π to sustain the oscillation may not be met and hence suppress the lasing in the laser system. At the same time, it also increases the generation of ASE as there is not enough lasing stimulated emission in the laser system to suppress the ASE.

Figure 4.2(b) shows the output spectrum with and without an acoustic wave at a pumping power of 27 mW. Due to the high pumping power, higher inversion populations can be generated and thus the lasing region was broader with more lasing peaks. This meant that more modes can be presented under such pump power. When the same modulation was done under the same sound level of 500 Hz sound wave, however it is observed that the modulation did not suppress all the lasing at this pumping level. The lasing region was observed to be narrower riding on top of a higher ASE level. The suppression of the lasing signal by sound wave modulation became insufficient due

to the higher pump power applied which results in a net gain of the laser system for modes with wavelength situated in the higher ASE region.

Other than the changes in the optical spectrum, the optical output intensity is expected to change based on the increase of the ASE level as shown in Figure 4.3, which shows the optical output power fluctuation in the time domain, measured using Lecroy digital oscilloscope (WaveJet 352A) under the modulation of a 500 Hz sound wave at different sound amplitude. The measurement started when there is no sound, followed by the increases of the sound level to 70 dBA, 80 dBA, 90 dBA, 100 dBA, and 110 dBA SPL (SPL or sound pressure level given were measured using Castle sound level meter (GA213)). Each slot was measured for a period of 1 second.

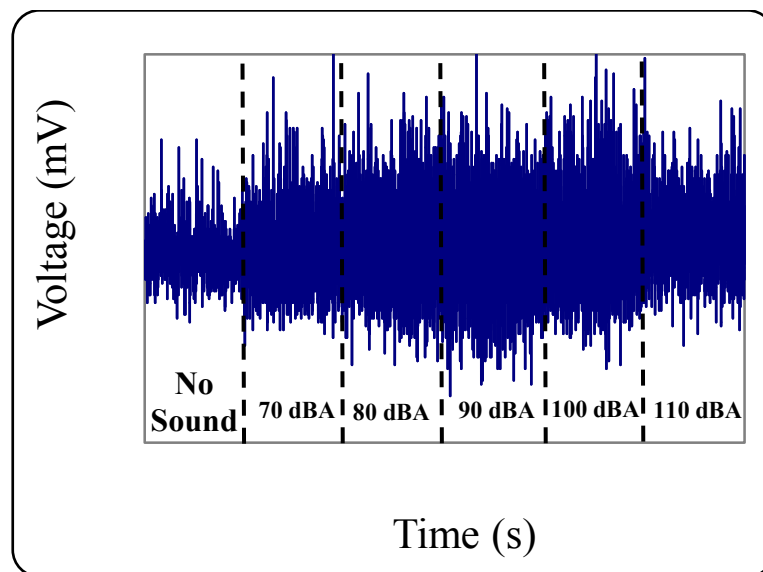


Figure 4.3: Optical output fluctuation under modulation of 500 Hz sound wave at different sound pressure level.

When the sound wave is present, the optical phase will experience periodic changes following the modulation of the sound wave. The compression and rarefaction of the imparted sound waves will cause the optical phase to be shifted and thus causes modulation of the optical signal intensity. As a result, the optical signal now carries the same information as carried in the sound waves. Furthermore, the fluctuation amplitude of the optical output was increases as the amplitude of the sound wave increases,

following the pattern of the sound wave as shown in Figure 4.3. The optical fluctuation amplitude reached a saturation value when the modulation of the sound waves is at 90.0 dBA SPL. The sensing threshold using the OM at frequency of 500 Hz is 69.8 dBA SPL with a surrounding noise at 48.0 dBA SPL.

Other than the changes on the fluctuation amplitude, or more likely the oscillation amplitude, there were also fluctuations to the average output power from the OM. Figure 4.4 shows the responses of the optical output powers in terms of photodiode voltage at different sound level (the response of the optical output is linear to the photodiode voltage output). As observed, the photodiode output voltage did not show any responses to any sound below 70.0 dBA SPL. From 70.0 dBA up to 110.0 dBA SPL, the average voltage output increased linearly with the sound level.

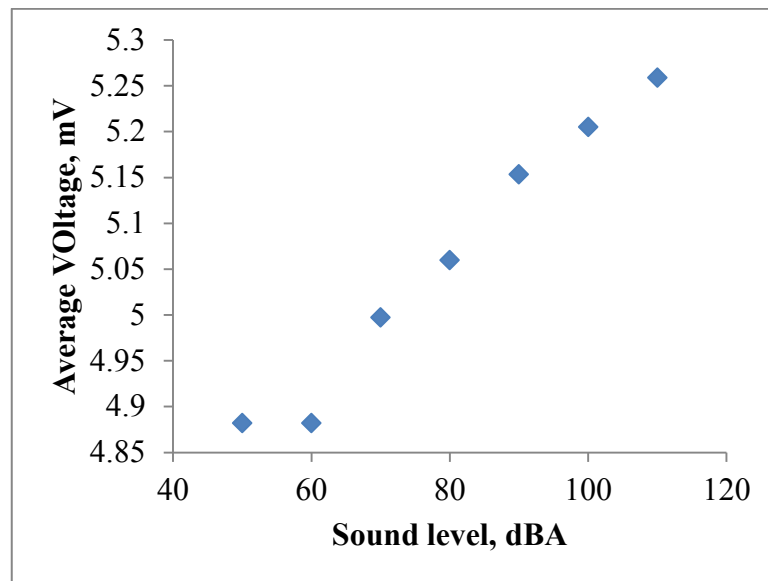


Figure 4.4: Average voltage output from photodetector as refer to the incident sound level.

After observation of the responses of the optical output power and fluctuation to modulation of sound wave at different frequencies, the response of the output pattern to the modulation pattern was studied. This is important as it represent the information

carried by the original sound wave. The modulation sound wave was generated by using multimedia speaker that connected to a personal computer. To make the analysis simpler, a 2 kHz sinusoidal wave was generated as the modulation source. Comparison of the output pattern of the OM with the electrical microphone were capture simultaneously using a digital oscilloscope, and is presented in Figure 4.5.

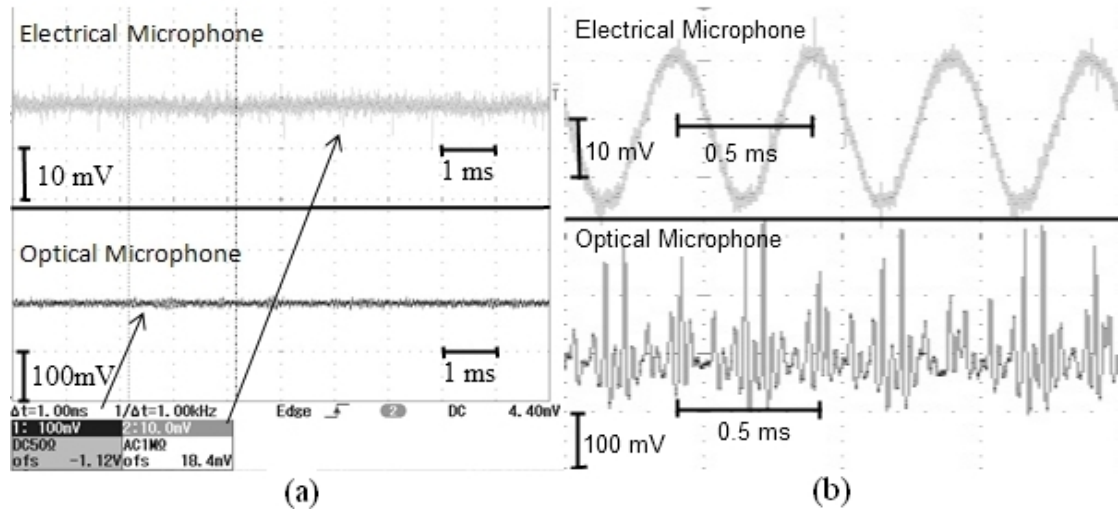


Figure 4.5: Comparison of (a) background noise without acoustic signal and (b) with a 2 kHz of acoustic signal between the electrical and the optical microphones captured using a digital oscilloscope.

In Figure 4.5, the output of the electrical microphone and the OM are in different scale ratios due to the difference in oscillation amplitude output from both microphones. Figure 4.5(a) shows the system noise from both microphones, while Figure 4.5(b) shows the output patterns from both microphones under modulation of 2 kHz of sinusoidal sound wave at 80.0 dBA. When compared the signal peak to noise ratio, OM has signal peak to noise ratio at 43.5 dB as compare to the electrical microphone at 39.1 dB. However, both microphones show an obvious difference from their modulation pattern. Electrical microphone carries electrical output in a form of 2 kHz sinusoidal wave which is similar to the sound wave, but the OM carries an optical output at 2 kHz in an almost periodical spiking pattern.

From the discussion in the previous section, it is understood that the sound wave induces a kind of loss modulation onto the OM. Continuous compressions and rarefactions will suppress the lasing in the fibre cavity as the refractive index and optical phase keeps changing, leading to cavity loss. However, when the oscillation is near to the peaks or troughs, there are turning points where the compression of the particles changing into rarefaction. At these short periods of time, the fibre laser cavity become temporally stable as the loss is at its minimum level. This condition is similar to the case where the system gain goes above the lasing threshold and it is where random spiking will be generated due to the dynamics of fibre laser. This is the reason why the highest peaks from the OM are observed near the peaks and troughs of the sinusoidal wave in electrical microphone.

Although the output pattern is different from the sound wave pattern, it does not lose the frequency component of the sound wave. When the OM was used to record human voice into a personal computer, the recorded voice was able to reproduce when played it back using multimedia speaker, but with a lot of noise and hissing in the background. The hissing sound is attributed to the multiple sharp spikes from the OM. To understand the significance of the disturbance of the spikes to the original signal, a Fast Fourier Transform (FFT) was performed on the optical output which was recorded for 5 s under the modulation of different frequency sound wave. The frequencies were chosen between 100 Hz to 20 kHz, which covers the human vocal or listening band as shown in Figure 4.6.

Figure 4.6 shows the FFT spectrum of the recorded output powers modulated at frequency 200 Hz, 1 kHz, 10 kHz and 20 kHz in (a), (b), (c), and (d) respectively. Multiple sharp peaks were observed instead of only one peak at the modulation frequency. Those peaks showing in the FFT spectrum share a similarity in that all the peaks frequency is a multiple of the modulation frequency. In other words, those are

harmonics of the modulation frequency. These harmonics frequencies are contributed by the main pulses train and satellite pulses between the main pulses which will be discussed more details in next section. For modulations of frequencies lower than 4 kHz, a large number of harmonics frequencies in FFT spectrum were observed, as shown in Figure 4.6(b). Some harmonics even have a magnitude higher than the modulation frequency due to the high intensity pulses that exist in between the main pulses.

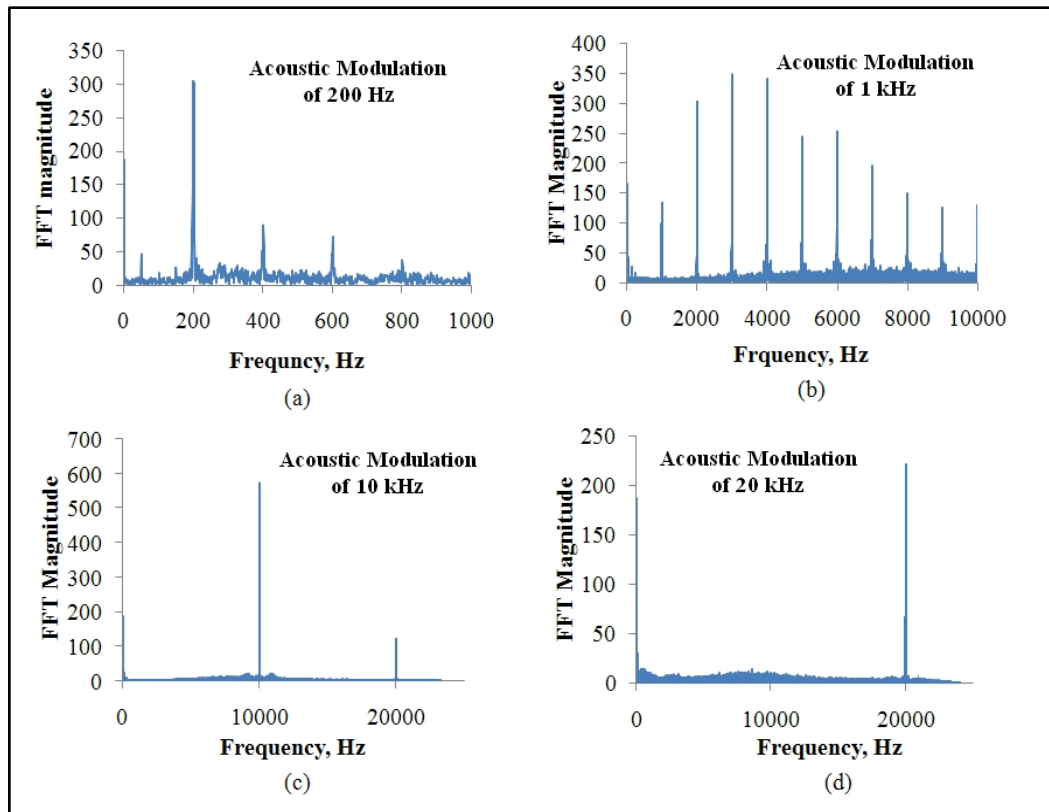


Figure 4.6: The FFT positive output for sound generated at (a) 200 Hz, (b) 1 kHz, (c) 10 kHz and (d) 20 kHz.

Other than the 25 km SMF used as the sensing medium, other fibre lengths are also tested. Figure 4.7 shows the optical spectrums of different lengths of SMF used as sensing medium. For sensing mediums with length of 1 km and below, the optical spectrums were similar while for length of 25 km and 50 km, significant drop in the ASE level can be observed. Simultaneously, the lasing region becomes smaller and the lasing power become higher and the fluctuation at the ASE level also higher when the

length increases. When a longer fibre is attached to the OM, higher loss is induced in the laser cavity and this in turn will reduced the ASE level and lasing region. However, it provides higher sensitivity due to the larger interaction area. If the sensitivity of the sensing medium were compare at 500 m, 25 km, and 50 km, the 500 m medium is the most insensitive length as it can only sense a 500 Hz sound wave of above 79.6 dBA SPL. This is followed by the 25 km medium at 69.8 dBA SPL and then the 50 km medium at 66.2 dBA SPL.

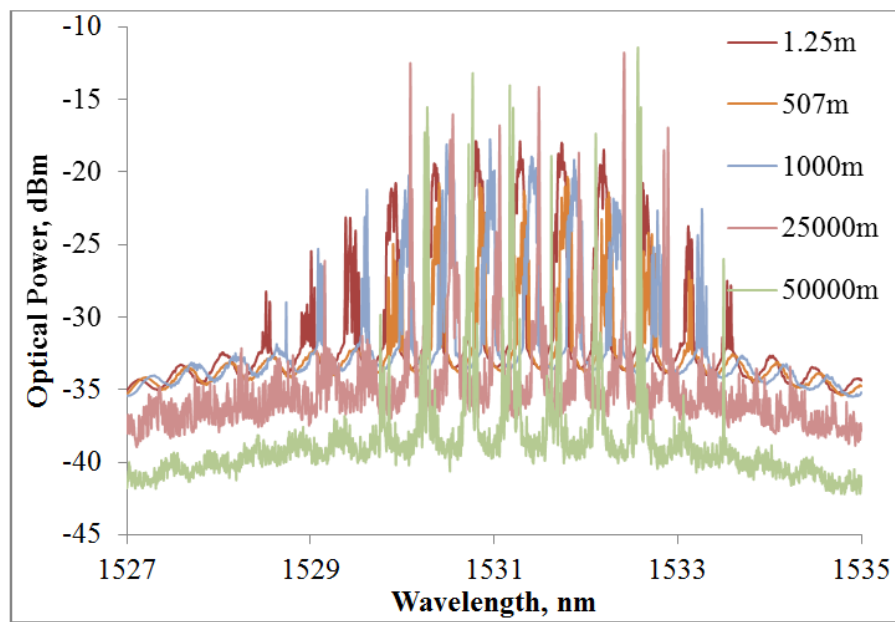


Figure 4.7: Optical spectrum output with different SMF length as sensing medium pumping at 30.8 mW.

Pump power plays an important role in laser dynamics as it defines the laser parameters such as latency, RO frequency, and spiking intensity. Therefore, an understanding of this effect of pump power on the average output power and modulation amplitude are important. Figure 4.8(a) shows the average voltage output read from the photo-detector when different length of sensing SMF was pumped with different powers. The average output voltage increase linearly with pump power. When a 10 kHz of sound wave at 90 dBA SPL was generated near the fibre, the average

output voltage for SMF with lengths of 5 km and 10 km increased. The 20 m medium setup did not show significant changes as the sensitivity to sound wave is too low while the 10 km of SMF setup experience a larger increment especially at higher pump powers.

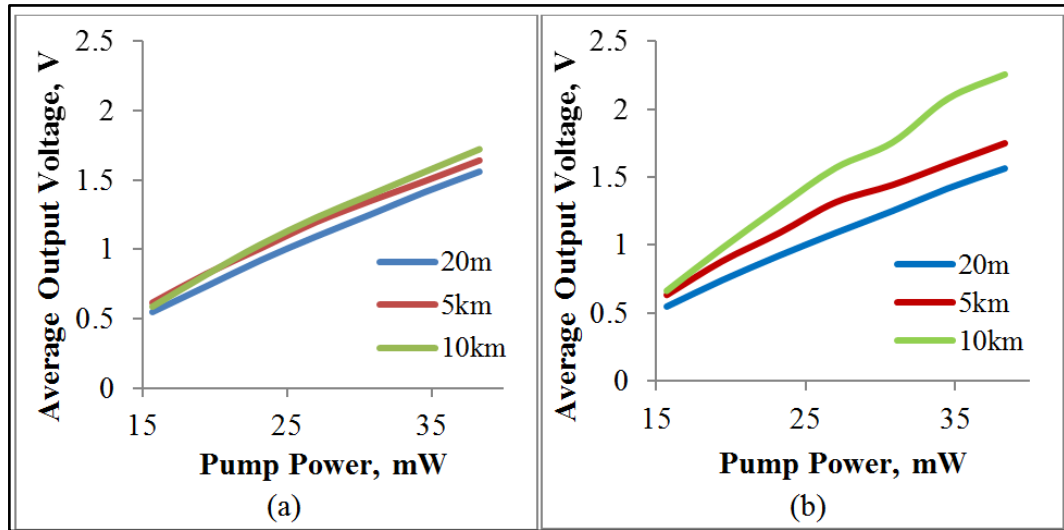


Figure 4.8: Average output voltage from photo-detector at different pump power when connected to different length of SMF as sensing medium (a) without present of sound wave and (b) with the present of 10 kHz sound wave.

To measure the sensitivity of our OM, the standard deviation of the system noise was compared with the standard deviation from the output under modulation as explained above. Standard deviation is then used to calculate the power fluctuation amplitude from the average, and larger fluctuations mean that a particular configuration is more sensitive of the sensing medium to acoustic waves. Figure 4.8 shows the standard deviation of the photo-detector output with and without sound modulation. By comparing Figure 4.9(a) and (b), it is obvious that the optical output power was oscillating at an amplitude which is about 6 times larger than the power fluctuation of the system for SMFs of 5 km and 10 km. Due to long SMF used in the setup, the sensor is able to distribute along a large area in a few tens of meters length. Depends on the requirement sensitivity, longer fibre can be customized into the sensor setup.

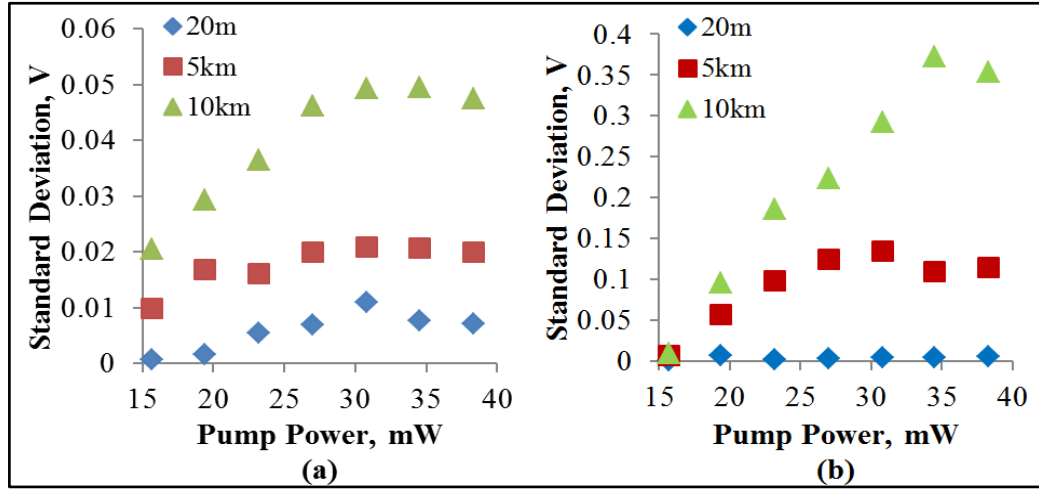


Figure 4.9: Standard deviation of the photo-detector output voltage for (a) background noise and (b) modulated signal at different pump power.

Long SMFs (a few km lengths) are not practical to be used as single point sound sensors. Such a long setup is more suitable for distributed sensing or large area sensing. All these while, most sound sensors are limited to number of sensing points. For distributed sound sensor, it requires a setup which is expensive as well as a complex network algorithm. With this setup, however there is an unlimited sensing point that can cover a large area by distributing the sensing fibre to the sensing region evenly, as the interaction of the sound wave with the OM can be done in any part of the sensing. In distributed sensing, the sensitivity of a site is dependent on the fibre length exposed to the site. As the sensing fibre is pulled over a long distance, a short spool of fibre can be placed at the site which requires a higher sensing sensitivity. Hence, an “unlimited” sensing points acoustic sensor with large area sensitivity has been presented which delivered part of the second objective in this research.

4.3 Special SMF (SSMF) as Sensing Medium

One might think that carrying a 25 km fibre spool around to use as an optical microphone is very bulky, heavy and not practical. Hence, a different type of fibre with high sensitivity was considered to replace conventional SMF in order to reduce the

system length. It was mentioned in previous section that the transmitted energy into the fibre is low due to the poor acoustic impedance matching. After the energy transmitted into the fibre, the energy needs to travel for another 60 μm (with 125 μm fibre diameter and 4.8~6.2 μm of core diameter) before it reaches the fibre core and interacts with the light in the core. To reduce the transmission path of acoustic energy in fibre optic, a reduced diameter single mode special fibre (SM1500 (4.2/80)) which only has 80 μm of cladding diameter was chosen to be used as the sensing medium.

There are two advantages of choosing this kind of Special SMF (SSMF). First, it can reduce the energy transmission path down to 37.9 μm , which will eventually leads to increase of sensitivity, and second, there is a smaller bending radius due to the small fibre diameter. To demonstrate the increase in sensitivity of this setup, a fibre length as short as 10 m was used in this experiment. The SSMF was spooled on a flat surface in a single layer circular form with an inner diameter of 3.5 cm and an outer diameter of 5.5 cm, as shown in Figure 4.10. It was placed to face the sound wave source during experiment to optimize the interaction surface area. Initially, the setup with a 10 m of SSMF was modulated with a 500 Hz sound wave as in previous case to do a comparison of their sensitivity. If a 10 m of conventional SMF is used, the sensitivity is expected to be very poor. However with this SSMF, the lowest sound level can be detected is 70.6 dBA SPL at 500 Hz and 69.8 dBA at 1 kHz [8] which is about the same level as 25 km SMF medium [4]. Due to the short length SSMF used that can spool into a flat circle within a diameter length of 5.5 cm, hence it is suitable to used as a point sensing medium which can deliver the second part of the second objective.

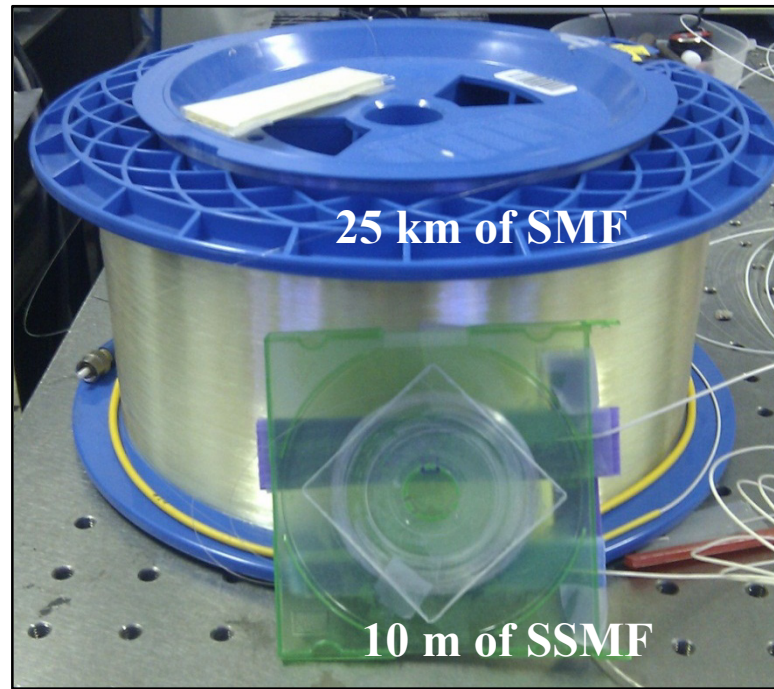


Figure 4.10: Comparison between 25 km of SMF sensing medium and 10 m of SSMF sensing medium in the foreground. The SSMF fibre spool is placed in a mini-CD cassette.

In the previous section, discussion on conventional SMF as sensing medium was mainly done on the responses of the optical output intensity to the acoustic modulation intensity. There is similar characteristic behaviour when the SSMF is used as sensing medium, but with different values. In this section, the discussion will revolve around frequency domain analysis such as the operating frequency and the resonance frequency. For testing in a broader operating frequency band, a 2 cm diameter piezoelectric transducer was chosen to be used as the acoustic source instead of a multimedia speaker as the latter is limited to a highest frequency of 20 kHz. The piezoelectric transducer was connected to the HP8116A function generator to generate different frequency acoustic wave. The OM under 17.5 mW of pump power was modulated by sound wave generated using piezoelectric drive with 16.0 V output with the frequency ranging from 1 kHz up to 50 kHz.

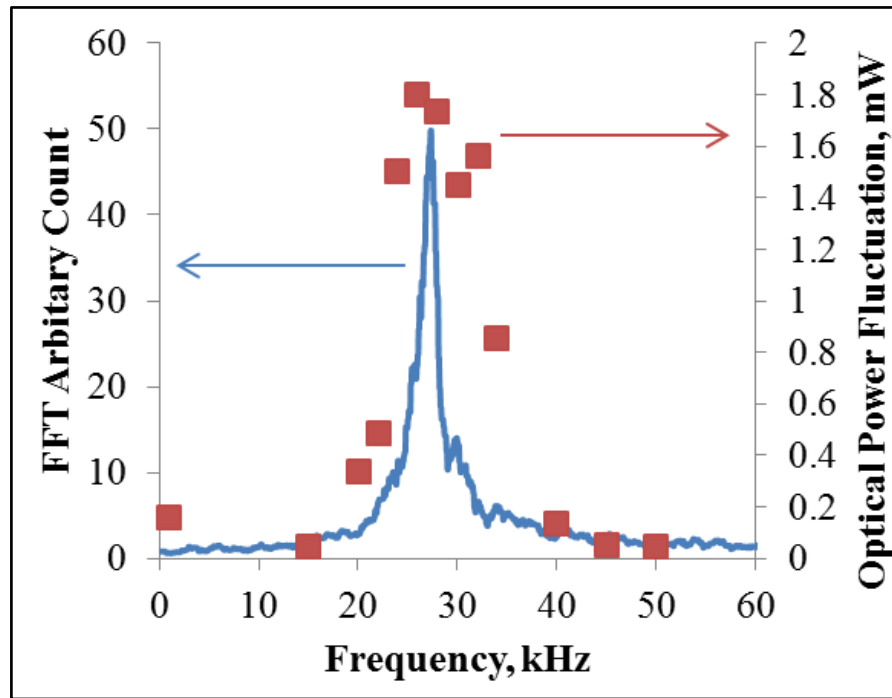


Figure 4.11: Comparison of the resonance frequency distribution with the optical power fluctuation under acoustic modulation at different frequency.

Figure 4.11 shows the plot (square dots) of the optical output power fluctuation (or oscillation amplitude) under the modulation of acoustic waves at different frequency. From the plot, it is obvious that the OM output power has very high fluctuation, which then implies high sensitivity, when it was modulated at frequencies ranging from 25 kHz to 35 kHz. The high sensitivity at the particular region is closely related to the resonance frequency distribution of the OM. The resonance frequency distribution of the OM pumped at 17.5 mW is also plotted in Figure 4.11 for comparison. When sensitivity of the OM at frequency near to the peak of the resonance frequency (27 kHz in this case) is compared to other frequency such as 15 kHz or 45 kHz, the difference can be as high as 14 dB. This high sensitivity region covers the frequency range between 8 kHz to 10 kHz.

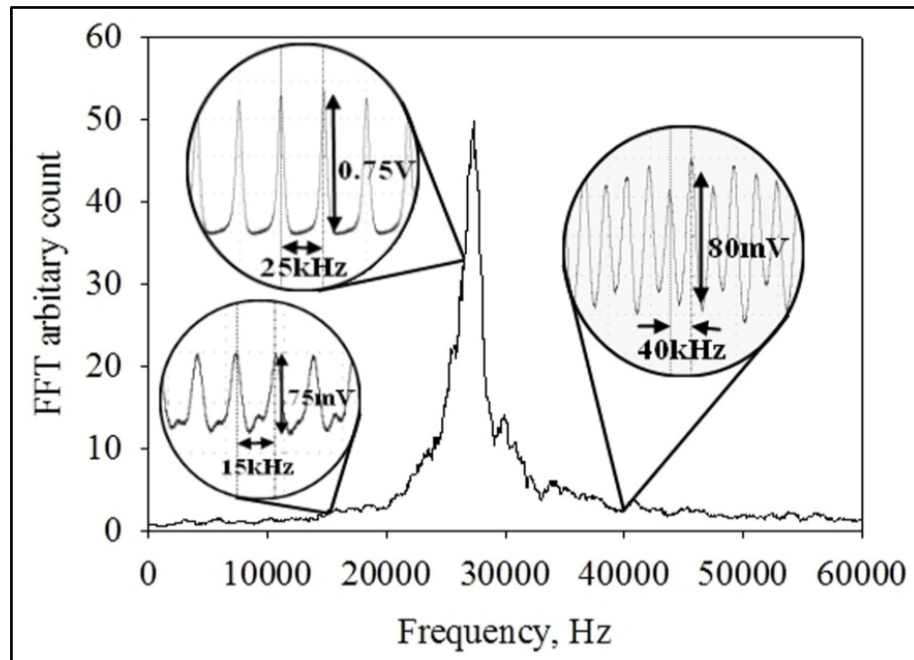


Figure 4.12: Optical output pattern under modulation of different frequency of acoustic wave.

Besides the difference of the optical power fluctuation amplitude when modulated by different acoustic frequencies, the output patterns were different at different frequencies. Figure 4.12 shows the optical output pattern under the modulation of acoustic wave at frequencies 15 kHz, 25 kHz, and 40 kHz. The 40 kHz output pattern is the closest to the original acoustic wave pattern, while both 15 kHz and 25 kHz are in pulses form. For the 15 kHz modulation output, it shows an additional small pulse in between the main pulses instead of a clean pulse train for 25 kHz as shown in Figure 4.12. For a better understanding of this phenomenon, a series of output pattern modulated at different frequency were captured using digital oscilloscope and presented in Figure 4.13. The OM was pumped at 49.6 mW which had the resonance frequency at 71.5 kHz. It was modulated by sinusoidal waves frequencies ranging from 13 kHz up to 75 kHz.

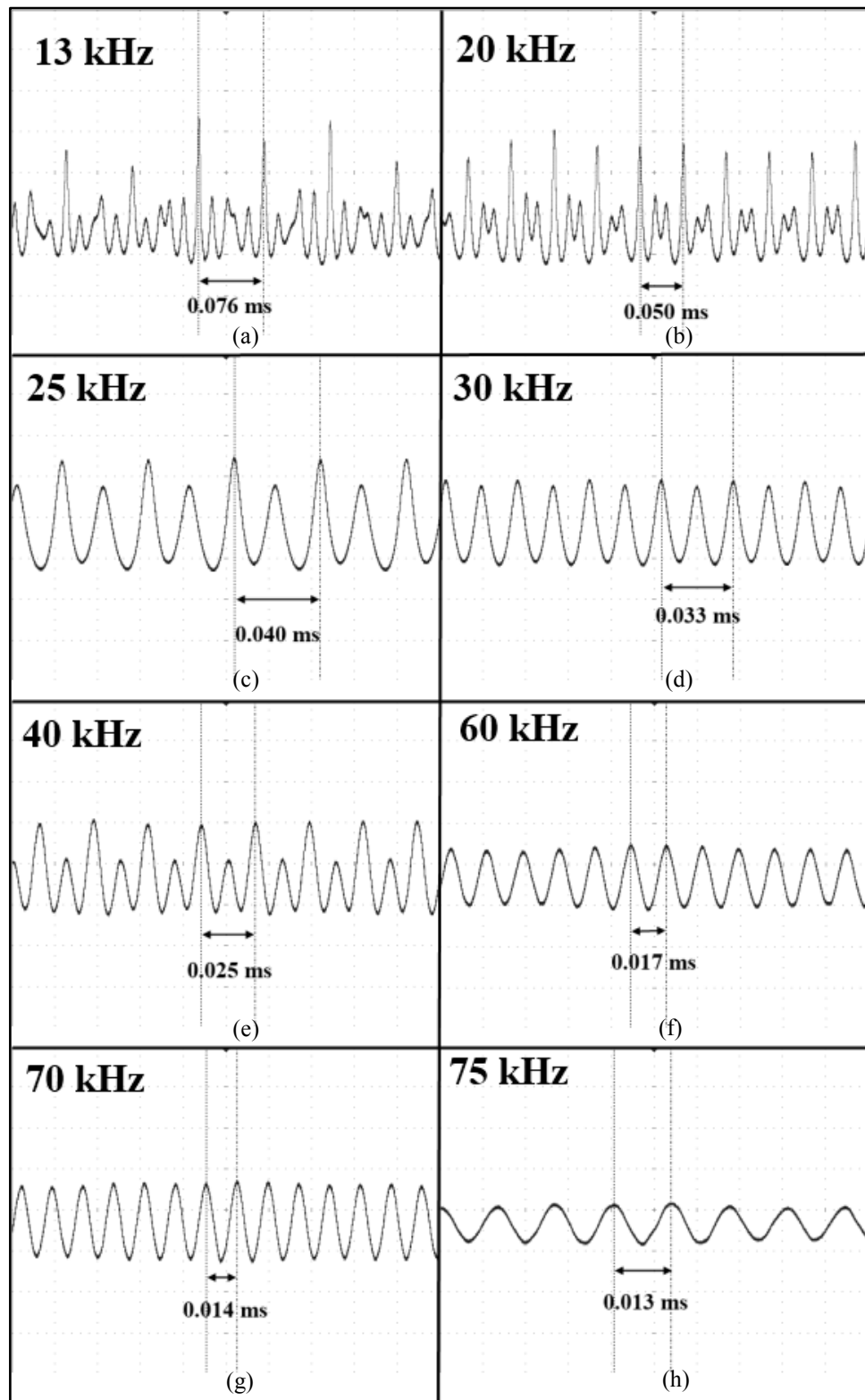


Figure 4.13: Optical output pattern under the sinusoidal acoustic wave modulation at different frequency.

At low modulation frequencies, in addition to the main pulses from the modulation frequency, there were other spikes in between the main pulses. These satellite pulses were reduced from four at 13 kHz to 2 at 20 kHz, and finally just one at 25 kHz and 30 kHz, and 0 for 60 kHz and beyond. At all modulation frequencies, these sub-pulses share two common behaviours: (a) the time spacing in between these main pulses and satellite pulses are always the same, and this will contribute to the harmonics frequencies when viewed in frequency domain, and (b) the repetition rate that contributed by these main and satellite pulses train will always fall around the resonance frequency peak.

Hence the optical output pattern can basically be separate into 3 different regions if the modulation pattern is in sinusoidal form: (a) region with multiple satellite pulses where the modulation frequencies are always lower than the resonance frequency distribution, (b) region with pulses in the modulation frequency, and (c) region with a sinusoidal form of oscillation which is the closest to the original modulation wave form as shown in Figure 4.14.

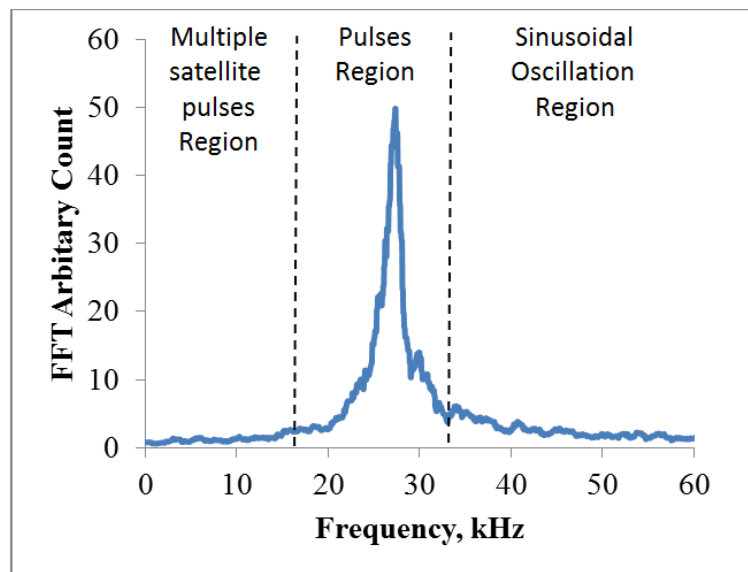


Figure 4.14: Different regions from the resonance frequency distribution categorize based on the output pattern.

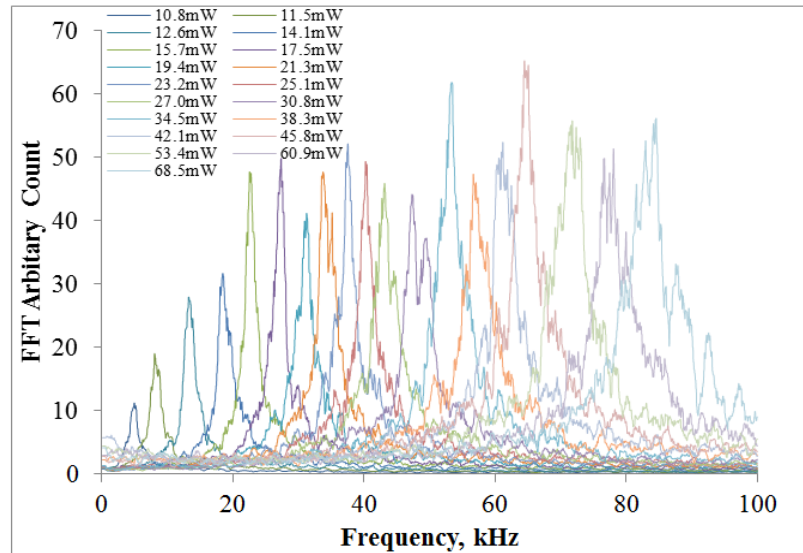


Figure 4.15: Resonance frequency of the OM noise at different pump power.

Figure 4.15 shows the FFT spectrum distribution of the optical output power fluctuation at different pump powers. The resonance frequency can be tuned from 4.5 kHz up to 85 kHz with just 68.5 mW pump power. A resonance frequency tuning of up to 100 kHz is possible with a higher pump power laser diode. The high sensitivity bandwidth of the OM at a set pump power is rather narrow at 8~10 kHz centred at the resonance frequency. Nevertheless, the sensing of the modulation frequency from 100 Hz to 100 kHz is possible using the same OM by varying the pump power level. The results of the acoustic wave modulation from 100 Hz up to 100 kHz has been reported[8]. From the above discussion, it can be seen that the noise of the OM carries a lot of important information such as operating band, sensitivity, and output pattern.

Although the setup with a 10 m of SSMF has a tuneable range as wide as 100 kHz, the sensitivity is low as compared to electrical microphones. To enhance the sensitivity of the OM, a longer SSMF was used in the OM. However, a detailed study needs to be done to understand more about the characteristic changes due to the change of sensing fibre length.

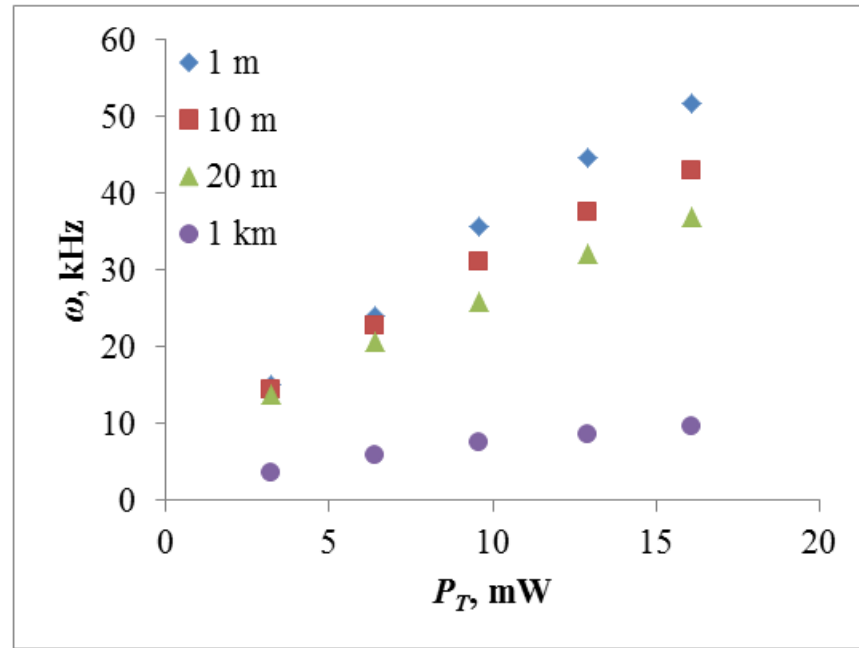


Figure 4.16: Relation between resonance frequency, ω and pump power above lasing threshold, P_T with 80 μm SSMF sensing medium at length 1 m, 10 m, 20 m and 1 km.

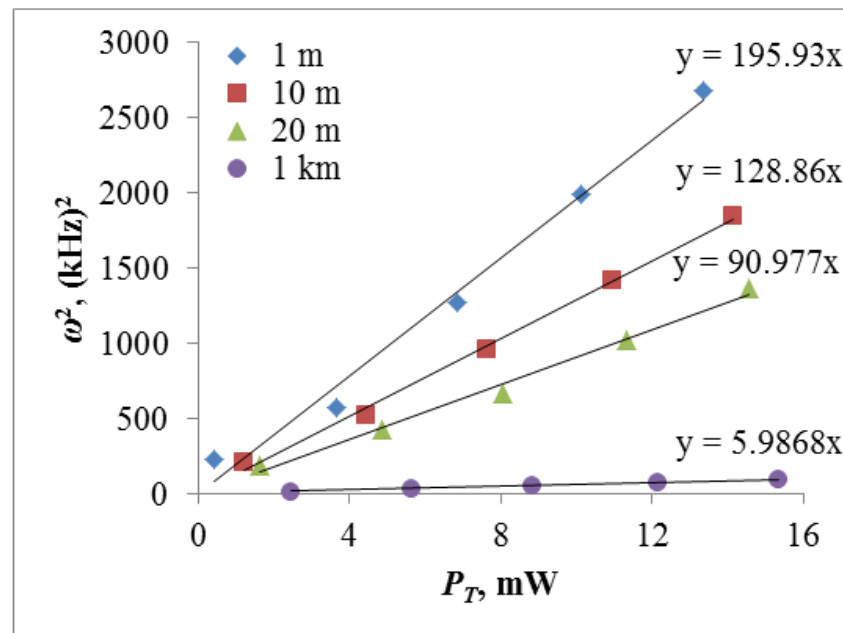


Figure 4.17: The linear relation between parameter ω^2 and pump power above lasing threshold, P_T with different SSMF length.

Figure 4.16 shows the relationship between resonance frequency, ω and pump power above the lasing threshold, P_T with a 80 μm SSMF sensing medium at length 1 m, 10 m, 20 m and 1 km. From Figure 4.16, it was observed that the tuning range of the resonance frequency is larger at shorter lengths. However, the resonance frequencies of shorter length fibres are more unstable and fluctuate in larger scale. In the graph, P_T is used instead of the pump power to match the Eq. (3.3) and to ease the calculations for the k value. To obtain the k value, ω^2 against P_T is plotted and shown in Figure 4.17. Trend lines and the equations were added to the plots of each fibre length. From Eq. (3.3), it is known that $\omega^2 = kP_T$ and therefore, k will represent the gradient of the graph in Figure 4.17.

The k parameter depends on the fibre length as observed in Figure 4.17, thus, their relation can be figured out by plotting the k parameter against fibre length as shown in Figure 4.18. Due to the large fibre length different between 1 km and others, a logarithm scale is used in the graph. From Figure 4.18, linear relation between the k parameter with the Fibre length in a logarithmic scale can be observed.

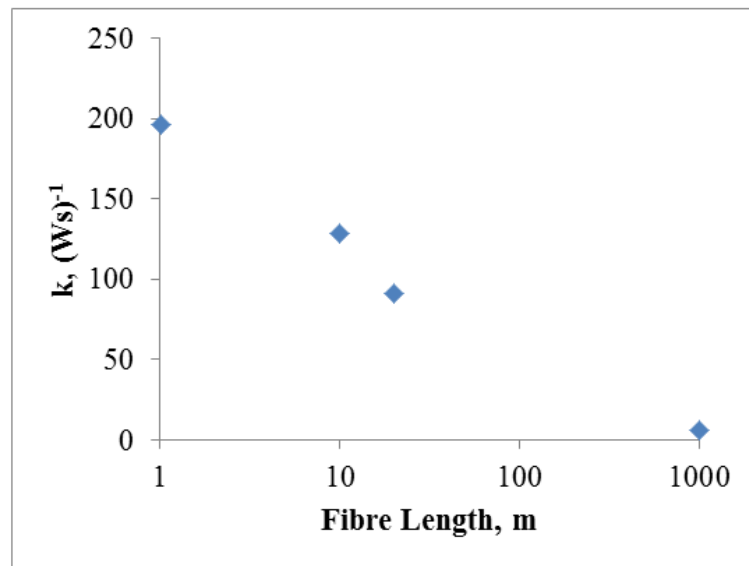


Figure 4.18: The relation between the constant, k and the SSMF fibre length in logarithm scale.

There are few advantages for using a 1 km SSMF as sensing medium: (a) larger sensing area is possible for a larger area distribution sensing, (b) higher sensitivity where the detection level of a 500 Hz sound wave was reduced to 66.7 dBA SPL, and (c) the ability to tune the pulses region or the highly sensitive zone to lower frequency as shown in Figure 4.19.

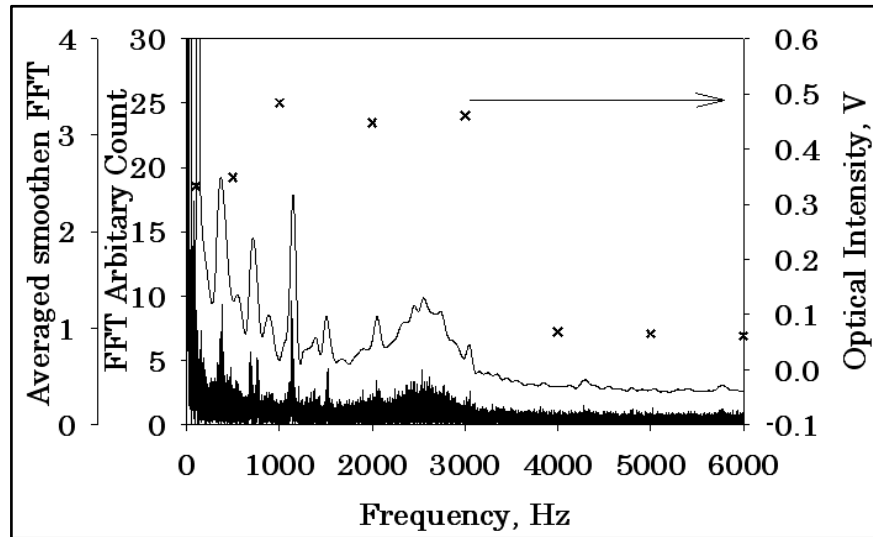


Figure 4.19: Modulated optical amplitude as compared with the intensity noise frequency distribution for a 5 s record of the detected laser output.

Figure 4.19 shows the noise FFT spectrum computed using Matlab for the optical power captured for 5 s on a digital oscilloscope using a linear photodiode (dark trace) (voltage displayed on the oscilloscope is proportional to the optical power). Figure 4.19 also shows the same data, after averaged with neighbouring data, represented by a single trace. For comparison, data points are shown for the average magnitude of the peak modulation of the laser output at an incident sound level of 95 ± 2 dBA SPL - at frequencies ranging from 100 Hz up to 6 kHz. It can be observed that the modulation of the laser output has an approximately constant magnitude - from low frequencies up to the main broad resonance frequency distribution. At frequencies above the resonance frequency, the modulation amplitude drops substantially. It has been discussed that by studying the intensity noise behaviour, the sensitivity at different

operating frequency bands of the acoustic sensor can be obtained. For the aforementioned reasons, the noise spectrum and modulation were obtained at a pump power level just above the lasing threshold, in order to produce the highest sensitivity at the lowest frequency possible and match the response at the human vocal frequency range (60 Hz to 7 kHz), thereby acting as an effective optical microphone. Greater sensitivity at progressively higher frequencies is obtainable by tuning the pump power to progressively higher levels.

4.4 EDF Length

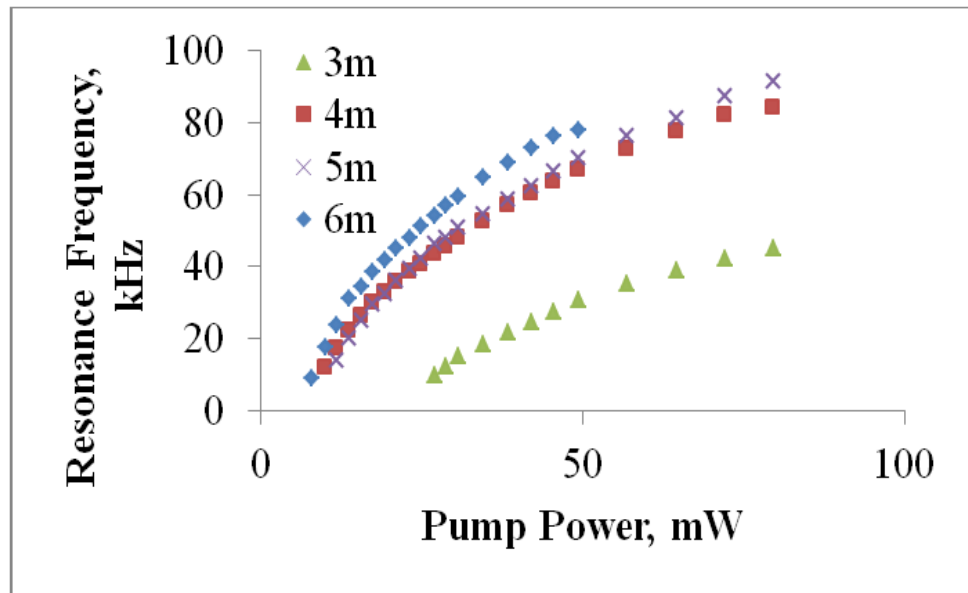


Figure 4.20: The resonance frequency of different EDF length under different pump power.

Besides types of sensing fibre, cavity length and pump power, the EDF length is another parameter that is very important in this experiment. EDF is the only gain medium in the setup which decides the gain parameter, g in Eq. (3.8). Since the resonance frequency is important in this setup, the changes of the resonance frequency based on different EDF lengths were studied. Figure 4.20 shows the changes of resonance frequency under different pump power with EDF (FIBERCORE Ltd. ISOGAIN I6) of 3 m, 4 m, 5 m, and 6 m. To maintain the cavity length, shorter EDF was spliced with extra SMF to obtained a total cavity length at about 16 m. This is

important as the cavity length will also affect the resonance frequency, maintaining the total cavity length will reduce the uncertainty in the results.

From Figure 4.20, it is obvious that for EDFs with lengths at 4 m, 5 m, and 6 m, the resonance frequencies have similar response to the pump power variation, while the response for a 3 m EDF is relatively far away from the longer lengths. Looking at EDF lengths of 4 m, 5 m, and 6 m, we can observe large increments of the resonance frequency at low pump power, the difference getting smaller when higher pump powers are used. There exist optimums EDF lengths for efficient absorption of pump power and signal amplification. In this OM configuration, the optimum EDF length was observed to be 4 m or longer. The short EDF length of 3 m limited the amplification of the feedback signal causing an increase of the lasing threshold. Hence, higher pump powers were needed to achieve higher gain per length in the gain medium, which is about 9 mW in this case. The increment of the resonance frequency is also getting smaller when the pump power increase due to the lower gain efficiency of the gain medium in such a short length.

Other than the EDF length, Erbium ions concentration in EDF plays an important role in fibre laser dynamics behaviour. Erbium ions concentration and clustering is the key parameter in generating dynamic self-pulsing in fibre lasers[9]. Many research and theoretical studies have been demonstrated especially on ion-ion interaction or ion pairs of Erbium in the excited state[10]. However, self-pulsing is one of the behaviour that should be avoided to maintain the output fluctuation in a minimum level. Hence, study of high concentration of EDF doped fibre is not considered in this thesis.

4.5 Design and Prototype

Instead of having the OM for laboratory use only where expensive and bulky laboratory instruments are used, the setup was designed to be a portable and customizable device. From previous section, the setup is known to be customizable to operate at different frequency band with different sensitivity by using different length or type of sensing medium. In this prototype, the setup was separated into 3 different sections: (a) Main module, (b) sensing medium, and (c) detector. The main module consists of a laser diode (LD) driver, a 980 nm LD, a 980 nm/1550 nm WDM, and 3 m of EDF. All of them were packed into a 13.0 (L) x 7.5 (W) x 1.5 (H) anodized aluminium case which was designed to fit all three items above in a minimum space. The aluminium case was anodized to create an oxide layer on top of the casing so that it became insulator. This step is important as laser diode is extremely sensitive to static discharge, and any short circuit will damage the laser diode. Figure 4.21 shows the interior of the main module. The module can be power up from standard power point using USB traveller charger (5 V- 1 A) with USB output.

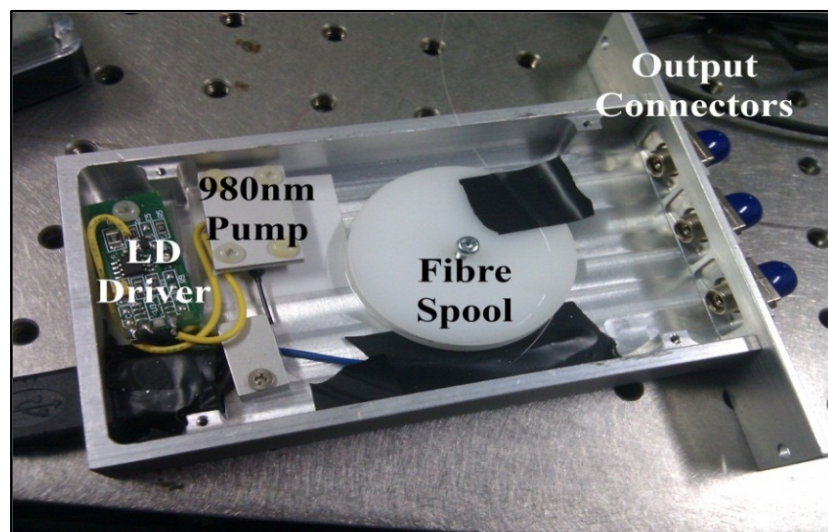


Figure 4.21: Interior part of the OM module.

The laser driver used in the main module is tuneable, which means that different current level can be used to drive the laser diode by turning the screw node on the driver. Through current control, the pump power of the pump can be controlled and this leads to the tune ability of the resonance frequency or operating band. The three output connectors were prepared for laser output at point A and point B as shown in Figure 4.1, with an extra port for interchangeable EDF. Although direct splicing of the sensing medium to the fibre laser can be more stable and smaller size, it will lose the flexibility on replacing the sensing medium. By using connectors, replacement of different sensing mediums is possible. Hence with this flexibility, the main module can be equipped with different sensing mediums with different capability such as for point sensing, distribution sensing, or large tuneable sensing medium and also different shape of sensing mediums like cylindrical, circular, or sphere in different size and diameter. Figure 4.22 shows the sensor prototype with sensing medium.

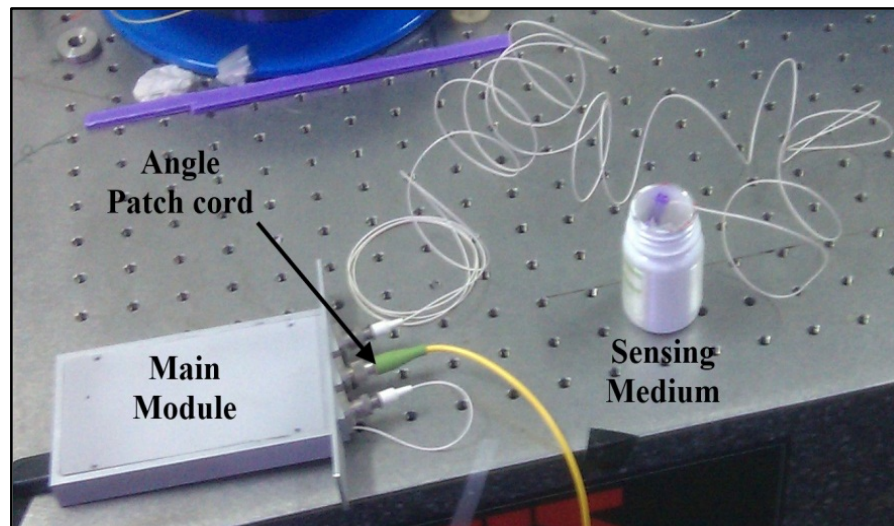


Figure 4.22: The sensor prototype with a 20 m SSMF sensing medium in cylindrical shape spool on a plastic bottle with 3.5 cm outer diameter.

The whole prototype starting from the main module to the sensing medium is sensitive to acoustic waves, hence the main module should place near to the sensing zone as well to avoid noise from unwanted acoustic signal in other places. However, long distance sensing and monitoring are always preferable. For long distance monitoring, optical transmission is still the first choice compared to electrical transmission due to its low loss transmission, free from electromagnetic interference and other advantages mentioned in Chapter 1. Unfortunately, connecting a standard long SMF patch-cord to output A is not recommended as the connector interfaces will induce back-reflection and create an extra fibre laser cavity. This extra cavity becomes part of the sensor as well and it will pick up all the acoustic waves along the transmission path. As to avoid this situation, an angle patch-cord can be used to transmit the output signal to the photodetector for long distance. The schematic drawing of the setup is shown in Figure 4.23.

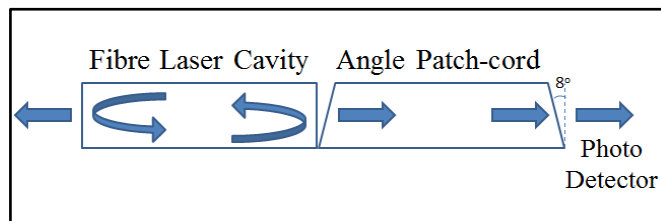


Figure 4.23: Schematic drawing of the fibre laser cavity connected to an angle patch-cord.

The angle patch-cord is a conventional SMF with angle connector. Both end surfaces of the connectors are cut with a small angle which is 8° from the normal. The purpose of the design of this kind of connector is to avoid any back reflection caused by the fibre ends in the connector. When an angle connector is connected to a flat connector, there is an air gap in between both connectors causing Fresnel's reflection at the fibre end. The optical signal transmitted from the cavity is then captured by the angle patch-cord and transmitted to the other end of the patch-cord and capture by photodetector. Since there is no back reflection from the angle patch-cord, there will not

be any feedback of the optical signal back to the fibre laser cavity. Therefore, any disturbance on the transmission fibre will not affect the stability of the fibre sensor.

The prototype has been tested by placing the main module and sensing medium in room A while a 50 m transmission fibre was used to direct the output to monitoring room B. Acoustic waves in room A were successfully detected and transmitted to the monitoring room without any pick up of the acoustic wave along the transmission path. The optical output power was then converted into electrical signals using a linear photodetector and recorded using a personal computer. The sound wave in room A can be heard when the recorded sound was played back but it was accompanied by a strong background noise. A strong hissing sound caused by the power fluctuation and sharp pulses from the optical output can be heard throughout the playback. To obtain a better performance from the sensor, a dual wavelength mode competition fibre laser system is built to observe the acoustic modulation below the dynamics threshold which will be discussed in next chapter.

4.6 Summary

In this chapter, sensing of airborne sound using the proposed acoustic sensor or optical microphone has been demonstrated. Two types of sensing mediums were used in the experiments, one was a 25 km conventional SMF while the other one was a 20 m of thin cladding SSMF. The conventional SMF fibre was able to sense a 500 Hz sinusoidal monotone sound at level as low as 69.8 dBA SPL with a background noise at 48.0 dBA SPL. The response of the average output power and the modulation amplitude were proportional to the SPL. However, when compared to electrical microphone, the OM shows modulation output in pulses form instead of sinusoidal form. These pulses show periodic arrangement which contributes to the generation of harmonic peaks in frequency spectrum. Different length of fibre were tested and it was found that the

longer the fibre, the greater the sensitivity of the sensor. Due to the long sensing medium formed by the long fibre in the length of 25 km, hence the objective of large area sensing with “unlimited” sensing point in this research has been achieved.

A reduction of the fibre length from 25 km to 20 m was successful by replacing the conventional SMF with a thinner cladding SSMF at sensitivity of 70.6 dBA SPL for 500 Hz and 69.8 dBA SPL for 1 kHz of sound wave. The modulated optical output amplitude was found to be related to the resonance frequency distribution of the system noise. Based on the modulated output pattern, the resonance frequency distribution is divided into three different regions, which are (a) Multiple Satellite Pulse Region at low frequency region, (b) Pulses Region at the resonance frequency peak region, and (c) sinusoidal oscillation region. As it is possible to tune the Pulses Region by changing the pump power, the sensing of airborne acoustic waves from 100 Hz to 100 kHz with a small operating window of 10 kHz was reported. The tune ability depends on the cavity length and pump power which can be related to the equation developed in Chapter 2. In this section, the short SSMF that used in the setup has the advantages of point sensing application where it was spool in a flat circle with only 5.5 cm of diameter. With this capability the second part of the second objective has been achieved. 1 km of SSMF was also tested to bring the sensitivity of the OM down to 66.7 dBA SPL.

The influence of the EDF length has also been demonstrated. Although the EDF length in the setup did not contribute to significant changes in the sensor, insufficient length of the EDF will significantly increase the pumping threshold and reduce the tuning range of the resonance frequency to the pump power. At the end of this chapter, a prototype of the setup was presented. The small size and portability of the OM with convenient interchangeable sensing medium was demonstrated. Other than that, an angle patch-cord was used as transmission medium for far distance monitoring purpose to eliminate surrounding noise on the transmission path.

References

- [1] N. Bilaniuk, "Optical microphone transduction techniques," *Applied Acoustics*, vol. 50, pp. 35-63, 1997.
- [2] Z. Wang and Y. Hu, "Frequency response of fiber-optic hydrophone with a novel mechanical anti-aliasing filter of side cavities," in *Communications and Photonics Conference and Exhibition (ACP), 2009 Asia*, 2009, pp. 1-2.
- [3] B. Culshaw, D. E. N. Davies, and S. A. Kingsley, "Acoustic sensitivity of optical-fibre waveguides," *Electronics Letters*, vol. 13, pp. 760-761, 1977.
- [4] C. H. Pua, S. F. Norizan, S. W. Harun, and H. Ahmad, "Non-membrane optical microphone based on longitudinal modes competition," *Sensors and Actuators A: Physical*, vol. 168, pp. 281-285, 2011.
- [5] P. C. Becker, N. A. Olsson, and J. R. Simpson, *Erbium-Doped Fiber Amplifiers - Fundamentals and Technology*. San Diego: Academic Press, 1999.
- [6] E. Desurvire, *Erbium-Doped Fiber Amplifiers - Principles and Applications*. New York: John Wiley & Sons, 1994.
- [7] A. E. Siegman, "Laser spiking and mode competition," in *Lasers*, ed CA, USA: University Science Books, 1986.
- [8] C. H. Pua, H. Ahmad, S. W. Harun, and R. M. D. L. Rue, "Direct Airborne Acoustic Wave Modulation of Fabry-Perot Fiber Laser (FPFL) over 100 kHz of Operating Bandwidth," *Applied Optics*, vol. 51, p. Paper Accepted, 2012.
- [9] H. L. An, E. Y. B. Pun, X. Z. Lin, and H. D. Liu, "Effects of ion-clusters on the intensity noise of heavily erbium-doped fiber lasers," *Photonics Technology Letters, IEEE*, vol. 11, pp. 803-805, 1999.
- [10] F. Sanchez, P. Le Boudec, P.-L. François, and G. Stephan, "Effects of ion pairs on the dynamics of erbium-doped fiber lasers," *Physical Review A*, vol. 48, pp. 2220-2229, 1993.

Chapter 5

Enhancement and Other Applications

5.1 System Enhancement

5.2 Arrayed Waveguide Grating (AWG)

5.3 Experimental Setup

5.4 Mode Competition

5.5 Summary

References

5.1 System Enhancement

In the previous chapter, an all optical fibre acoustic sensor assembly with an optical fibre used as the sensing medium has been demonstrated. The direct modulation of electromagnetic waves propagating in the fibre core by acoustic waves based on laser dynamic behaviour is a new idea that realizes unassisted optical microphone (OM) [1]. The realization of an unassisted OM has opened the possibility of accessing the large and promising area of distributed sensing. Despite the limited multi-point sensing capability of the current setup, the proposed method is an effort towards unlimited point sensing.

Although this method overcomes the barrier where by optical airborne acoustic sensing is now possible without the need of an intermediate medium such as a diaphragm, it still suffers from various issues. The most pressing issue is the random fluctuation of optical output power due to laser dynamics which cause to the unstable noise of the sensor. Another issue is the transient generation during the onset of modulation which will distort the original acoustic wave pattern even though wave frequency detection is still possible. The third issue is the sensitivity of the sensor is still low compared to a diaphragm-transduced OM. This section will introduce the implementation of dual wavelengths mode competition to increase the sensitivity of the proposed methods.

There are various methods to obtain a dual wavelength fibre laser, including the use of a high birefringence fibre loop mirror [2], fibre grating Sagnac loop [3], highly nonlinear fibre ring laser [4], Arrayed Waveguide Grating (AWG) [5], and more [6, 7]. This experiment uses a 1x16 AWG for dual wavelength selection purposes and an Erbium Doped Fibre (EDF) as an amplifying medium in the laser cavity.

5.2 Arrayed Waveguide Grating (AWG)

AWGs are built with three main parts, two inputs/outputs waveguides, two slab waveguides (or free propagation zones, FPZ) and one arrayed waveguide with equal length difference between adjacent array waveguides as shown in Figure 5.1.

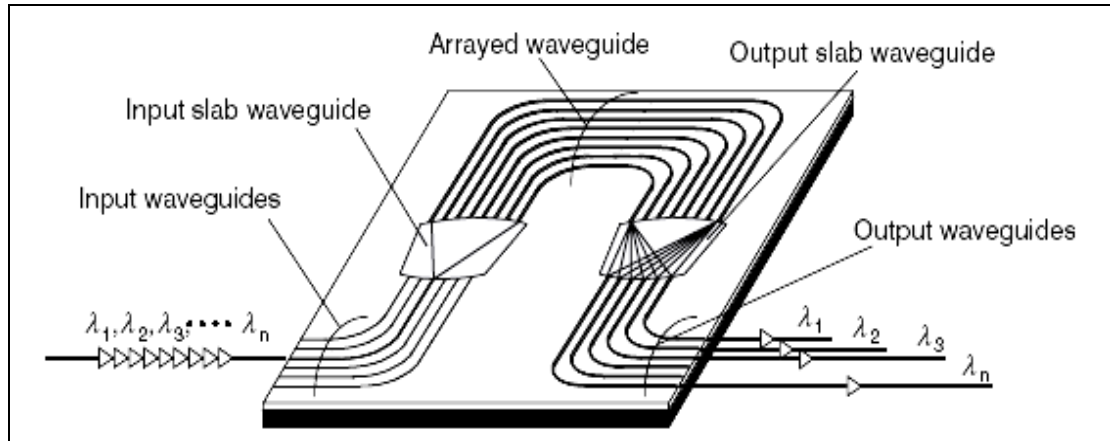


Figure 5.1: Structure of AWG

As a demultiplexer, the device transmits multiplexed optical signals with different wavelengths (λ_1 to λ_n) from the input waveguides to the first FPZ. When the input signals enter the first FPZ they will diverge in the FPZ, coupled into, and transmitted through the arrayed waveguide as shown in Figure 5.2. The length of the arrayed waveguides is designed such that the optical path length difference, ΔL , between adjacent waveguides is equal. The equal length difference between adjacent array waveguides will create a phase difference, so that wavelength-dependent focusing occurs at spatially separated points at the end of the second FPZ as shown in Figure 5.3. Thus signals of different wavelengths can be coupled to separate waveguides at the outputs of the AWG. The basic operation of the AWG demultiplexer is the same as the basic operation of AWG multiplexer. Hence the AWG demultiplexer can be used as a multiplexer in the reverse direction because of the reciprocity [8, 9].

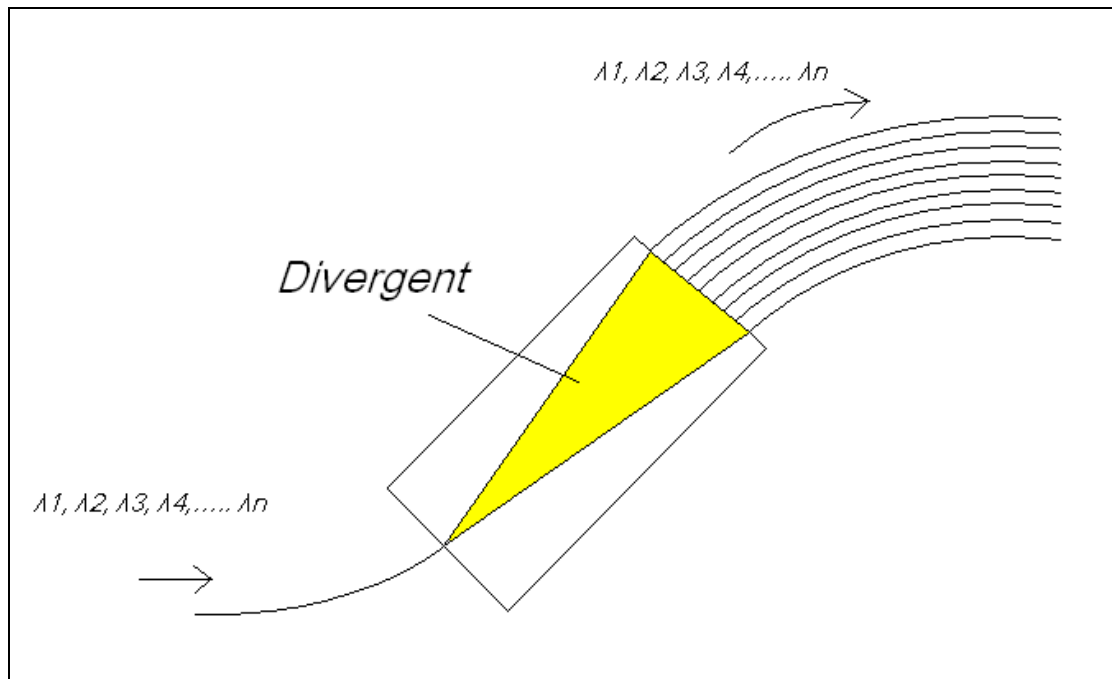


Figure 5.2: Divergent of multiplexed wavelength to arrayed waveguides in first FPZ.

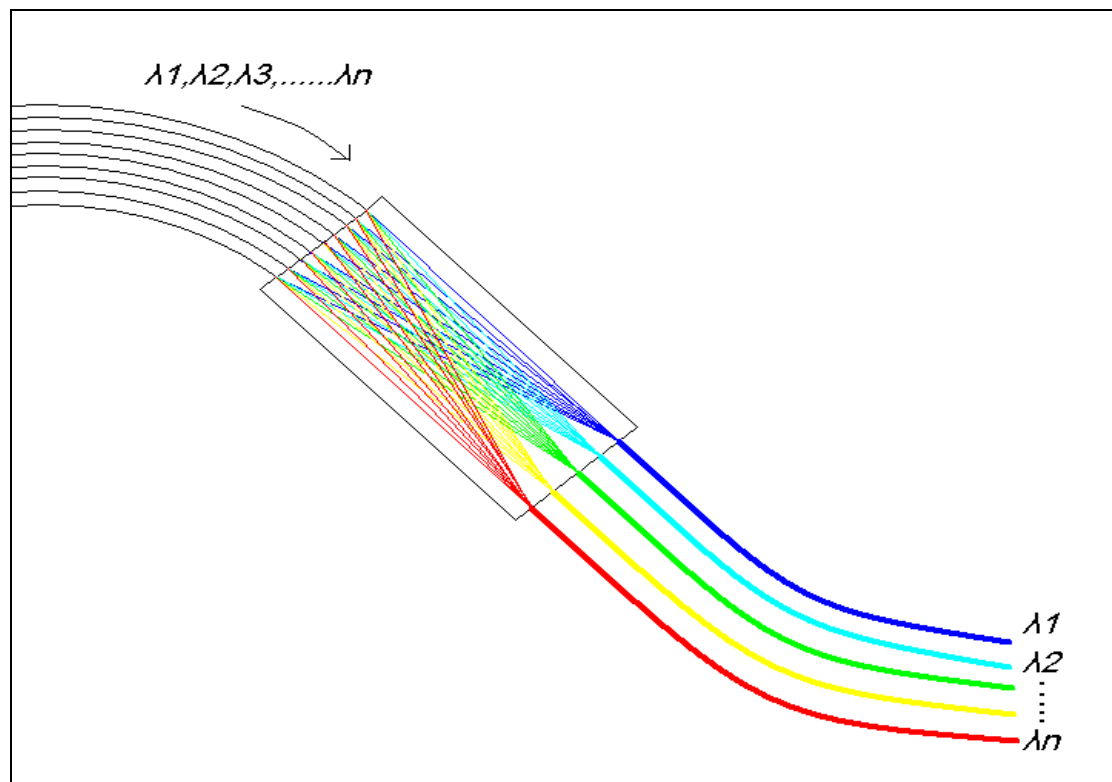


Figure 5.3: Optical ray path of different wavelength at second FPZ.

5.3 Experiment setup

The experiment setup is shown in Figure 5.4. A 980 nm laser diode pump was used to create the conditions for inversion population in the EDF and generate Amplified Spontaneous Emission (ASE). The ASE that propagates toward the AWG will be sliced into 16 different wavelength outputs at each physical channel. Among the 16 channel outputs, 2 selected channel outputs B_1 and B_2 will have a flat-cleaved output to produce a 4% back reflection or feedback to the system while the other 14 channels will have angle-cleaved output to avoid any back reflection or feedback. The 2 selected wavelengths will be partly reflected back to the cavity and induce stimulated emission when passing through the 5 m EDF. The amplified dual wavelength signal will experience an additional 4% back reflection at the other end of the laser cavity, labelled as output A, completing a dual-wavelength laser cavity.

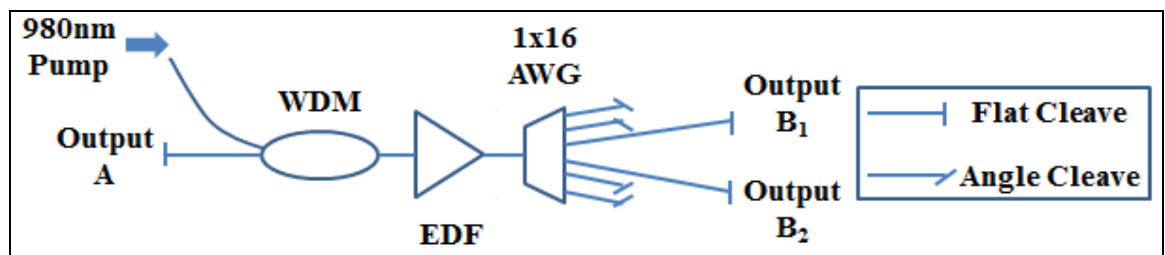


Figure 5.4: AWG enhancement OM.

Figure 5.5 shows the optical spectrum of the dual wavelength fibre lasers from output A with lasing wavelengths of 1532.10 nm and 1532.90 nm. Dual wavelength lasing in such a system is unstable due to mode competition caused by strong homogeneous broadening and cross gain saturation of the EDF [10]. Although there already exist various methods which are able to stabilize multi wavelengths lasing by eliminating or reducing the mode competition [5, 11, 12], these steps are not taken as the natural response of the system is of interest in this work. The setup is pumped with 23.2 mW to generate a dual-wavelength fibre laser from both B channels. To obtain

similar levels of optical output power from both B channels, micro bending is introduced to the higher output power channel to induce losses in the channel.

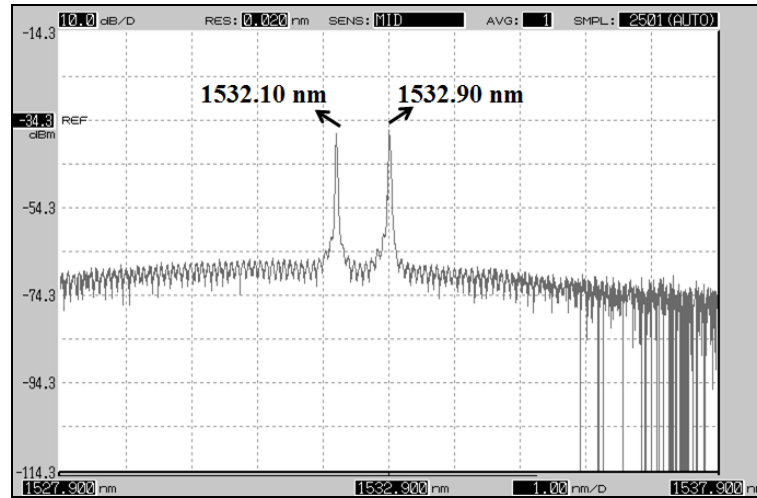


Figure 5.5: Optical spectrum of dual wavelength fibre laser pumped at 23.2 mW.

5.4 Mode Competition

Figure 5.6 presents the outputs power from outputs A, B₁ and B₂, measured using a digital oscilloscope. Figure 5.6(a) shows output A which contains the total optical output of the fibre laser in the backward direction at a voltage level of 2.18 V. This output is stable at low frequencies with noise or fluctuation power in the range of 19.7 kHz to 22.0 kHz and peak fluctuation at 20.8 kHz measured using the Fast Fourier Transform (FFT) method from the build-in MATH function in the digital oscilloscope. The FFT spectrum was displayed on the digital oscilloscope panel as shown in Figure 5.6(a). This noise frequency has already been discussed in [1], known to be caused by the fibre laser dynamics, and depends on parameters like pump power, laser cavity length, erbium concentration, cavity reflectivity, and cavity loss. Figure 5.6(b) on the other hand, shows the optical power from output B₁ and B₂ which represent the optical output of wavelengths 1532.10 nm and 1532.90 nm respectively at 260 mV independently. It is observed that the fluctuations of the optical output power between the two wavelengths are totally inverted. The increase of optical power of one

wavelength will cause the optical power of the second wavelength to decrease by the same magnitude.

To identify the inverted characteristic of both outputs, a summation of both outputs was done using the build-in Math function in the digital oscilloscope. The result was a stable output similar to output A at a much lower voltage level (averagely at 532 mV) due to few factors. One factor is the difference between the output power levels from the forward and backward directions of the fibre laser. As that the fibre laser is not pumped in such a way that the condition for population inversion throughout the length of the EDF is not satisfied (at the low pump powers used), reabsorption will happen towards the end of the EDF where there is less population inversion. A second factor could be the losses caused by AWG, due to insertion and coupling losses. An additional contributing factor is the loss caused by the other 14 channels. However, these losses are at the ASE level and therefore are less significant.

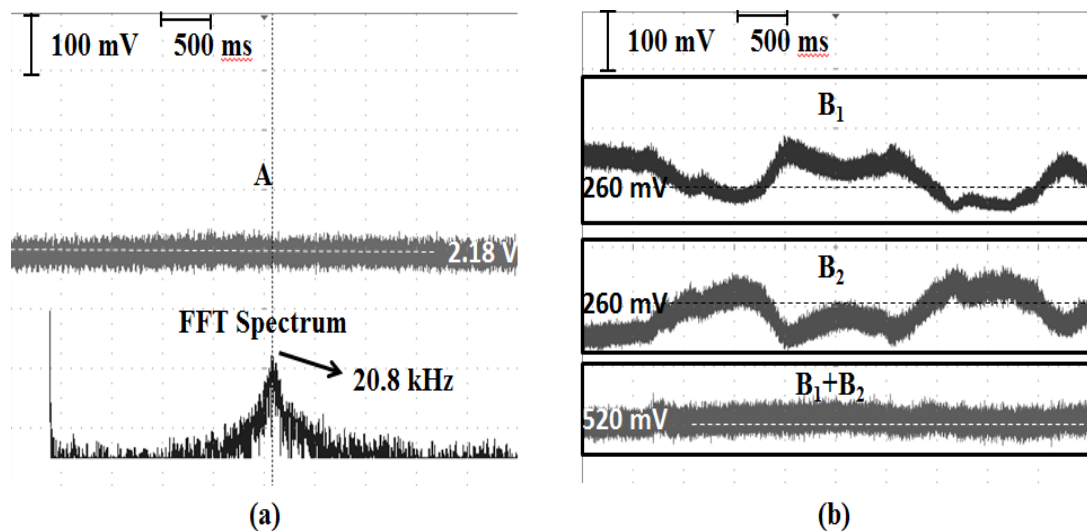


Figure 5.6: Optical output from (a) output A and (b) B_1 and B_2 with FFT frequency distributions that measured and calculated using build in MATH function of the digital oscilloscope.

Analysis of the optical powers fluctuation in the frequency domain was done by studying the FFT of the optical power fluctuation. Figure 5.7(a) and (b) show the optical output power from outputs B₁ and B₂ measured by a digital oscilloscope for a period of 5 s with the FFT frequency distribution of B₁ and B₂ showed at the bottom. From both FFT spectrums, three distribute peaks at frequency 3.50 kHz, 5.45 kHz, and 20.8 kHz were observed. The 20.8 kHz peak is caused by the resonant frequency of the fibre laser system as mentioned previously which exist on all the optical outputs. The other two peaks at 3.50 kHz and 5.45 kHz are caused by the resonant frequency of each mode which oscillates at different wavelengths and can only be observed in outputs B₁ and B₂. The existence of both resonant frequency peaks at both outputs indicates that they are correlated. The FFT frequency distribution from outputs B₁ and B₂ are almost identical with only slight differences in the magnitude and is not significant for further analysis. Furthermore, due to the instability of the outputs power, these two low frequency peaks are unstable as they fluctuate considerably; fluctuations which are related to their output powers. The relationship of the lasing power of each wavelength to the low resonance frequency peak at a more stable condition is discussed in next section.

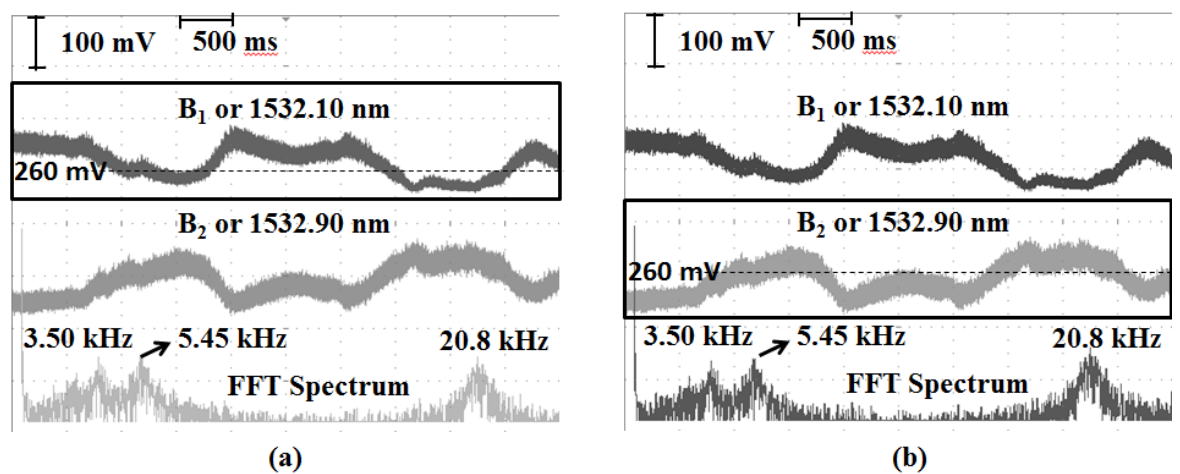


Figure 5.7: Optical output from both output B₁ and B₂ with calculated FFT frequency distribution for (a) output B₁ and (b) output B₂.

Observation of mode competition behaviour for the fibre laser under chaotic conditions was done by the introduction of a small impact (knocking using metal ruler) near the fibre laser. The perturbation generated will cause the laser to undergo chaos condition and produce random spiking effect similar to transient effect which is well explained in laser dynamics behaviour [13, 14]. Figure 5.8(a) shows the spiking generated at both output B_1 and B_2 due to the laser dynamic transient effect. For better visualization, outputs B_1 and B_2 were slightly offset at a different magnitude from the base level to prevent overlapping on the oscilloscope panel. It is obvious that under the chaotic condition, the laser at 1532.90 nm from B_2 is dominant, producing major high energy spikes as compared to B_1 . When both outputs were overlapped, it can be observed that most spikes generated in B_1 will fill up the empty gap between spikes generated in B_2 . Under the chaos condition, mode hopping became dominant process in the fibre laser will only allow one mode to survive at a time. The total output from B_1 and B_2 can be obtained by adding both outputs as presented in Figure 5.8(b). The domination of the pulsing effect is thought to be related to the stability and laser peak power.

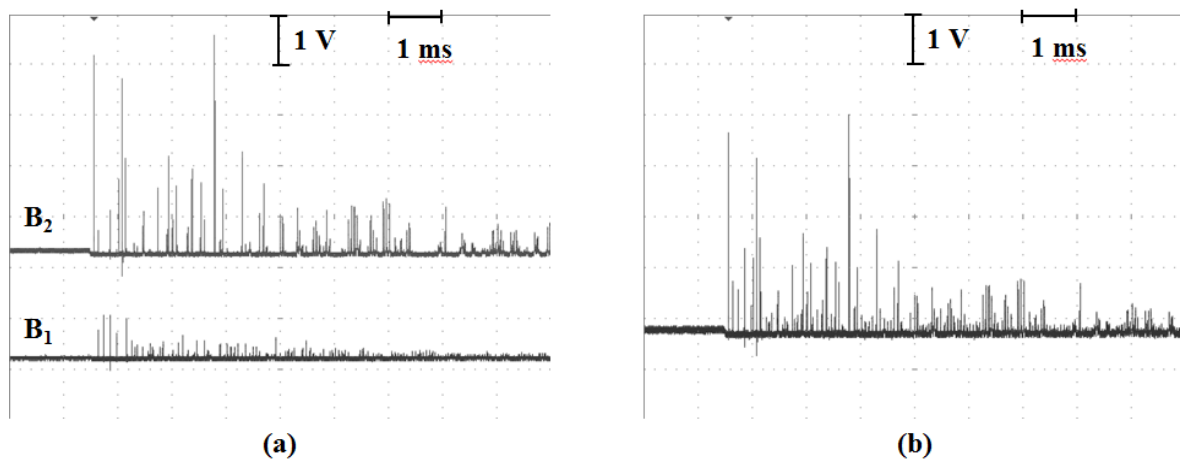


Figure 5.8: Random spiking due to the transient effect from outputs (a) B_1 and B_2 and (b) summation from both of them.

In the previous chapter, acoustic modulation is done based on the dynamic behaviour of the fibre laser without looking into the details about the modes competition behaviour. The perturbation affecting the optical output power of the laser must be large enough to provide significant impact on the laser system gain or loss parameters. If the perturbation is small, the loss introduced on one mode will be compensated by gain of another mode leading to unobservable changes in the total output power a process similar to mode competition, as shown in Figure 5.6. To observe the effect of these small perturbations to the oscillation of the two wavelengths, a 500 Hz low amplitude acoustic waves was generated near the fibre laser using a multimedia speaker connected to a personal computer. The amplitude of the acoustic waves was increased slowly until output B_1 and B_2 respond to the acoustic wave. Figure 5.9 shows optical output from B_1 and B_2 under the modulation of the aforementioned 500 Hz acoustic waves at (a) 65.0 dBA SPL and (b) 88.3 dBA SPL. Both optical outputs show sinusoidal waves forming at 500 Hz. The larger modulation amplitude shown in Figure 5.9(b) is due to larger acoustic wave amplitude. Another difference between Figure 5.9(a) and (b) that can be observed is the outputs in B_1 and B_2 are “out of phase” by 180° in (a) while they are “in phase” in (b).

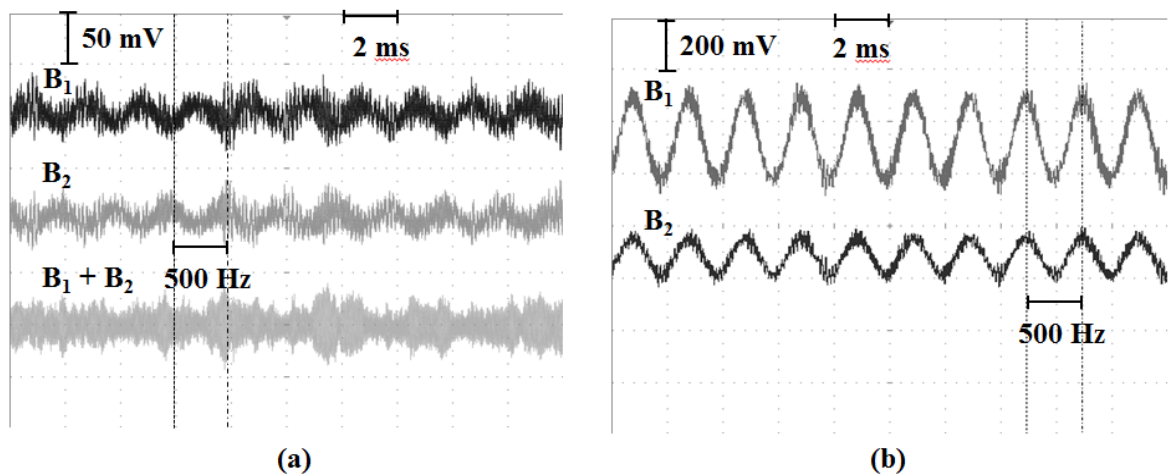


Figure 5.9: Optical output from B_1 and B_2 under the modulation of 500 Hz acoustic waves at amplitude of (a) 65 dBA and (b) 88.3 dBA SPL.

It is believed that outputs from B_1 and B_2 are “out of phase” not because of any delay or changes of path length which then cause a phase shift between output B_1 and B_2 . The interaction of the acoustic waves with the fibre causes modulation on the modes oscillating in the fibre laser. However, the acoustic modulation at this amplitude (65.0 dBA) is far too weak to modulate the total gain and loss of the system. Hence, when one of the modes experience changes in gain or loss, the other mode will experience the opposite effect to compensate for the changes in the system in order to maintain stable lasing conditions. Thus, when both the outputs from B_1 and B_2 in Figure 5.9(a) are sum out or measure the total output from A, the modulation effect in the laser can hardly be observed. However, in Figure 5.9(b), the acoustic amplitude is large enough to modulate the total gain and loss of the fibre laser system where both outputs from B_1 and B_2 exhibit an “in phase” modulation. Furthermore, the modulation pattern from the total output either directly from output A or from the summation of B_1 and B_2 as shown in Figure 5.9(a). Compared to the modulation measurement from the total output power, the measurement of a single wavelength from the dual wavelength fibre laser significantly increased the sensitivity of the fibre laser to the acoustic wave although the noise to signal ratio is comparable high. An improvement of the sensitivity of more than 23 dB has been achieved without sensing medium. With the sensitivity threshold at 65 dBA SPL, the third objective of the research has been achieved.

However, the details about the nature of the interaction between the sound wave and the dual wavelengths laser is still under intense investigation, especially on the selection of wavelength used to modulate and is in phase with the sound wave and the wavelength which will compensate the gain and loss which is out of phase with the sound wave.

Although Figure 5.7 shows large optical power fluctuation (~ 150 mV) of the optical power from output B_1 and B_2 at average output level of 260 mV, these fluctuation can be reduce by stabilizing the setup condition. Figure 5.10 shows the optical outputs from B_1 and B_2 without any micro bending at 1530.52 nm and 1532.07 nm, pumping at 15.7 mW. The differences between Figure 5.7 and Figure 5.10 are that the optical output in Figure 5.10 is more stable and there are only two resonance frequency peaks as compared to Figure 5.7 Under stable conditions, the energy transfer from one mode to another is reduced significantly causing a reduction in the power fluctuation amplitude. In this case, the low frequency noise is expected to be lower from the output of the module.

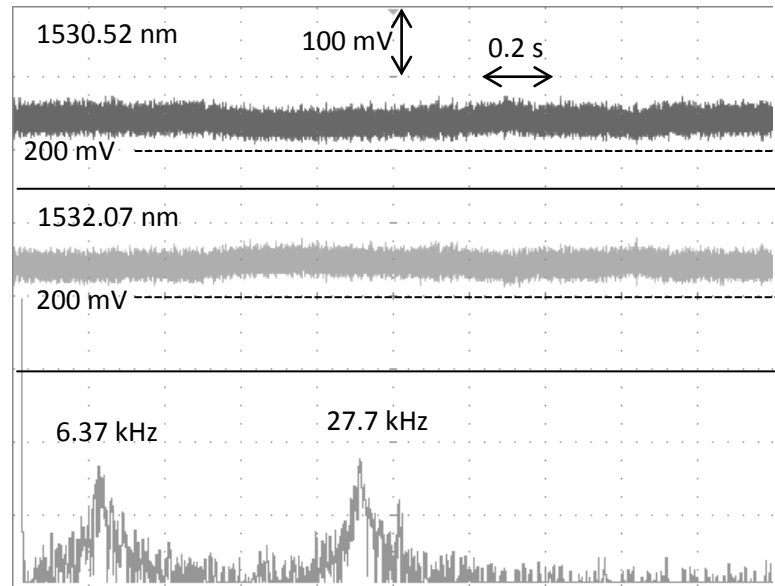


Figure 5.10: Optical output from both output B_1 and B_2 at frequencies 1530.516 nm and 1532.068 nm with calculated FFT frequency distribution pumping at 15.6 mW.

At different pump powers, the shifting of the first and second resonance frequencies show similar trend as discussed in previous chapter but with the different k values, shown in Figure 5.11. The k values for the first resonance frequency (FRF) and the second resonance frequency (SRF) are $99.5 \text{ W}^{-1}\text{s}^{-1}$ and $4.6 \text{ W}^{-1}\text{s}^{-1}$ respectively. FRF is related to the dynamic behaviour of the system while the SRF is contributes by mode competition effect.

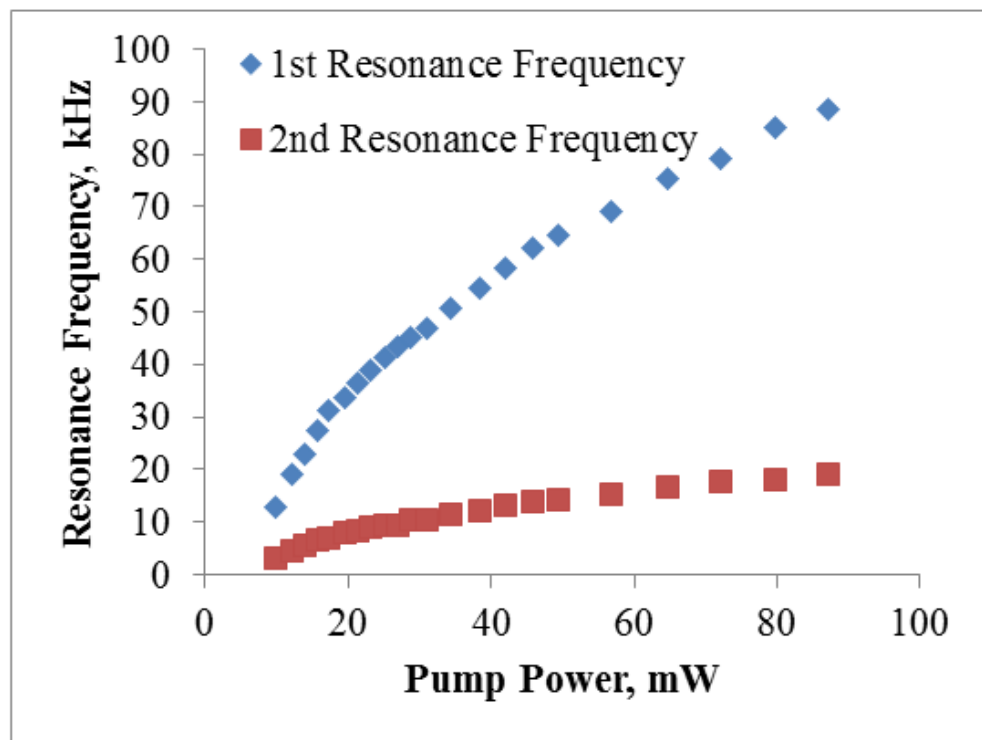


Figure 5.11: Relation between first and second resonance frequency with pump power.

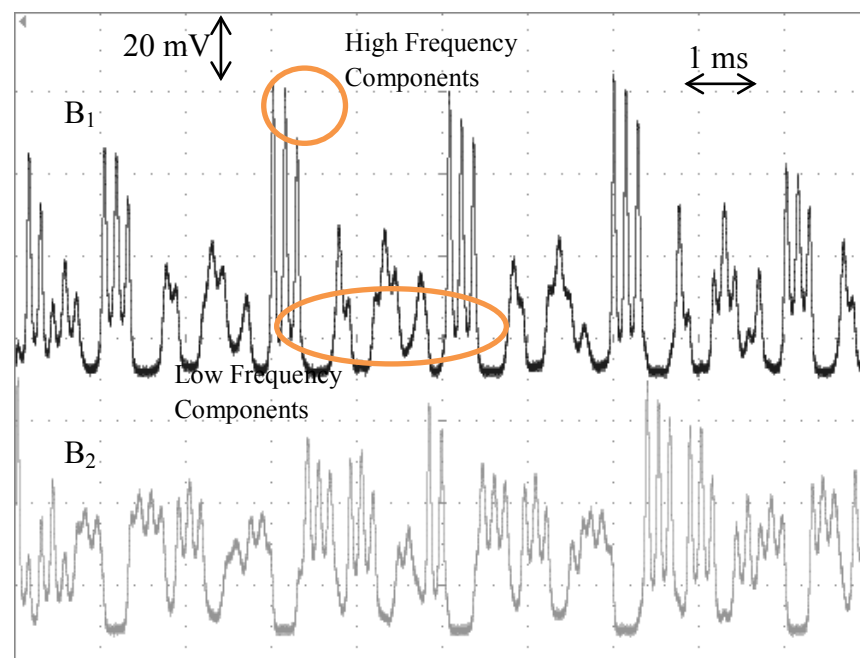


Figure 5.12: Screen capture of optical output power from B₁ and B₂ simultaneously under the modulation of sound wave at 500 Hz with a digital oscilloscope.

A clearer observation of the second resonance frequency generation can be formed by analysing Figure 5.12. Figure 5.12 shows the optical output from B_1 and B_2 under the modulation of a sound wave at 500 Hz. Under strong modulation, the total fibre laser output will tend to generate pulses at frequencies near to the FRF. However, due to the mode competition behaviour, there will be only one mode under such chaotic condition for the majority of the lasing duration. Thus when pulsing is observed in B_1 , the output in B_2 will remain low and flat and vice versa. The short period continuous pulses from both outputs caused by the laser dynamics behaviour are labelled as high frequency components and contributed to the FRF distribution. The SRF is caused by the effect of mode competition, which is the frequency of the periodic group pulses labelled as low frequency components.

Different combinations of the output channels from the 1x16 AWG are chosen to generate different spacing for the dual wavelength fibre laser as shown in Figure 5.13. Output B_1 is fixed at channel 1 of the AWG while B_2 is switched from channel 2 to channel 7 until lasing is impossible due to the large ASE level difference between the selected wavelengths. It is observed that the optical output power of B_2 is reduced from when the selected wavelength is higher. This is due to the reduction of the ASE level when switching to a higher wavelength; which also reduces the lasing efficiency. The low B_2 output power in Figure 5.13(a) is caused by the defect of the AWG.

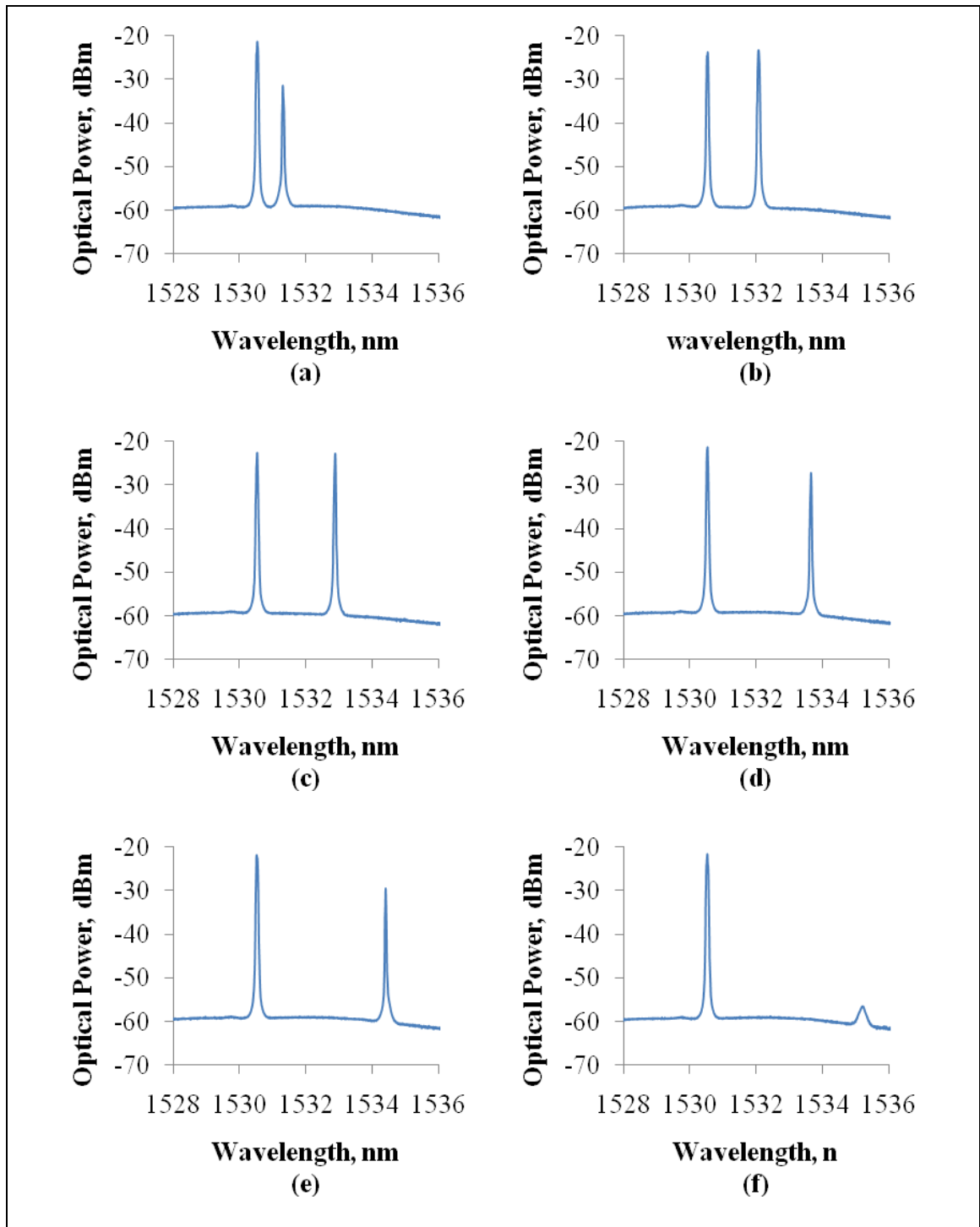


Figure 5.13: Dual wavelength fibre laser generated using 1x16 AWG with different channels combination at wavelengths: (a) 1530.52 nm and 1531.32 nm, (b) 1530.52 nm and 1532.07 nm, (c) 1530.52 nm and 1532.88 nm, (d) 1530.52 nm and 1533.65 nm, (e) 1530.52 nm and 1534.40 nm, and (f) 1530.52 nm and 1535.22 nm pumped at 15.7 mW.

FFT was performed for both outputs taken from all the combinations in Figure 5.13 to obtain their resonance frequencies. As was expected, they all share the same FRF at 27.5 ± 0.5 kHz due to the same laser cavity length and pump power. However, the SRF is different for each of them which implies that the mode competition behaviour between the dual wavelengths changes. The SRF for each case is 3.62 kHz, 6.37 kHz, 7.62 kHz, 6.75 kHz, 5 kHz, and disappear with respect to Figure 5.13(a) to (f). When the SRFs are plotted against the peak power of the B_2 outputs, SRF is found to be linearly dependant on the peak power of the B_2 output with the condition that B_1 is fix, as shown in Figure 5.14. The wavelength of B_2 and the spacing between B_1 and B_2 does not contribute to the change of the SRF. In Figure 5.13(f) there is no SRF in the FFT spectrum where lasing does not happen at 1535.22 nm.

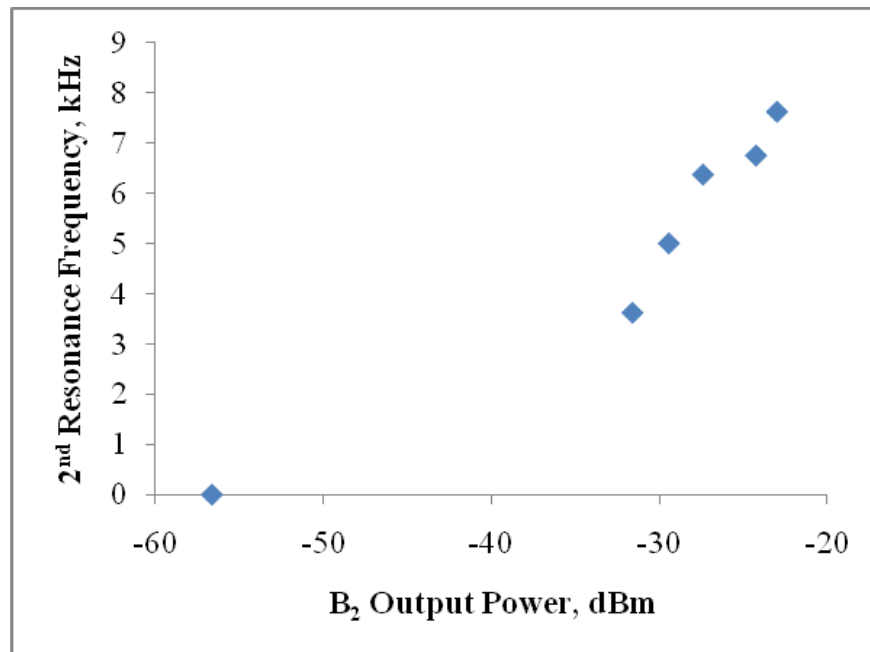


Figure 5.14: The relation between SRF with the peak power from output B_2 .

All the experimental result above determined that the low frequency components are related to the optical power of the lasing wavelength with lower peak powers. Figure 5.15(a) and (b) are the noise of the dual wavelength OM obtained simultaneously for a period of 2 s. Figure 5.15(a) shows the optical output together with the FFT analysis for wavelength 1530.52 nm while (b) for 1533.65 nm. It can be observed from the FFT distribution that the, wavelength 1530.52 nm wavelength with peak power at -21.25 dBm is dominant by high frequency fluctuation that fluctuates at 27.2 kHz while 1533.65 nm with peak power at -27.39 dBm is dominant by low frequency fluctuation that fluctuates at 6.75 kHz.

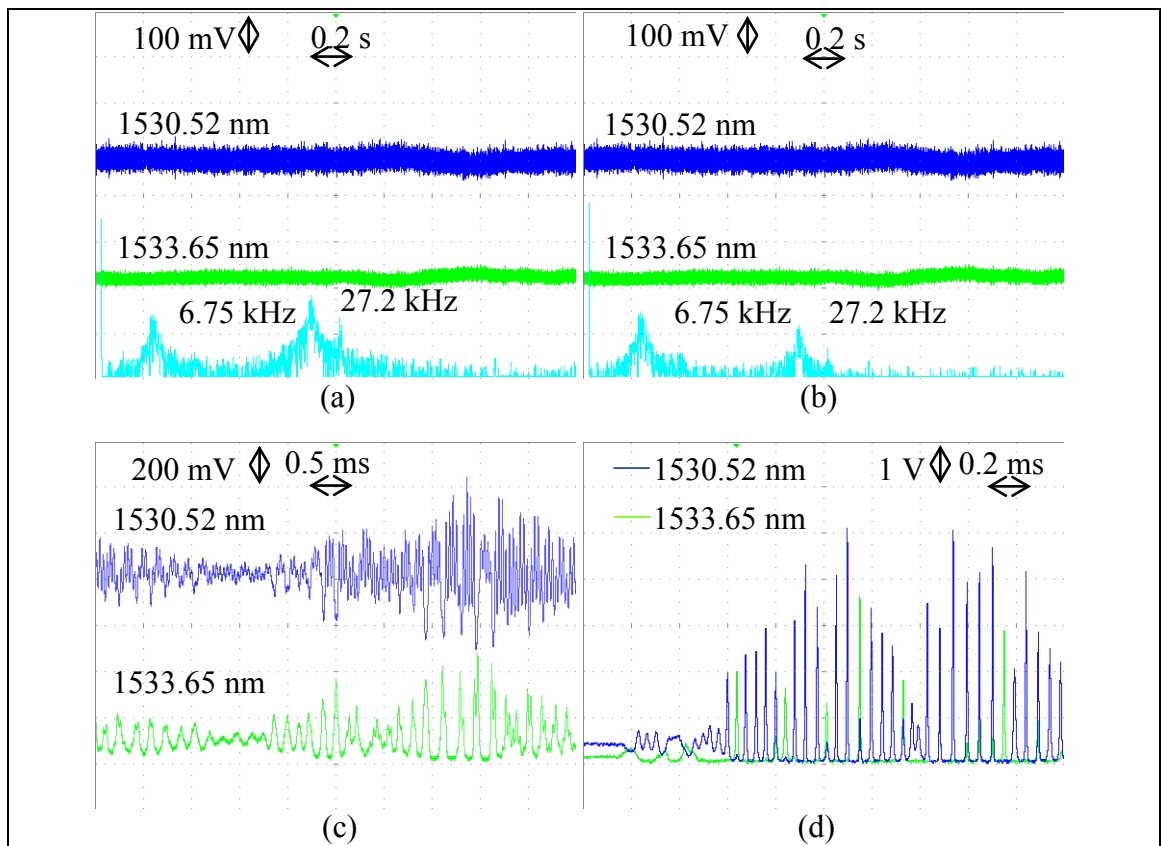


Figure 5.15: Digital oscilloscope readings from output B₁ and B₂ at wavelengths 1530.52 nm and 1533.65 nm with average peak power at -21.25 dBm and -27.39 dBm. (a) and (b) are noise readings with the frequency domain analysis for (a) 1530.52 nm and (b) 1533.65 nm. (c) is the chaos condition with a small acoustic disturbance incident on the OM while (d) is the chaos condition with a strong acoustic disturbance.

If a weak acoustic vibration is incident on the OM, optical power output from B_1 and B_2 are oscillating in an inverted direction where B_2 will reach the peak output when B_1 falls to the trough as shown in Figure 5.15(c). The oscillations of one wavelength will always tend to compensate the loss or gain of the other wavelength as long as the external perturbation is not strong enough to trigger the dynamic behaviour of the fibre laser. Since there are no changes on the total gain or loss in the fibre laser cavity, hence the total output power will remain the same even though there are changes of the optical power in each wavelength. Furthermore, it is obvious that the 1530.52 nm output is oscillating with considerable amount of high frequency fluctuation which is not observed in the 1533.65 nm wavelength case. Thus, the output from 1533.65 nm will have less noise under the modulation of low frequency acoustic wave.

Figure 5.15(d) shows the overlapped optical outputs from B_1 and B_2 under a strong perturbation. It can be observed that the combination of both outputs produce pulses which are almost periodic. However, when a strong pulse is generated by one wavelength, the other one will remain at the lowest output power and vice versa due to the competition of both modes.

Thus, by using a dual wavelength fibre laser with a significant power difference between the output wavelengths, a fibre laser with output dominated by low frequency oscillation can be obtained. This low frequency domain output is suitable to be used as a sensor for the human voice at a frequency between 80 Hz and 1100 Hz or for low frequency acoustic sensing as it will suppress the high frequency noise to a lower level.

5.5 Summary

In this chapter, a method was proposed to increase the sensitivity of the OM to airborne sound waves and simultaneously reduce the high frequency noise for audible noise recording. The enhancing method proposed is observing the power fluctuation of individual wavelength in dual wavelength competition condition. In generating dual wavelength fibre laser, the AWG method is chosen due to its flexibility on switching different operating wavelengths. The operating principle of the AWG was briefly introduced.

The optical outputs power from the dual wavelength fibre laser are observed from A, and the total output power and B_1 and B_2 which are each individual lasing wavelength output. From the total output power, the setup shows no significant difference from previous setup in terms of power fluctuation. The output is stable and fluctuates with its resonance frequency at 20.8 kHz. However, when the output power from each individual wavelength was observed, the optical power fluctuation of each individual wavelength is found to be larger and that the fluctuation pattern of one wavelength is an inversion of the other wavelength. This inversion of optical power fluctuation is due to the compensation of gain and loss of one wavelength by the other wavelength since the total gain of the system remains the same.

This power compensating behaviour is based on the modes competition behaviour and can be observed during weak acoustic modulation. When a weak sinusoidal acoustic modulation below the triggering level of fibre laser dynamics is introduced, 180° out of phase sinusoidal outputs from the chosen wavelengths were observed. If the acoustic modulation is above the fibre laser dynamics threshold, the oscillation of both outputs will be in-phase again. When the modulation is below the laser dynamics threshold, the total laser gain remained the same, hence outputs from B_1 and B will oscillating with 180° phase difference to maintain the same total output

power. However, when the modulation is above the threshold, it modulates the gain and loss of the fibre laser system generating an in-phase optical output. The results proof that without any extended sensing medium, sensing below the laser dynamic threshold can improve the system sensitivity for more than 23 dB. The sensing threshold is now down to 65 dBA which delivered the third objective of the research.

In addition, in dual wavelength modes competition, two resonance frequencies were observed in the FFT spectrum. One at a higher frequency which depends on the whole laser system condition such as the cavity length and pump power. While the other one at a lower frequency if depends on the power difference between the two lasing wavelengths. This low frequency fluctuation is contributes by the resultant of modes competition where it shows how frequent does the domination of mode changing in the laser cavity.

Besides that, the wavelength with lower lasing power will oscillate at lower frequencies due to it less competitiveness with the other wavelength which eliminates the high frequency fluctuation. It shows a cleaner modulation pattern for audible acoustic wave sensing as compared to the higher lasing power wavelength.

References

- [1] C. H. Pua, S. F. Norizan, S. W. Harun, and H. Ahmad, "Non-membrane optical microphone based on longitudinal modes competition," *Sensors and Actuators A: Physical*, vol. 168, pp. 281-285, 2011.
- [2] X. P. Dong, L. Shenping, K. S. Chiang, M. N. Ng, and B. C. B. Chu, "Multiwavelength erbium-doped fibre laser based on a high-birefringence fibre loop mirror," *Electronics Letters*, vol. 36, pp. 1609-1610, 2000.
- [3] S. Xuewen, J. Shan, and H. Dexiu, "Fiber grating Sagnac loop and its multiwavelength-laser application," *Photonics Technology Letters, IEEE*, vol. 12, pp. 980-982, 2000.
- [4] C. Zhe, S. Hongzhi, M. Shaozhen, and N. K. Dutta, "Dual-Wavelength Mode-Locked Erbium-Doped Fiber Ring Laser Using Highly Nonlinear Fiber," *Photonics Technology Letters, IEEE*, vol. 20, pp. 2066-2068, 2008.
- [5] H. Ahmad, M. Z. Zulkifli, A. A. Latif, and S. W. Harun, "Tunable dual wavelength fiber laser incorporating AWG and optical channel selector by controlling the cavity loss," *Optics Communications*, vol. 282, pp. 4771-4775, 2009.
- [6] P. J. Moore, Z. J. Chaboyer, and G. Das, "Tunable dual-wavelength fiber laser," *Optical Fiber Technology*, vol. 15, pp. 377-379, 2009.
- [7] C. H. Yeh, C. W. Chow, F. Y. Shih, C. H. Wang, Y. F. Wu, and S. Chi, "Tunable Dual-Wavelength Fiber Laser Using Optical-Injection Fabry-Pérot Laser," *Photonics Technology Letters, IEEE*, vol. 21, pp. 125-127, 2009.

- [8] M. K. Smit, "Progress in AWG design and technology," in *Fibres and Optical Passive Components, 2005. Proceedings of 2005 IEEE/LEOS Workshop on*, 2005, pp. 26-31.
- [9] P. Munoz, D. Pastor, and J. Capmany, "Modeling and design of arrayed waveguide gratings," *Lightwave Technology, Journal of*, vol. 20, pp. 661-674, 2002.
- [10] H. Xiaoying, D. N. Wang, and C. R. Liao, "Tunable and Switchable Dual-Wavelength Single-Longitudinal-Mode Erbium-Doped Fiber Lasers," *Lightwave Technology, Journal of*, vol. 29, pp. 842-849, 2011.
- [11] X. Liu, X. Yang, F. Lu, J. Ng, X. Zhou, and C. Lu, "Stable and uniform dual-wavelength erbium-doped fiber laser based on fiber Bragg gratings and photonic crystal fiber," *Opt. Express*, vol. 13, pp. 142-147, 2005.
- [12] J. Im, B. Kim, and Y. Chung, "Tunable single- and dual-wavelength erbium-doped fiber laser based on Sagnac filter with a high-birefringence photonic crystal fiber," *Laser Physics*, vol. 21, pp. 540-547, 2011.
- [13] Y. I. Khanin, *Fundamentals of Laser Dynamics*. Cambridge: Cambridge International Science Publishing Ltd., 2006.
- [14] T. Erneux and P. Glorieux, *Laser Dynamics*. New York: Cambridge University Press, 2010.

Chapter 6

Conclusions

6.1 Conclusions

6.2 Future Works

6.3 Other Applications

6.1 Conclusions

A thorough report of the work on acousto-optic sensor based on fibre laser dynamics has been presented in this thesis. The purpose of this acousto-optic sensor is to resolve current issues of achieving unassisted optical microphone. Chapter 2 explored the principles of EDFL dynamics from basic rate equations of EDFL. From the rate equations, the steady state, linear stability, and turn on transient effect of EDFL are discussed analytically. Same theoretical analysis was performed in the EDFL condition and the modulation of EDFL by pump and loss are discussed.

Optical Microphone:

In chapter 3, the basic setup of the acoustic sensor which was formed with free running Fabry-Perot fibre laser with an EDF as the gain medium has been demonstrated. In this condition, multiple lasing peaks are observed due to the broad emission spectrum and long fibre laser cavity. The output power is found to be fluctuating at a frequency region of 22.5 kHz when pumped with a power of 15.7 mW. This fluctuation frequency is found to be related to the pump power and is known as the resonance frequency. The stronger the pump power, the higher the resonance frequency and they can be related by the Eq. (3.7),

$$\omega^2 = 120P - 1400 \quad (6.1)$$

where ω is the resonance frequency and P is the pump power.

The turn on transience of the fibre laser is demonstrated by switching the pump power from zero to a level above the lasing threshold. There are three different regions that were observed in the turn on transient which are the latency region, spiking region, and relaxation oscillation region. All three of them depended on the pump power being above the threshold.

As the pump power increase,

- (a) the turn on time decrease,
- (b) the spiking power increase, and
- (c) the damping effect decrease.

In addition, the relaxation oscillation measured in the turn on transient experiment is found to be very close to the resonance frequency measured from the fibre laser noise.

Modelling of the turn on transient effect was presented in the same chapter by using the equations developed from the same rate equations. The model was successful in simulating the pulsing and relaxation oscillation regions, but they failed to produce the latency period values close to the experiment results. This is due to the over simplification and linearization on the equations used in the model during its development. End of the chapter demonstrated the modulation of the fibre laser using both pump modulation and loss modulation. Both modulations show similar behaviour in the transient region, but loss modulation is behaved in chaotic condition which is much difficult to analyse. The loss modulation shows that the setup is sensitive to the vibration which is one of the acoustic waves form without any diaphragm as intermediate. Hence, the first objective of the research was achieved in this section.

In chapter 4, an unassisted optical microphone is presented by adding a 25 km long conventional SMF fibre as sensing medium. A 500 Hz sound wave with 100 dBC SPL is generated to modulate the OM. Suppression of the lasing in EDFL by the acoustic modulation is observed. Furthermore, the fluctuation intensity and the average output power is observed to be higher when under modulation of a higher sound level and they are almost linearly dependent. When compared to electrical microphone, OM will have slightly higher signal to noise ratio at 43.5 dB. However, it seems to have an output pattern which is in a more spiking form instead of the

conventional sinusoidal form of the incident sound. This spiking effect is generally generated by the laser dynamic behaviour due to the loss modulation during the compression and rarefaction of the fibre particles. These generated spikes are found to be periodic and observable as a contribution to the resonance frequency when we observed the FFT spectrum of the OM output. They also simultaneously contributed to the hissing background noise during sound recording.

The sensitivity of the OM is found to be different when it is connected to SMF with different lengths due to the difference in the interaction surface area. A 500 m SMF sensing medium will have a lower sensitivity, down to the sound level of 79.6 dBA SPL, while a 25 km and a 50 km will have sensitivity of 69.8 dBA SPL and 66.2 dBA SPL respectively. This means that the longer the fibre, the higher the sensitivity of the OM. Hence with the 25 km long fibre, the objective to obtain a large area sensing that can distribute out for length more than 10 m length is achieved.

A fibre spool of a few tens of kilometre length is only suitable for large area distribution sensing as it is very bulky to operate as a single point sensing device. Replacing the sensing medium to an 80 μm SSMF was shown to enhance the sensitivity and indirectly achieving the objective of reducing the fibre length for sensing medium.

High Sensitive Optical Microphone:

An 80 μm fibre with a smaller cladding thickness allows higher penetration of acoustic energy into the fibre core. To achieve similar sensitivity with a 25 km at about 70 dBA SPL, only 10 m of SSMF was needed and this reduced the fibre length dramatically. Utilizing a shorter fibre laser cavity length has a large effect on the noise resonance frequency. From experimental results, a shorter laser cavity will offer a larger tuning range of the noise resonance frequency. This noise frequency is found to be important in acoustic modulation as the sensitivity of the OM to different frequency is

dependent on the resonance frequency distribution of the OM. The difference in sensitivity of the OM to the frequency falls at the peak of the resonance frequency with the frequency out of the resonance frequency distribution can be as large as 14 dB.

Other than having dissimilar sensitivity, the resonance frequency distribution also determined the optical output pattern when modulated at different frequencies which can be basically categorized into 3 different regions which are:

- (a) multiple satellite pulses region where other than the main pulses generated at the modulation frequency, there exist multiple satellite pulses in between main pulses; and the frequency of these satellite pulses will always fall within the resonance frequency peak distribution,
- (b) pulses region where large pulse are generated at the modulation frequency, and
- (c) sinusoidal oscillation region where the output pattern is similar to the acoustic wave pattern which modulated the OM.

To achieve high sensitivity, the pulses region is given priority, but the region is limited to a window of about 8 ~ 10 kHz. The modulation of acoustic wave from 100 Hz up to 100 kHz is possible by connected a 10 m SSMF and changing the pump power from 10.8 mW to 68.5 mW. Besides 10 m, SSMF at length of 1 m, 20 m, and 1 km are tested and their k value were calculated which represent the resonance frequency tuning ability at different pump power. Their k values are 195.93 (Ws)^{-1} , 128.86 (Ws)^{-1} , 90.98 (Ws)^{-1} , and 5.99 (Ws)^{-1} for SSMFs of lengths 1 m, 10 m, 20 m, and 1 km respectively. The larger the k value, the wider the resonance frequency tuning range. By using a 10 m of SSMF, a sensing medium spool in a flat circle with diameter not more than 5.5 cm can be achieved to deliver the second objective of this research.

Further Sensitivity Enhancement:

Fibre laser dynamics based OM realized the unassisted OM for airborne sound sensing. However, the sensitivity is low compared to commercially available microphones. Modulation of the optical wave in the OM is possible only when the laser dynamics is triggered. A dual wavelength fibre laser was shown to enhance the sensitivity of the OM to a level lower than the laser dynamics triggering level.

An AWG was chosen to generate a dual wavelength fibre laser by attaching it to the EDF end. The total output power from the OM is stable and similar to the previous setup with a high frequency fluctuation at frequency 20.8 kHz. We observed larger output fluctuations when the output of individual wavelength was observed separately from AWG's output channels due to the modes competition. Mode competition between these two wavelengths caused their powers to fluctuate in an inverted direction. This means that the gain of one wavelength will cause a comparable loss to the other wavelength, stabilizing the summation of both outputs. This is because the total gain of the OM is constant although the gain of each wavelengths fluctuating.

In weak sinusoidal acoustic wave modulation regimes (65 dBA SPL) at 500 Hz where the dynamic behaviour is not being triggered, the output of each wavelength shows modulated sinusoidal waveform instead of a spiking behaviour. However, the sinusoidal waves of both outputs were 180° out of phase and were inverted waveforms of one another. The summation of both output resulted in a stable output where the modulation cannot be observed due to the constant gain of the OM. When the acoustic wave intensity was increased (to 88.3 dBA SPL) above the dynamic triggering level, both outputs will be in phase causing the total output power to fluctuate. The ability to sense the acoustic wave below the dynamics triggering level improved the OM sensitivity for more than 23 dB when no sensing medium is connected. Thus, with the

sensitivity enhancement, the third objective has been achieved by improving the sensing threshold down to 65 dBA only.

The output power of each wavelength is observed to fluctuate at two different frequencies. The FRF distribution is caused by the fibre laser system while the SRF is caused by mode competition between the two wavelengths. The laser will always tend to oscillates at the FRF which determines by the gain, cavity loss, and cavity length. However, when there is dual wavelength mode competition, mode hopping is occur between two wavelength and cause the oscillation take place in turn by each wavelength. This was observed clearly when the OM was modulated under a strong acoustic wave. When one wavelength obtained a higher gain to generate pulses, the optical power of the other wavelength will remain stable at a relatively low level. This is inverted when the other wavelength obtained a higher gain following mode competition. This effect caused the generation of the SRF which actually the frequency of mode hopping.

From the study, the SRF is related to the different in power of the two lasing wavelengths, but not on the selected wavelengths or the spacing between the wavelengths. The larger the power difference, the lower the SRF. This implies that the ability for one wavelength to compete with other wavelength is dependent on its lasing power. Hence, wavelengths with comparably lower power will generate a lower repetition rate pulses when it is modulated above dynamic threshold. Such behaviour offers the ability to generate of cleaner pulses at a low repetition rate when modulated at low frequencies or at audible frequencies.

In conclusion, an unassisted optical fibre based microphone which is sensitive to airborne sound based on the principles of laser dynamics and dual wavelength modes competition have been demonstrated. The dual wavelength mode competition is responsible for sensitivity enhancement with sensing threshold at 65 dBA as well as

noise reduction. The flexibility of the OM design allows us to connect different sensing mediums at different length, making it possible for us to have “point” sensing with sensor size less than 6 cm diameter in circle or “unlimited” sensing points for large area distribution sensing which can be distributed out for length longer than 10 m. The OM is capable of detecting vibrations, audible sound, as well as ultrasound of up to 100 kHz. The achievements have fulfilled all the objectives of this research.

6.2 Future Work

The foremost and on-going development of this project is to optimize the modulated output of the acoustic sensor so it is as close as possible to the modulation acoustic wave. More work can be done in the study of dual wavelength competition in fibre lasers as there are a considerable number of unexplored characteristic and might have the potential for a better acoustic sensor. The dual wavelength fibre laser sensor offers smoother oscillations at low intensity modulations and cleaner pulse generation at high intensity modulation.

In addition, a more detailed study is planned for the sensing medium. Different shapes and arrangements of attaching the sensing mediums will most likely impact the sensor sensitivity and applications. Different designs of sensing mediums for single direction sensing or multiple direction sensing will be carried out as well. The material of the sensing medium will be one of the more interesting studies, as well additional effects such as the effects of the nonlinearity of the fibre to the modulation of the acoustic wave.

6.3 Other Applications

The acoustic sensing discussed in this thesis is focussed on airborne sound sensing and partly on vibration. Other than the application as optical microphone and ultrasound sensor, the sensor design is suitable for hydrophones as well [1]. Some tests were done on the special designed optical microphone for hydrophone usage during this project and the results are convincing as it exhibit behaviour similar to OM. There might also be additional application in building health structure monitoring [2] or as seismic sensors [3] which is one of the applications which we are keen to look into.

References

- [1] Z. Wang and Y. Hu, "Frequency response of fiber-optic hydrophone with a novel mechanical anti-aliasing filter of side cavities," in *Communications and Photonics Conference and Exhibition (ACP), 2009 Asia*, 2009, pp. 1-2.
- [2] F. Ansari, "Structural health monitoring of slab-column connections using FBG sensors," *Journal of Civil Structural Health Monitoring*, vol. 14, pp. S1 - S7, 2012.
- [3] A. Laudati, F. Mennella, M. Giordano, G. D'Altrui, C. C. Tassini, and A. Cusano, "A Fiber-Optic Bragg Grating Seismic Sensor," *Photonics Technology Letters, IEEE*, vol. 19, pp. 1991-1993, 2007.

Appendix



Non-membrane optical microphone based on longitudinal modes competition

Chang Hong Pua^{a,*}, Siti Fatimah Norizan^a, Sulaiman Wadi Harun^b, Harith Ahmad^a

^a Physics Department, Faculty of Science, University of Malaya, Kuala Lumpur 30603, Malaysia

^b Electrical and Electronic Department, Faculty of Engineering, University of Malaya, Kuala Lumpur 30603, Malaysia

ARTICLE INFO

Article history:

Received 18 November 2010

Received in revised form 13 April 2011

Accepted 13 April 2011

Available online 22 April 2011

Keywords:

Fibre optic sensors

Acousto-optical devices

Optical microphone

Longitudinal mode competition

ABSTRACT

We propose and demonstrate a simple and cost effective non-membrane optical microphone (OM) consisting of only a standard erbium doped fibre amplifier (EDFA) and a 25 km of conventional single mode fibre (SMF) as the sensing medium. A photo detector is used for data acquisition. The proposed setup utilizes the disturbances in the competing longitudinal modes in a low reflectivity fibre resonator whereby airborne acoustic waves impacting the surface of the fibre will modulate the intensity of the optical signal in the fibre. This modulation frequency is analyzed using the fast fourier transform (FFT) technique to extract the information embedded in the optical signal. The experiment shows that the system is capable of picking up the airborne acoustic waves and can find many potential applications.

© 2011 Elsevier B.V. All rights reserved.

1. Introduction

The principal of optical microphones (OMs) has gained significant interest as a medium of communications since the early 1880s with the invention of the first “photophone” by Bell [1]. Since then, advances in optics and photonics technology have motivated many approaches towards the development of optical microphones, with the usage of fibre gratings [2,3], Fabry–Perot [4,5], Michelson [2,6] and Mach–Zehnder interferometers [3,7] and also the use of cantilevers [8,9]. Of late, OMs has seen a renewed interest in the area of research and development especially due to its advantages such as immunity to harsh environments, free from electromagnetic (EM) interference which can find usage in areas of flammable and explosive environments [4]. OMs operate on a slightly different principal as that of electrical based microphones, whereby the OM uses an optical carrier signal. In this manner, airborne sound or acoustic waves modulate onto the carrier signal, where it then passes the information onto a data retrieving system. Basically, the OM can be configured to detect intensity, polarization or phase modulation [1] that put this device into a higher footing as compared to other electrical based systems.

Typically, optical fibres as such have poor sensitivity to airborne acoustic waves, and this is attributed largely to the impedance mismatch between the fibre and the surrounding air. As a result to overcome this issue, membranes or similar low-mass structures are normally implemented in an OM as to mediate the impedance

difference. However, this adds into the complexity of the setup of the OM. This requires additional transduction stages involving the displacement of the membrane due to acoustic pressure, the phase shift arising from the displacement of the membrane and also its effect on the optical intensity, and finally the conversion of the optical signal to an electrical signal, where it needs to be processed [1]. On top of this, sophisticated techniques such as homodyne or heterodyne detection systems are required.

As a means to overcome this complexity as mentioned above, a novel and simple OM based on phase modulation phenomena is proposed in this paper. The proposed setup is able to detect airborne acoustic waves ranging from 100 Hz to 20 kHz without the need for a membrane or a low-mass structure, and therefore reducing the transduction stages to only two steps, namely, the transduction of the acoustic pressure in the form of modulation onto the optical signal in the fibre, which is due to the phase shift and also the retrieval of the optical modulation into an electrical signal. This significantly reduces the complexity and cost of the system but it comes with certain limitations such as the modulation pattern being in a pulse instead of sinusoidal that causes “hiss noise” when the modulation signal is reproduced in the acoustic form and the generation of a series of harmonic frequencies. Hence, voice over fibre is possible with this setup but a good filtering system is required as to improve the performance before it can be commercially viable.

2. Experimental setup and principle

The proposed setup consists of a 3 m erbium doped fibre (EDF) that is pumped by a 980 nm laser diode capable of generating up to 160 mW. On top of this, a 980/1550 nm wavelength division

* Corresponding author. Fax: +60 3 79674282.

E-mail addresses: shen82@siswa.um.edu.my, harith@um.edu.my (C.H. Pua).

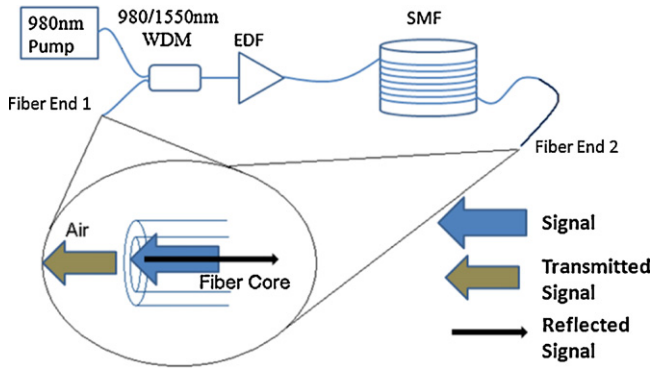


Fig. 1. Illustration of all optical microphone experimental setup.

multiplexing (WDM) coupler is used as to combine the free-running laser signal with the pump into a 25 km conventional single mode fibre (SMF-26) as shown in Fig. 1. The EDF generates amplified spontaneous emission (ASE) in the C-band region (1520–1560 nm) when pumped at 980 nm via the excitation and de-excitation of the erbium ions in the EDF. The generated ASE then travels in both directions of the optical fibre, in the forward and backward direction. The 1550 nm port of the WDM coupler is left unconnected and cleaved at 90° as to provide the 4% Fresnel reflection which in this case acts as a mirror in this cavity. The other end of the fibre, after the 25 km spool of SMF-26 is also left unconnected and cleaved at 90° so as to create the second mirror for the cavity. Basically, this cavity acts as a linear cavity with mirrors of low reflectivity at either end as shown in the inset of Fig. 1. In this setup, the EDF provides the active gain medium for the required amplification on the modulated signal and with the two mirrors, laser oscillation can be created.

As in any laser cavities, either in bulk or fibre based optics, there will be quite a large number of longitudinal modes oscillating at the same time. This can only take place when the gain of the amplifying medium exceeds the loss of the gain cavity. This can also be translated as to when the ASE overcomes the loss of the cavity. Those longitudinal modes falls within the maximum gain region will survive better as compared to those modes at the end of the gain curve. These modes are observed to be around the region of 1529 nm. The longitudinal modes within this region will oscillate simultaneously and will undergo mode competition as a result of the gain and homogenous nature of the EDF.

The longitudinal modes that are utilized as the information carriers in this setup are those modes that satisfy the specific conditions of the resonator geometry, the reflectivity of the mirrors and the gain spectrum of the medium. The modes of oscillation generated are in the form of standing wave patterns that are produced between the two fibre ends. The wavelength (or frequency) that are produced will be governed by Eq. (1):

$$\Delta\lambda_{\text{res}} = \frac{\lambda_0^2}{n_r L} \quad (1)$$

where L is the length of the cavity, and in this case is the sum of the length from the WDM, EDF and the 25 km SMF-26. λ_0 is the centre wavelength, and n_r is the effective refractive index of the core. Depending on the bandwidth of the gain spectrum above the threshold, it is possible to generate multiple periodic sequences of longitudinal modes. The sustainability of these longitudinal modes is highly dependent on the phase interference of the oscillating light and as such small external disturbance like airborne acoustic waves can cause phase shifts of the longitudinal mode and thus reduce lasing, or in an extreme case can terminate the lasing of some modes. Utilizing this phenomenon, it is thus possible to detect

acoustic waves traveling in the air that impact on the optical fibre surface.

As the light waves oscillate in the resonator, one of the important parameters that are connected to the oscillating modes is the resonator lifetime, or sometimes called the photon lifetime. This is given in Eq. (2):

$$\tau_{\text{res}} = \frac{L_{\text{opt}}}{c_0 |\ln(GV\sqrt{R_1 R_2})|} \quad (2)$$

where c_0 is the speed of light, R_1 and R_2 are the reflectivity of both end mirrors, V is the transmission constant which also includes the optical fibre loss and G is the amplification gain. The laser threshold is reached at $GV\sqrt{R_1 R_2} = 1$ and when $GV > 1$, it will show an increase in the resonator life time [11]. Since R_1 and R_2 are fixed in the setup, G and V play an important role in the lasing process. On top of this, the resonator will sustain oscillations for frequencies that correspond to a round-trip phase shift that corresponds to a multiple of 2π . For a resonator devoid of active atoms, which are sometimes called 'cold' resonators, the round trip phase shift is simply $k2L = 2\pi\nu L/c = q2\pi$. Those modes that satisfy this phase shift of 2π will be the modes that oscillates. Any external disturbances that changes these phase shifts of 2π will inhibit these modes from oscillating. This implies that any external disturbance, for instance in the form of an acoustic wave can disrupt those modes that oscillate and can cause instability in the laser resonator. This instability provides the necessary mechanism whereby the external disturbance is being translated into the optical carrier wave that is then detected optically.

3. Experimental results and discussion

The experimental results as shown in Fig. 2 illustrate the optical spectrum of the ASE generated with and without the presence of acoustic waves at 2 pumping powers of 16 mW and 27 mW. Due to the broad ASE spectrum of the EDF emission and also the long cavity setup which consists of a 25 km SMF-26, huge numbers of longitudinal modes which can be created within the 1530 nm region. These modes can also be computed by using Eq. (1) for the case of a 'cold' resonator. In the case when there is no acoustic wave acting on it, a broad ASE spectrum with spikes is present as shown in dark blue lines in Fig. 2(a). As a result of homogenous broadening in the EDF, there will be a tendency of mode competition occurring, that can result in instabilities in the lasing action. When this fibre is exposed to acoustic waves, the condition of a phase shift of 2π to sustain the oscillation may not be met. Due to the presence of the acoustic wave and as a result of the compression and rarefaction of the acoustic wave in the fibre, this causes a change in the refractive index and will lead to a phase shift of the oscillating modes. Fig. 2(b) shows the output spectrum with and without an acoustic wave at a pumping power of 27 mW. This pump power is higher than that of Fig. 2(a) and this power is able to generate more population inversion, exceeding that of the threshold value and thus can support more oscillation modes. This can be seen in Fig. 2(b) whereby even when the acoustic wave is being applied to the system, there are still oscillating modes riding on top of the ASE spectrum, but less as compared to the case of without the acoustic waves.

In most cases many longitudinal modes can oscillate simultaneously, however, different modes have different gain, loss and saturation parameters due to the spectral emission probability of the EDF. These different modes will then compete for the available population inversion in the laser gain medium [10] and the oscillation of one mode will reduce the gain available for the other modes, thus making the lasing wavelengths unstable. Under such unstable lasing conditions, the lasing effect will be suppressed when there is any external disturbance such as an acoustic wave. As longitudinal

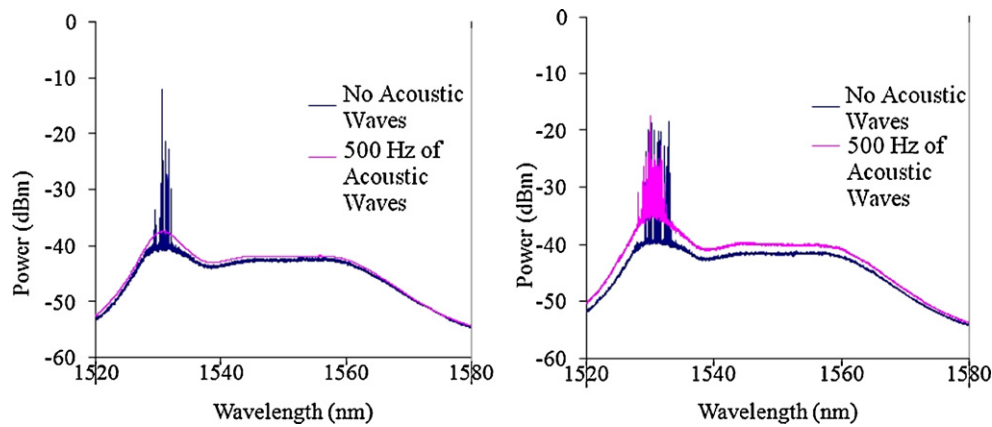


Fig. 2. Optical spectrum of the ASE generated with and without the presence of the acoustic waves at different 980 nm pumping powers to the EDF: (a) 16 mW and (b) 27 mW.

modes are standing waves created due to the cavity geometry, thus the interaction of the acoustic waves with the fibre causes uneven tension and vibration and hence changes the phase of the propagation signal. This change of phase will destroy the original standing waves that buildup in the cavity and thus causes the system to lose its lasing characteristic temporary as mentioned earlier.

However the total suppression of the lasing effect is highly dependent on the parameters G and V in Eq. (2). To obtain total lasing suppression, the 980 nm pump laser power is tuned as to determine the value of G in the system, so that its value is near the lasing threshold that is given by $GV\sqrt{R_1R_2} = 1$. As such, when the fibre interacts with the acoustic waves, it will experience a phase change that induces a loss in the system that in turn reduces the value of V . This will make $GV\sqrt{R_1R_2} < 1$ and hence inhibit the lasing action. On the other hand, in the case of a higher pump powers, any change of V due to external factors will not cause $GV\sqrt{R_1R_2}$ to be less than 1 due to the high value of G , which will therefore still support some modes to oscillate. Furthermore, the destruction of the standing waves as a result of the phase shift will reduce the stimulated emission process in the system and therefore more energy will be released in the form of spontaneous emission and causes the ASE level to increase. The increase in the ASE level will contribute to the increment of the total optical output power. As to observe this, Fibre End 2 is connected to an amplified photo detector where it will convert the optical signal into an electrical output that can then be displayed through an electronic oscilloscope. The output is then recorded for the case of a 500 Hz tone that is taken at different amplitudes at intervals of 1 s as shown in Fig. 3(a).

As can be seen from Fig. 3(a), the output power shows a random fluctuation with time, even without the presence of the acoustic waves. These fluctuations are attributed to the free oscillations of the various possible oscillating modes, optical phase noise as well as secondary factors such as temperature, pressure and tension changes [1]. When the acoustic wave is applied, the optical phase will experience periodic changes following the modulation of the acoustic waves. The compression and rarefaction of the imparted acoustic waves will cause the optical phase to be shifted and thus causes modulation onto the optical signal intensity. As a result, the optical signal now carries the same information as carried in the acoustic waves. Furthermore, the vibration amplitude of the optical output is increased as the amplitude of the acoustic wave increases, following the pattern of the acoustic vibration as shown in Fig. 3(a) for different input powers (given in terms of dB whereby the output power is measured against a reference point). The optical amplitude will reach a saturation value when the modulation of the acoustic waves is at -20 dB or more (90 dBA in the unit of acoustic waves). The sensitivity of the OM is measured using a Castle

sound level meter (GA213) as a reference and the sensitivity of the OM at a frequency of 500 Hz is 69.8 dBA taken in an environmental surrounding with a 48.0 dBA noise level.

Fig. 3(b) shows a plotted average optical power output against that of the applied acoustic power that shows a linear behavior until a value of -15 dB where saturation takes place. As the power of the acoustic wave increases, more energy of this wave will be imparted onto the optical signal in the optical fibre. This will result into higher losses in the system and thus suppresses lasing activity and at the same time generate more spontaneous emission, thereby increasing the ASE power level.

A comparison is performed between the OM and a standard electrical microphone simultaneously whereby both microphones are placed side by side at a distance of 1 m away from the source and this is shown in Fig. 4. Fig. 4(a) shows the screen shot of the noise level of both microphones as taken from the oscilloscope while Fig. 4(b) shows the output of both microphones when 2 kHz of the acoustic signal is being imparted to them. As can be seen, the responses of the OM are much higher as compared to electrical microphone; indicating that it is more sensitive. However the OM also carries a higher output noise level as compared to the electrical microphones. Besides this, the electrical microphone produces a nice sinusoidal waveform, closely matching the form of the acoustic wave. However, in the case of the OM, the output waveform is in the form of random spikes against times. The reason for this is that during the modulation, the system will be able to build up the population inversion and lasing will occur as a result of the shorter resonator lifetime as compared to the modulation signal. Thus multiple pulses can be generated within the modulation frequency.

Analysis is done as to extract the information carried by the modulated optical signals at Fibre End 2 (the lower trace of Fig. 4(b)). This setup is tested using acoustic signals of different frequencies, ranging from 100 Hz to 20 kHz in order to determine the bandwidth and accuracy of the OM. The acoustic signals are generated using a typical personal computer multimedia speaker. The Fast Fourier Transform (FFT) is performed using Matlab on these 5 s long samples. Fig. 5 shows the FFT results from the obtained optical output signals and only the positive parts of the graph are given for clarity.

Given in Fig. 5(a) is the extracted FFT signal of which shows the applied acoustic wave at 200 Hz with the accompanying harmonics at 400, 600 and 800 Hz. The line before 200 Hz is associated with the noise of the system. Similarly, the FFT of the applied acoustic wave at 1000 Hz as given in Fig. 5(b) shows many harmonics at 2000 Hz, 3000 Hz and so on, with any lines below 1000 Hz associated to the noise of the system. The same case is presented for applied acoustic waves at 10 kHz and 20 kHz as given in Fig. 5(c) and (d). For Fig. 5(c),

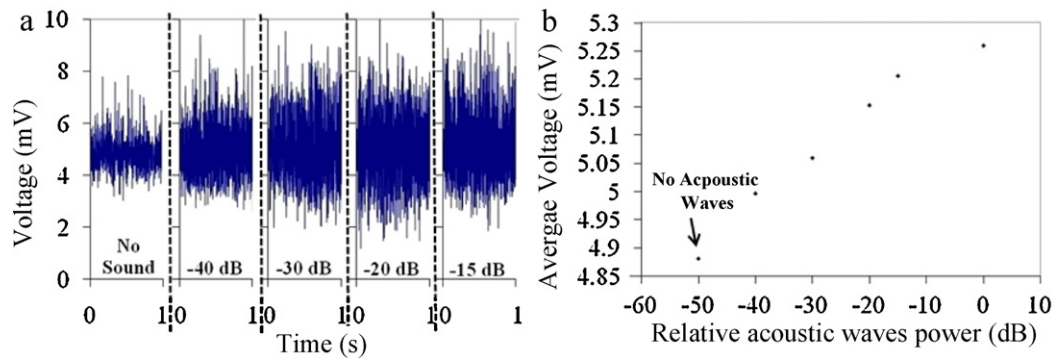


Fig. 3. (a) Electrical output from an oscilloscope after the photo detector, taken at different power levels of the acoustic wave at 500 Hz (that are generated by no acoustic signal, -40 dB, -30 dB, -20 dB and -15 dB of the acoustic signal power) and (b) the average electrical output for 1 s with the presence of acoustic waves of different power levels. The power level measurements are being taken against a fixed reference point and are given in dB and not in dBm.

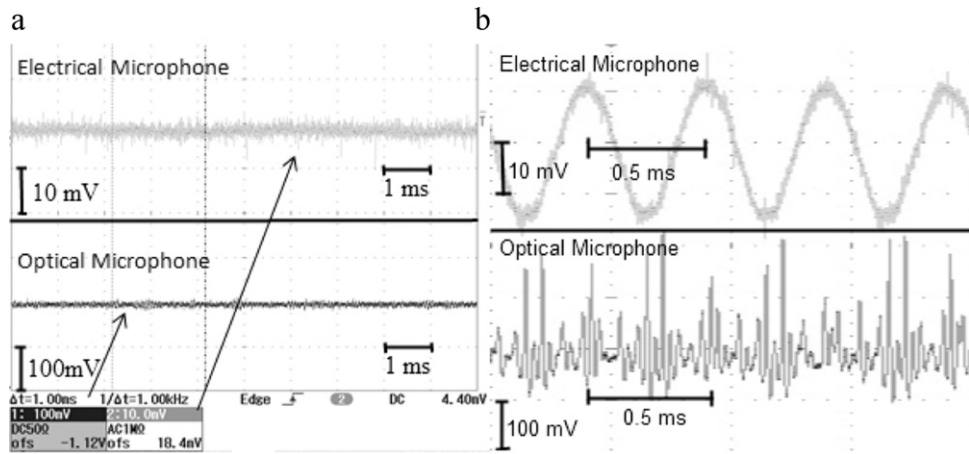


Fig. 4. Comparison of (a) background noise without acoustic signal and (b) with 2 kHz of acoustic signal between electrical and optical microphones.

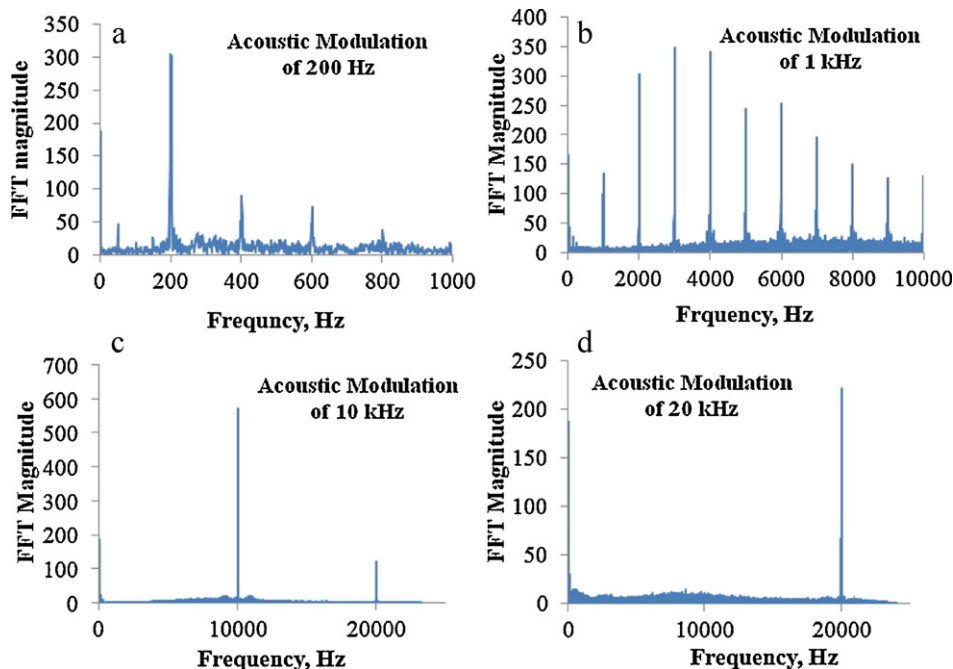


Fig. 5. The FFT positive output for sound generated at (a) 200 Hz, (b) 1000 Hz, (c) 10 kHz and (d) 20 kHz.

the FFT of the applied acoustic wave at 10 kHz shows a harmonic at 20 kHz, whilst in the case of Fig. 5(d) no harmonics are observed from the FFT spectrum.

The harmonic frequencies are coming from the side pulses generated in between the main frequency as shown in Fig. 4(b). The generation of the side pulses are due to the shorter resonator life-time as compared to that of the modulation signal as explained above. The existence of the harmonic waves comes about when the modulation amplitude is strong enough to suppress the random lasing so as to allow a higher population inversion to buildup and this will generate stronger side pulses. The presence of stronger side pulses will produce dominant, and at times higher amplitude harmonic frequencies as in the case of Fig. 5(b). In this setup, dominance of harmonic frequencies can be observed for the case of modulation frequencies between 800 Hz and 6 kHz. As the modulation frequency of the acoustic wave increases, such as in the case of 10 kHz, only a single harmonic is being observed. This is due to the low-amplitude side pulses being generated for this frequency. With further increases of the modulation frequency of up to 20 kHz, there are no harmonics observed from the FFT analysis. At this frequency, the modulation frequency is of the same magnitude as that of the build-up time for the oscillation, thereby inhibiting any random generation of laser oscillations. The existing experimental setup can only accommodate the present bandwidth being studied due to the limitation of the multimedia speaker. In an actual system, a sophisticated filtering technique is required to extract the frequencies of the object and reconstruct them back.

4. Conclusion

In conclusion, a non-membrane OM is presented using a conventional single-mode optical fibre (SMF-26) as the sensing medium in conjunction with a low-reflectivity erbium doped fibre laser for detecting airborne acoustic waves. The presence of the airborne acoustic waves is able to provide the necessary phase shift that will result in the suppression of the self-lasing effect and also to modulate the optical signal output power. The result shows that as the frequency of the acoustic waves vary from 100 Hz to 20 kHz, the optical output of the erbium doped fibre lasers will be modulated accordingly. From this modulation, the acoustic wave frequencies can be reproduced using the FFT technique. This method allows for an effective approach of detecting airborne acoustic waves for applications such as OMs, hydrophones and in the areas of ultrasound sensing.

Acknowledgements

The authors gratefully appreciate the financial support for this work provided by the University of Malaya (PPP Grant No: PS327/2009C), and all the facilities provided by The Photonic Research Centre, University of Malaya.

References

- [1] N. Bilaniuk, Optical microphone transduction techniques, *Applied Acoustics* 50 (1997) 35–63.
- [2] J.P.F. Wooler, B. Hodder, R.I. Crickmore, Acoustic properties of a fibre-laser microphone, *Measurement Science and Technology* 18 (2007) 884–888.
- [3] T. Iida, K. Nakamura, S. Ueha, A microphone array using fibre Bragg gratings, in: *Optical Fibre Sensors Conference Technical Digest, OFS 2002*, vol. 231, 2002, pp. 239–242.
- [4] J.K. Holger, O.P. Christian, R. Ingo, A fibre-optical microphone based on a Fabry–Perot interferometer applied for thermo-acoustic measurements, *Measurement Science and Technology* 21 (2010) 015302.
- [5] H. Sagberg, A. Sudbo, O. Solgaard, K.A.H. Bakke, I.R. Johansen, Optical microphone based on a modulated diffractive lens, *IEEE Photonics Technology Letters* 15 (2003) 1431–1433.
- [6] J.H. Chu, Y.H. Bak, B.K. Kang, U. Kim, K.W. Oum, J.G. Choi, D.S. Ko, Michelson interferometric detection for optoacoustic spectroscopy, *Optics Communications* 89 (1992) 135–139.
- [7] L. Kruger, H.J. Theron, Optical fibre Mach–Zehnder microphone, in: *Microwave and Optoelectronics Conference, IMOC 2007, SBMO/IEEE MTT-S International*, 2007, pp. 389–391.
- [8] M. Feldmann, S. Buttgenbach, Microoptical distance sensor with integrated microoptics applied to an optical microphone, in: *IEEE Sensors*, 2005, pp. 769–771.
- [9] K. Wilcken, J. Kauppinen, Optimization of a microphone for photoacoustic spectroscopy, *Applied Spectroscopy* 57 (2003) 1087–1092.
- [10] A.E. Siegman, Laser spiking and mode competition, in: *Lasers*, University Science Books, CA, USA, 1986 (Chapter 25).
- [11] R. Menzel, *Lasers*, in: *Photonics*, Springer-Verlag, Berlin, Heidelberg, New York, 2001 (Chapter 6).

Biographies

Chang Hong Pua was born in 1982. He received his B.Sc. and M.Sc. degrees in physics, from University of Malaya, Kuala Lumpur, Malaysia in 2006 and 2009, respectively. His M.Sc. research was related to fabrication process of planar light-wave circuit (PLC). He is currently a Ph.D. candidate in Photonics Research Center, Physics Department, Faculty of Science, University of Malaya who work on fibre optic acoustic sensor. His research interests include fibre optic sensor and applications, high power fibre lasers, and planar lightwave circuit.

Siti Fatimah Norizan received her B.S. degree from University of Malaya, Kuala Lumpur, Malaysia in 2008, majoring computational and electronic physic. Currently pursuing her Ph.D degree at Photonics Research Center, Physic Department Faculty of Science, University of Malaya. Her research is mainly in multiwavelength Brillouin Fibre Laser, fibre optics amplifier and fibre sensor.

Sulaiman Wadi Harun received the B.E. degree in electrical and electronics system engineering from Nagaoka University of Technology, Japan in 1996, and M.Sc. and Ph.D. degrees in Photonics from University of Malaya in 2001 and 2004, respectively. Currently, he is a full professor at the Faculty of Engineering, University of Malaya. His research interests include fibre optic active and passive devices.

Harith Ahmad has his B.Sc. (Hons) in 1979 from University of Malaya, his M.Sc. in high voltage technology and Ph.D. in laser technology in the year of 1980 and 1983 respectively from University of Wales, U.K. His initial works are mostly in solid state lasers and diode pumped solid state laser. Late in 1995, he undertakes research in optical fibre devices such as optical amplifiers and others and then move on to planar waveguides. His current research interest is in the areas of non linear optical effect in optical fibres and optical fibre sensors. His current position is a professor at Physics Department, University of Malaya.

Direct airborne acoustic wave modulation of Fabry–Perot fiber laser (FPFL) over 100 kHz of operating bandwidth

Chang Hong Pua,^{1,*} Harith Ahmad,¹ Sulaiman Wadi Harun,²
and Richard M. De La Rue^{1,3}

¹Physics Department, Faculty of Science, University of Malaya, 50603 Kuala Lumpur, Malaysia

²Electrical Engineering Department, Faculty of Engineering, University of Malaya, 50603 Kuala Lumpur, Malaysia

³School of Engineering, University of Glasgow, G12 8LT Scotland, UK

*Corresponding author: shen82@siswa.um.edu.my

Received 28 September 2011; revised 19 January 2012; accepted 9 February 2012;
posted 10 February 2012 (Doc. ID 154144); published 11 May 2012

The idea of applying a simple Fabry–Perot fiber laser (FPFL) set-up in a free-running condition as an acoustic sensing medium is proposed. Conventional optical microphone requires a stringently aligned diaphragm to mediate the acoustic impedance mismatch between air and silica fiber. Motivated by the difficulty of optical sensing of airborne acoustic waves, a new sensing method is proposed to sense acoustic waves without the assistance of a diaphragm as transducer. By studying the output power fluctuation of the FPFL, the operating bandwidth and sensitivity of the proposed sensing method are determined. The tunability of the resonant frequency from 5 kHz to 85 kHz allows sensing of acoustic waves in the range of 100 Hz to 100 kHz. Tuning of the resonant frequency can be performed by changing the optical pumping power from as low as 10 mW to 68.5 mW or higher. © 2012 Optical Society of America
OCIS codes: 190.3100, 280.4788.

1. Introduction

The birth of photonic technology has brought about a huge revolution in telecommunication, optoelectronic devices, and other applications such as environmental sensing. Replacement of copper wire by optical fiber in telecommunication, use of optoelectronic devices instead of electronic devices, and optical sensors instead of chemical, mechanical, or electrical sensors is becoming ubiquitous. Fiber optic sensing is one of the technologies that has attracted much interest due to its advantages such as compactness, flexibility, immunity to electromagnetic interference, inherent electrical isolation, superior dielectric properties, etc. [1,2].

Acousto-optic (AO) sensing is a field that began in 1880 when the first hydrophone was patented by

A. G. Bell [3]. Since then, research in acousto-optic sensors has expanded into optical microphones [4,5], ultrasound sensors [6], SONAR, vibration sensors [7], acoustic emission (AE) sensors [2], and seismic sensors [8]. Over a number of years, a variety of methods has been developed to exploit acousto-optic sensing, including Fabry–Perot interferometers [9], distributed feedback fiber lasers [10], and fiber Bragg gratings [11]. Ref. [10] has a similarity to the present work in that unassisted fiber was used in the experiments. It presents detailed analysis of the effect of an incident acoustic wave in air—in terms of the dynamic temperature and pressure effects that are produced and are strongly frequency dependent. Many of the AO sensing set-ups that have been demonstrated require stringent alignment, complicated apparatus and expensive instrumentation.

In this paper, we study the response of a free-running Fabry–Perot fiber laser (FPFL) to acoustic waves due to competition of multiple longitudinal

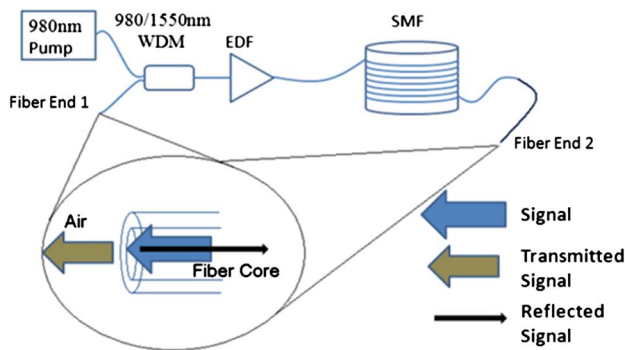


Fig. 1. (Color online) Experimental setup of linear cavity fiber laser.

modes in the laser. The interest in this study arises from the simplicity of the Fabry–Perot fiber laser setup—with only a 980 nm diode pump laser, WDM coupler, and Erbium Doped Fiber (EDF), which results in a flexible and compact sensor package. The set-up also offers customizability where different fiber or optical devices can be added into the basic setup to change the laser cavity length, cavity loss, and reflectivity. The operating power level can be tuned from as low as 10 mW up to 70 mW to suit different sensitivity and operating bandwidth requirements. This study provides a proof of concept for the feasibility of building new AO sensors for acoustic wave sensing in the bandwidth range from 100 Hz to 100 kHz, using the method proposed. In contrast to our previous work [12], where 25 km of standard single mode fiber (SMF) was used, the present work only uses 10 m of special fiber to achieve similar sensitivity, with larger spectral range up to 100 kHz.

2. Experimental Set-up

The experimental setup is a standard FPFL consisting of a 980 nm/1550 nm coupler, Erbium Doped Fiber (EDF) as gain medium, 10 m of bare (without jacket) special SMF (FiberCore SM1500 [4.2/80]) as part of the cavity, and a photodetector to convert the optical output to an electrical output at Fiber End 2, as shown in Fig. 1. The total length of the fiber set-up is about 20 m—in a cascade of 3 m of EDF, 7 m of coupling and connecting fiber, and 10 m of special SMF as sensing element. The 10 m special fiber is spooled on a compact disk (CD) holder to form a flat circular shape—so that the acoustic waves can have a strong interaction with the fiber surface. The setup before the SMF fiber is packaged into a homemade portable laser/amplifier device, together with the 10 m SMF, which is connected to it as shown in Fig. 2. This special SMF has been selected because of its thinner cladding (80 μm), which reduces the travel distance required for a radially propagating acoustic wave in the fiber cladding before it interacts with the optical signal in the fiber core and therefore translates into higher sensitivity. A similar set-up using a conventional SMF has also been studied to provide a reference. There are two reasons why a shorter fiber length has been selected in this research. One is the

size of the sensor, since shorter fiber cavity lengths are preferable for point sensing or small area sensing due to the resulting compactness—as compared with possible use of a few tens of kilometers of fiber on a drum [12]. A second reason is the tunability of the resonance frequency, which will be discussed later.

The linear cavity was formed by the $\sim 4\%$ Fresnel reflection from the cleaved fiber end that is exposed to air, as shown in Fig. 1. During the experiment, the 980 nm pump light is coupled into a 3 m long EDF section, without any seed signal. C-band amplified spontaneous emission (ASE) is generated by the erbium ions during excitation by the 980 nm pump. The power of the pump laser is increased until self lasing starts to occur in a wavelength region with positive net gain. A high inverted population is created at large pump power levels—and laser oscillation will take over from amplified spontaneous emission in the wavelength region that has the highest photon emission into the linear cavity. When lasing occurs under free running conditions with excitation of multiple axial modes there is no control of oscillating wavelength. Hence, multiple lasing peaks with broad ASE spectrum can be observed using an optical spectrum analyzer.

In the case of optical oscillation in an erbium doped fiber laser that is homogeneously broadened, mode competition becomes an issue. Modes with different gain, loss and saturation parameters, due to the spectral distribution of the emission probability of the EDF, will compete for the available population inversion in the laser gain medium [13]. Oscillation of one mode will reduce the gain available for another, hence the competition among the modes creates an unstable lasing condition. Longitudinal modes are modes created under a specific condition of resonator geometry and reflectivity. Oscillations at a particular optical wavelength generate a standing wave within the resonator. These standing waves must obey the rule that the resonator length L_{opt} has to be an integer multiple mode number, p_{mode} of half the possible wavelengths, λ_p , of the laser, according to the basic equation

$$\lambda_p = \frac{2L_{\text{opt}}}{p_{\text{mode}}} \quad (1)$$

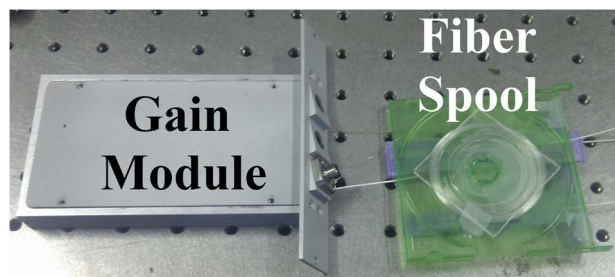


Fig. 2. (Color online) Er-doped fiber gain section pumped by 980 nm laser diode module with the fiber spool.

and the frequency spacing is, approximately given by

$$\Delta\nu = \frac{c}{2nL}, \quad (2)$$

where c is the speed of light, n is the fiber effective index and L is the cavity length, with $L_p = nL$. Competition among these modes will create an unstable, random lasing condition.

3. Results and Discussion

As mentioned in the previous section, multiple-mode competition will cause random self-lasing and leads to small, but rapid, fluctuations in the total optical output power. Figure 3(a) shows the optical output power measured using a fast oscilloscope and a linear photo-detector. It can be observed that the power fluctuation, observed as photodetector voltage, (<22.5 mV) is 7% of the average output power (320 mV) under 17.5 mW of pump power. At first sight, these fluctuations appear to be totally random. However, a certain frequency of regular fluctuation is clearly observable when the time scale is magnified to $500\ \mu\text{s}$ per unit distance along the horizontal axis, as shown in Fig. 3(a). This fluctuation falls within a

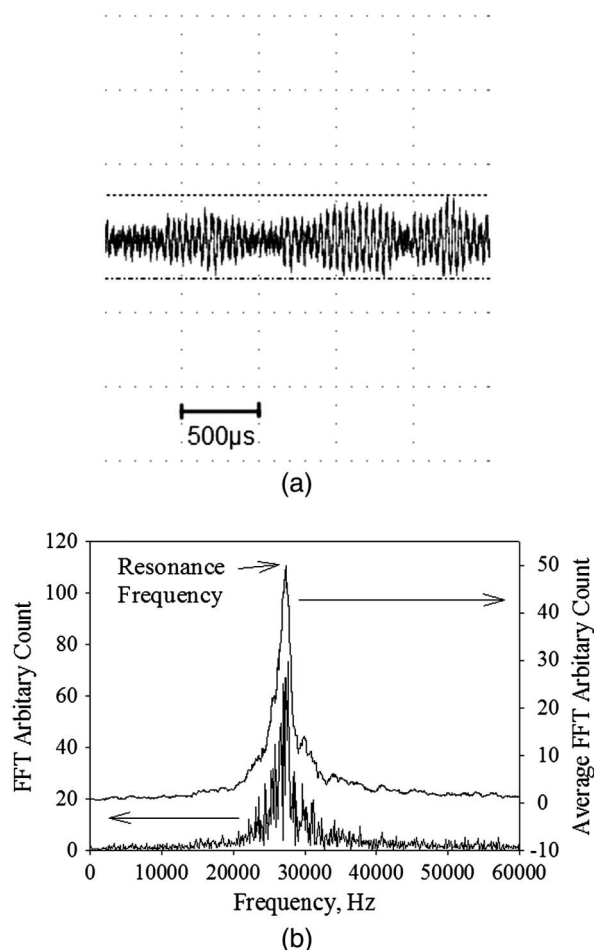


Fig. 3. Optical output noise from (a) electrical oscilloscope and (b) frequency spectrum analysis using FFT method.

limited frequency bandwidth under fixed operating parameters, when the Fast Fourier Transform (FFT) of the optical output is analyzed, as shown in Fig. 3(b). The average of the FFT counts was obtained, in order to create the cleaner spectrum shown in Fig. 3(b). We have observed a bulk noise spectral peak at ~ 27 kHz and identify it as a resonant frequency.

This resonant frequency does not exist at pump power levels below the lasing threshold (i.e. <6 mW), for which only ASE can be observed using the Optical Spectrum Analyzer (OSA). When the pump power is increased above 7 mW, random lasing peaks can be observed from the OSA in the 1530 nm wavelength region, superimposed on the ASE spectrum. From this point onwards, optical output power fluctuation can be observed, as shown in Fig. 3(a). The contribution of the observed frequency distribution centered at the resonance frequency is related to the self pulsing frequency of the FPFL. Successive FFT samples show significant variation in the estimated peak position, over a range of approximately 400 Hz.

The FPFL is generally known to be sensitive to acoustic waves. Acousto-optic modulation can be separated into three different techniques: which are amplitude modulation, phase modulation, and polarization modulation. This set-up applies amplitude modulation technique. When the acoustic waves or vibration interact with the FPFL, it will cause a certain degree of phase-shift on the current standing waves (modes) and hence generate destructive interference for modes that do not fulfill the condition described in Eq. (1). At the same time, random lasing is reduced and allows the system to build up a higher level of population inversion. The higher population inversion will contribute to a greater power laser pulse, at a frequency that falls within the resonant frequency distribution. Figure 4 shows the response for the optical output power, displayed on a fast oscilloscope, when a small impact occurs 1 m away from the FPFL, on the same optical table, generated by dropping a 253 gm piece of metal from a height of 1 cm above the table.

From Fig. 4, we can observe that the optical output power drops immediately after the impact, due to destructive interference and cavity loss within the cavity, followed by a sequence of pulses. The induced cavity loss causes a rapid drop in the optical power level, immediately after the impact, and allows the build-up of population inversion in the erbium ions. The higher level of population inversion leads to higher energy pulses being generated by the FPFL. The working principle is similar to acousto-optic Q-switching in a laser [14], where a high cavity loss is induced, in order to allow a larger population to build up. The highest pulse power generated is roughly 5 times larger than the average power before the impact. To understand in more detail about the characteristics of the FPFL as an acoustic sensor, we generated single tone acoustic waves to observe the acousto-optic interaction. The highly sensitive

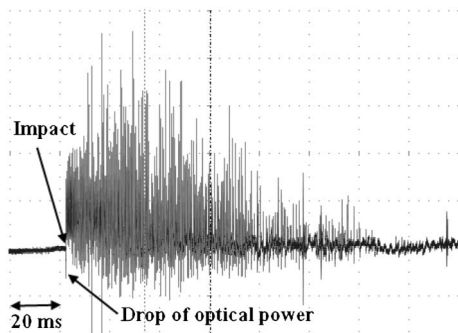


Fig. 4. Optical output of FPFL after the vibration impact.

nature of the FPFL allows direct interaction between an airborne sound wave and the light wave propagating in the fiber, something that was previously believed to be impossible without the assistance of a diaphragm or transducer, due to high impedance mismatch between air and glass [3]. The modulation of the optical output can be observed above an average sound level at as low as 69.8 dBA with 1 kHz acoustic waves.

The resonant frequency plays an important role in characterizing the “sensitivity” bandwidth of the system to acoustic wave modulation. Figure 5 shows three inset diagrams of the modulated optical output, captured using a digital oscilloscope, with an optical pump power level of 17.5 mW for different frequency sinusoidal sound tones, generated using a 2 cm diameter piezoelectric cylinder driven at 16 V amplitude by a signal generator facing directly onto the surface of the 10 m length of circularly spooled fiber, as shown in Fig. 6. Under this level of pump power, the system has a resonant frequency around 27.3 kHz, as shown in Fig. 5. The sound intensity levels generated at the different frequencies 15 kHz, 25 kHz, and 40 kHz were 93.9 dBA, 82.9 dBA, and 73.2 dBA respectively, measured using a sound meter. A-weighting parameter and extrapolation values (due to the A-weighting parameters that strictly apply only up to a frequency of 20 kHz) were used to calculate the sound intensity level in dB. The calculated sound levels were 99.9 dB, 94.4 dB, and 91.5 dB respectively.

There are several interesting phenomena that can be observed in Fig. 5, and one of them is that the output electrical signal at lower frequencies is in the form of discrete pulses instead of the sinusoidal wave-form of the incident sound waves. Besides that, it is also observable that higher amplitude optical pulses are generated when the tone is near the resonant frequency at 25 kHz, at a level that is approximately 10 dB larger than the output at 15 kHz and 40 kHz. Because the photo-detection process produces a photo current that is proportional to the incident optical power level, the *voltage* displayed on the oscilloscope is proportional to the incident optical power level. The observed signal level at 25 kHz therefore corresponds to an optical signal level that is 10 dB greater than the optical signal level at

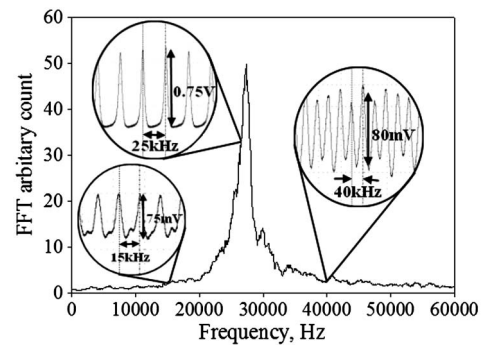


Fig. 5. Inset of Modulated optical output at 15 kHz, 25 kHz, and 40 kHz with respect to the average resonant frequency, with 17.5 mW pump power.

15 kHz. In terms of the resulting signal voltage levels, the electrical ratio is 20 dB.

Modulation by sinusoidal sound waves will cause the phase of oscillating modes to shift constantly—and to generate constructive and destructive interference within the laser cavity repeatedly. To study the relationship between the sensitivity of the setup and the resonant frequency, different frequency sinusoidal tones were generated and the peak-to-peak (P-P) oscillation value of the optical output was measured from fiber end 2 at a fixed pump power level of 17.5 mW. Figure 7 shows the resonant frequency distribution and the P-P optical output value when modulation at several different frequencies is applied. It is very obvious that the P-P value of the optical outputs is dependent on the resonant frequency distribution. Hence, by studying the resonant frequency distribution at different pump power levels, it is possible to tune the sensitivity range of the setup to meet the needs of acoustic wave sensing for different frequency range and bandwidth requirements. The high sensitivity spectrum covers a frequency band of about 8 kHz in the demonstrated setup and is followed by a pronounced drop to the low sensitivity region at a frequencies outside the range between 25 kHz and 33 kHz. With a resonance frequency at ~27.3 kHz, the device would be useful for high-sensitivity detection of ultrasonic waves at a known specific frequency. Possible applications included low frequency ultrasound detection (<100 kHz), e.g. for gas or vacuum leakage detection and SONAR. This device could also be useful for the detection of impulsive sound sources (e.g. sound

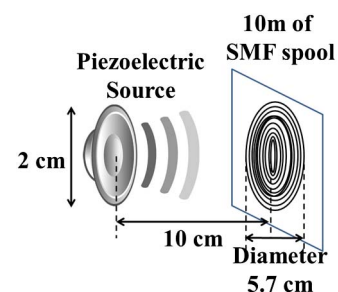


Fig. 6. (Color online) Acoustic excitation arrangement diagram.

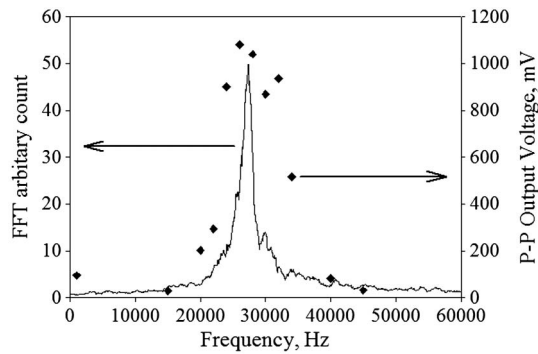


Fig. 7. Averaged resonant frequency distribution count (line) together with the average peak to peak (P-P) optical output (dots) from the modulated optical power at different frequencies.

generated by mechanical shock or impact), but the detection will be accompanied by a substantial amount of distortion. Such extreme changes of sensitivity cause problems for wide frequency band sensing, as spectrally flat sensitivity is almost always preferable in sensor applications. However, this characteristic could be useful in other applications that require high sensitivity and small frequency bandwidth at a known centre-frequency, together with filtering capability.

In our observation, the optical pulse repetition frequency not only depends on the acoustic wave modulation frequency but also on the resonant frequency. If the acoustic wave frequency is much lower than the resonant frequency, population inversion will build up in a shorter time than the modulation period. When a threshold is exceeded that is a function of the Er^{3+} lifetime and pumping rate, the system will begin to lase and thereby reduce the buildup of population inversion. Lasing occurs whenever the population inversion is sufficiently large to cause series of pulse trains with obvious major pulse with 3 kHz of repetition generated under modulation by 3 kHz acoustic waves. In addition, multiple side pulses were observed between the main pulses, because of easing of the population inversion buildup during the modulation period, as mentioned above. These side pulses will fit in between the main pulses, with the same time spacing, and the repetition frequency of all these pulses will always fall within the resonant frequency distribution, as shown in Fig. 8(a). As a result, this side pulse stream contributes to the harmonic frequency spectrum when Fast Fourier Transform (FFT) analysis is performed, as observed in [12].

On the other hand, when the modulation frequency is much higher than the resonant frequency, the optical output will be in sinusoidal form, instead of pulsed—as shown in Fig. 8(b). When the modulation frequency is very much higher than the resonant frequency, the sensitivity will be reduced, as mentioned above, due to weak suppression of modes in the cavity. This reduction in sensitivity will discourage the build-up of population inversion, which leads to no output pulse being generated.

Compression and rarefaction of the fiber caused by acoustic modulation, however, will still induce a certain degree of relative phase shift between the modes. The interference of the surviving modes will produce a clean sinusoidal optical output instead of pulses.

At pump power levels above 10.0 mW, which is the threshold for random lasing to occur due to modal competition, the optical power begins to fluctuate with a certain frequency distribution. Figure 9 shows the average frequency spectra of the recorded output power after Fast Fourier Transformation (FFT). Spectral distributions for different pump power levels are plotted and shown in Fig. 9(a).

The resonant frequency distribution represents the pulse frequencies or periods needed to build up inversion for lasing. As the pump power increases, more energy is absorbed by the gain medium and hence the population inversion build-up times that lead to lasing are shorter. Therefore, the observed resonant frequency shifts towards a higher frequency when the pump power is increased. We have also noticed that the shift in resonant frequency increases in a logarithmic manner with respect to pump power increase, as shown in Fig. 9(b). Hence, by tuning the pump power from 10.8 mW to 68.5 mW, the resonant frequency can be shifted from 5 kHz to 85 kHz. This result also means that the operating bandwidth can cover a range of frequencies, up to 100 kHz. In other experiments, we have noticed that a short cavity is the main factor in achieving a large resonance frequency tuning range with such an optical power range. The longer the cavity length, the smaller the tuning range, but the higher the sensitivity—as we have observed. Accordingly, in order to achieve a large tuning range, the potential sensitivity of the

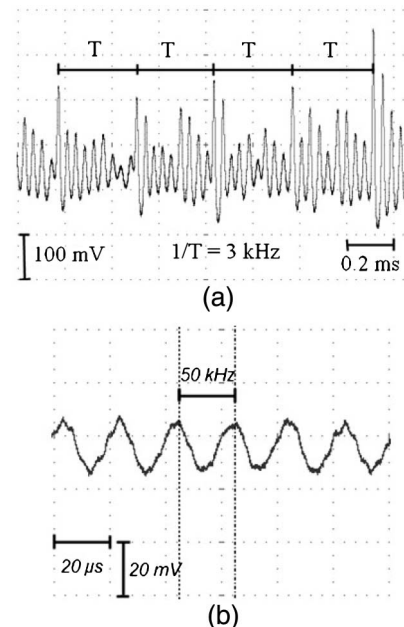


Fig. 8. Optical output under modulation of (a) 3 kHz and (b) 50 kHz acoustic waves, viewed on a digital oscilloscope.

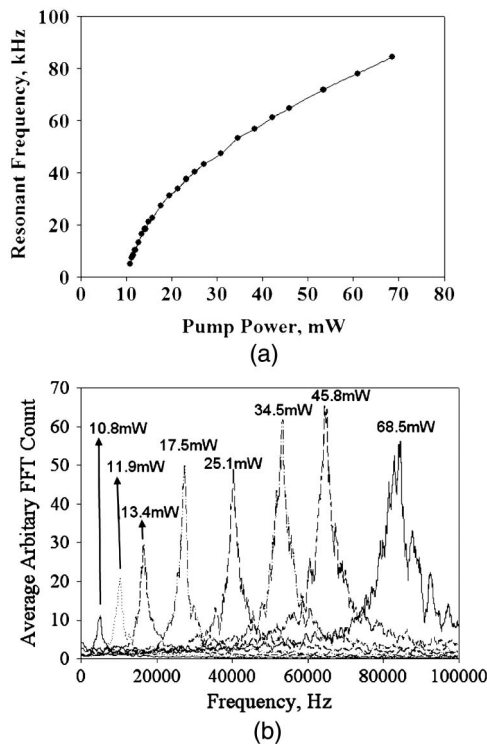


Fig. 9. (a) Averaged resonant frequency spectrum distribution of output power at different pump power, and (b) Resonant frequency at different pump power for 10 m SMF.

set-up has, in part, been sacrificed in the present research.

Considering the impact of temperature fluctuation during sensing to the laser stability, the FPFL set-up, excluding the diode pump laser, was heated using a hotplate to observe the shifting of the resonant frequency. An up-shifting in the resonant frequency by a maximum of 1 kHz is observed when the set-up is heated from room temperature (23 °C) up to 50 °C. Fluctuation of the resonant frequency close to 400 Hz, under a controlled environment may be caused by pump power fluctuation and the short sampling period of 2 s. We consider that shifting of the resonant frequency and sensitivity bandwidth by 1 kHz is not insignificant. Taking into account the 1 kHz fluctuation caused by the temperature changes and the 400 Hz fluctuation in the position of the resonance frequency, the setup has a high sensitive frequency band of about 6 kHz.

4. Conclusions

We have studied the response of an FPFL, operating in a free running condition, to both vibrations and airborne acoustic waves. Our results show that the interaction of acoustic waves with an FPFL will lead to laser pulses being generated by the FPFL. The

pulse frequency and amplitude are dependent on the resonant frequency of the FPFL, which can be obtained from the fluctuation of FPFL laser before external modulation. The resonant frequency distribution of a FPFL is determined by its operating bandwidth, which can be tuned from 10.0 mW to 68.5 mW by changing the pump power. With this ability, the set-up is able to sense airborne acoustic waves in a range from 100 Hz up to 100 kHz. We have also demonstrated a simple sensor set-up that has high sensitivity to airborne acoustic waves—a capability that was previously believed to be impossible without using a diaphragm or transducer. Since the whole fiber is sensitive to acoustic waves, it offers potential applications in both point sensing (short SMF fiber) and distributed sensing (long SMF), at a very low cost.

References

1. Z. Wang, Y. Hu, Z. Meng, and M. Ni, "Fiber-optic hydrophone using a cylindrical Helmholtz resonator as a mechanical anti-aliasing filter," *Opt. Lett.* **33**, 37–39 (2008).
2. T. Fu, Q. Li, Y. Liu, and J. Leng, "A novel embedded fiber optic acoustic emission sensor and its applications for monitoring failures of composite laminates," in *Smart Sensor Phenomena, Technology, Networks, and Systems 2009* (SPIE, 2009), 72931 A–72938.
3. N. Bilaniuk, "Optical microphone transduction techniques," *Appl. Acoust.* **50**, 35–63 (1997).
4. J. H. Cole, R. L. Johnson, and P. G. Bhuta, "Fiber-optic detection of sound," *J. Acoust. Soc. Am.* **62**, 1136–1138 (1977).
5. L. Kruger and H. J. Theron, "Optical fibre Mach-Zehnder microphone," in *Microwave and Optoelectronics Conference 2007 (IMOC 2007)* (SBMO/IEEE MTT-S International, 2007), 389–391.
6. D. Wiesler, H. Wen, A. B. Tveten, B. Danver, and A. Dandridge, "Fiber optic ultrasound sensors for medical imaging applications," in *Optical Fiber Sensors*, OSA Technical Digest Series, (Optical Society of America, 1997).
7. V. Kondakov, N. Meshcheryakov, and Y. Pod'yapolskii, "A fiber-optics sensor for monitoring vibration in the bearings of large stationary plant," *Meas. Tech.* **42**, 897–901 (1999).
8. A. Laudati, F. Mennella, M. Giordano, G. D'Altrui, C. C. Tassini, and A. Cusano, "A fiber-optic Bragg grating seismic sensor," *IEEE Photon. Technol. Lett.* **19**, 1991–1993 (2007).
9. J. K. Holger, C. O. Paschereit, and I. Röhle, "A fiber-optical microphone based on a Fabry-Perot interferometer applied for thermo-acoustic measurements," *Meas. Sci. Technol.* **21**, 015302 (2010).
10. S. W. Løvseth, J. T. Kringlebotn, E. Rønnekleiv, and K. Bløtekjær, "Fiber distributed-feedback lasers used as acoustic sensors in air," *Appl. Opt.* **38**, 4821–4830 (1999).
11. T. Iida, K. Nakamura, and S. Ueha, "A microphone array using fiber Bragg gratings," in Vol. 1 of *Optical Fiber Sensors Conference (OFS 2002) Technical Digest* (IEEE, 2002), 239–242.
12. C. H. Pua, S. F. Norizan, S. W. Harun, and H. Ahmad, "Non-membrane optical microphone based on longitudinal modes competition," *Sens. Actuators A* **168**, 281–285 (2011).
13. A. E. Siegman, "Laser spiking and mode competition," in *Lasers* (University Science Books, 1986).
14. A. E. Siegman, "Laser Q-Switching," in *Lasers* (University Science Books, 1986).

Study of Dual-Wavelength Mode Competition in an Erbium-Doped Fiber Laser (EDFL) Produced by Acoustic Waves

Chang Hong Pua, Harith Ahmad, Sulaiman Wadi Harun,
and Richard M. De La Rue, *Fellow IEEE*

Abstract—Distributed sensing using all-fiber laser-based acoustic sensors has been demonstrated recently for large area sensing. However, the sensitivity of this type of sensor has so far been much lower by comparison with currently available optical microphones. This paper studies the use of controlled interaction between the modes of oscillation in a fiber laser to enhance the sensitivity of acoustic wave detection. The responses of individual longitudinal modes to acoustic waves in a dual-wavelength fiber laser are demonstrated. With the experimental setup that has been developed, observation of a single wavelength output from the dual-wavelength laser shows optical responses to acoustic waves at 23 dB below the triggering threshold of laser dynamics, when compared with the previous scheme based on uncontrolled multimode operation.

Index Terms—Acoustic sensors, acousto-optic effects, erbium-doped fiber lasers, laser dynamics.

I. INTRODUCTION

IN OUR previous work [1], [2], we have demonstrated an all-fiber acoustic sensor in which the optical fiber forms the sensing medium. The direct modulation of optical frequency electromagnetic waves propagating in the fiber core by acoustic waves, based on the laser dynamic behavior, is a new approach to large area distributed acoustic sensing. Instead of limited multi-point sensing, the proposed approach is research directed towards sensing over an essentially unlimited number of points. The set-up can be connected to a long distributed optical fiber (with a typical length of 25 km) for large area sensing - or a short fiber spool (20 m) for point sensing.

Although our fiber-laser based method overcomes a conceptual barrier, so that optical airborne acoustic sensing is now possible without the need for an intermediate medium or a diaphragm, there are several problems that remain unsolved. The first issue is the random fluctuation of the optical output

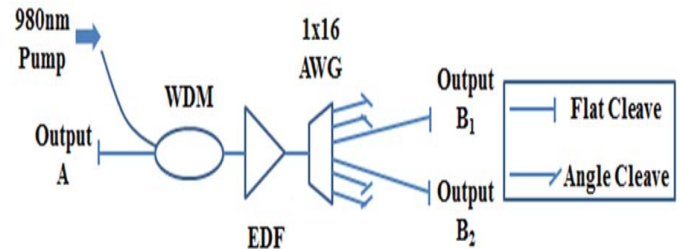


Fig. 1. Dual wavelength fiber laser setup constructed using 1×16 channels AWG.

power due to the laser dynamics that contribute to the unstable background noise of the sensor. The second issue is the transient generation during the modulation, which will distort the original acoustic wave pattern, although detection is still possible. The third issue is the absolute sensitivity of the sensor, which is still low compared to that of a diaphragm optical microphone.

In this paper, we shall describe how the mode competition behavior between light at the two selected wavelengths that are present in a dual-wavelength operation, linear-cavity, fiber laser enhances the sensitivity, in comparison with previous experiments.

II. EXPERIMENTAL SETUP

There are various methods for obtaining dual-wavelength fibre laser operation, including high-birefringence fibre loop mirrors [3], fiber-grating Sagnac loops [4], highly nonlinear fibre ring-lasers [5], Arrayed Waveguide Gratings (AWGs) [6] and so on [7], [8]. Our experimental set-up uses a 1×16 AWG for dual wavelength selection purposes and erbium doped fiber (EDF) as the amplifying medium in the laser cavity. The experiment setup is shown in Fig. 1. A 980 nm laser diode driven at a current of 79.2 mA is used to pump the 5 m long EDF at a power of 30.0 mW and to create a population inversion in the fiber. At this pump power, an Amplified Spontaneous Emission (ASE) spectra with an average power of 4.72 mW is generated. The ASE that propagates toward the AWG will be sliced into 16 different wavelength outputs, with one wavelength for each physical channel. Among the 16 channel outputs, 2 selected channel outputs, B₁ and B₂, have a flat-cleaved output to produce $\sim 4\%$ back-reflection as feedback to the system - while the remaining 14 channels are organized to

Manuscript received June 13, 2012; revised September 5, 2012; accepted September 11, 2012. Date of publication September 28, 2012; date of current version October 23, 2012. This work was supported in part by the University of Malaya under the HIR Grant Terahertz, UM.C/HIR/MOHE/SC/01, and the MOHE.

C. H. Pua and H. Ahmad are with the Department of Physics, University of Malaya, Kuala Lumpur 50603, Malaysia (email: shen82@siswa.um.edu.my; harith@um.edu.my).

S. W. Harun is with Department of Electrical Engineering, University of Malaya, Kuala Lumpur 50603, Malaysia (e-mail: swharun@um.edu.my).

R. M. De La Rue is with the School of Engineering, University of Glasgow, Glasgow G12 8LT, U.K. (e-mail: Richard.delarue@glasgow.ac.uk).

Color versions of one or more of the figures in this paper are available online at <http://ieeexplore.ieee.org>.

Digital Object Identifier 10.1109/JQE.2012.2219505

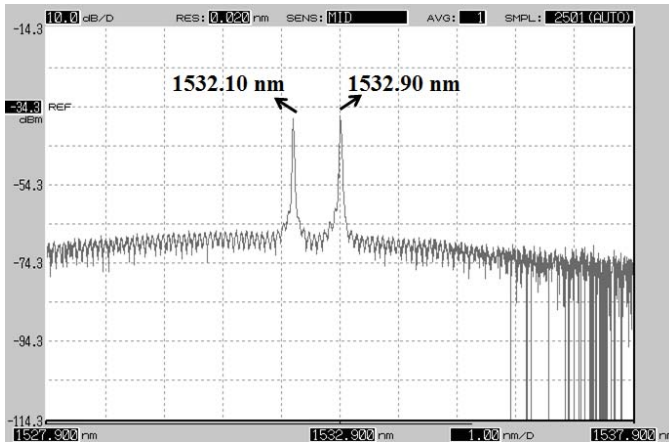


Fig. 2. Optical spectrum of dual wavelength fiber laser pumped at 23.2 mW.

have angle-cleaved outputs to avoid significant back-reflection. The two selected wavelengths are partly reflected back into the cavity and experience stimulated emission when passing through the EDF. The amplified dual wavelength signal then experiences another 4% back reflection at the other end of the laser cavity, which is labeled as output A – and the gain is sufficient to produce laser action at the two selected wavelengths. This setup forms a dual-wavelength laser cavity approximately 12 m long.

III. RESULTS AND DISCUSSION

Fig. 2 shows the optical spectrum of the dual-wavelength fiber laser obtained from output A, with lasing wavelengths of 1532.10 nm and 1532.90 nm. While for output B₁ and B₂, only single wavelength will be observed due to the demultiplexing effect of AWGs, B₁ will only carry the wavelength at 1532.10 nm and B₂ will carry the wavelength at 1532.90 nm. Dual wavelength lasing in such a system is unstable due to mode competition caused by strong homogeneous broadening and cross gain saturation of the EDF [9]. Although there already exist various methods that are able to stabilize multi-wavelength lasing by eliminating or reducing the mode competition, these methods have not been applied - since the natural response of the system without stabilization is the study of interest.

Fig. 3 presents the photodetected output power from output A and both outputs B, measured by a digital oscilloscope. Fig. 3(a) shows output A, which is the total optical output of the fibre laser in the backward direction, at a photo-detected voltage level of 2.18 V, and approximates an optical power of 1.15 mW. This output is stable at low frequencies, but exhibits fluctuations of the power level at frequencies in the range from 19.7 kHz to 22.0 kHz – with the peak fluctuation level at 20.8 kHz being measured using the built-in Fast Fourier Transform (FFT) capability of the MATH function in the digital oscilloscope.

The FFT spectrum displayed on the digital oscilloscope panel is shown in Fig. 3(a). The fluctuation noise has been discussed in [1] - and its frequency spectrum is directly related to the fibre laser dynamics - depending on parameters such as

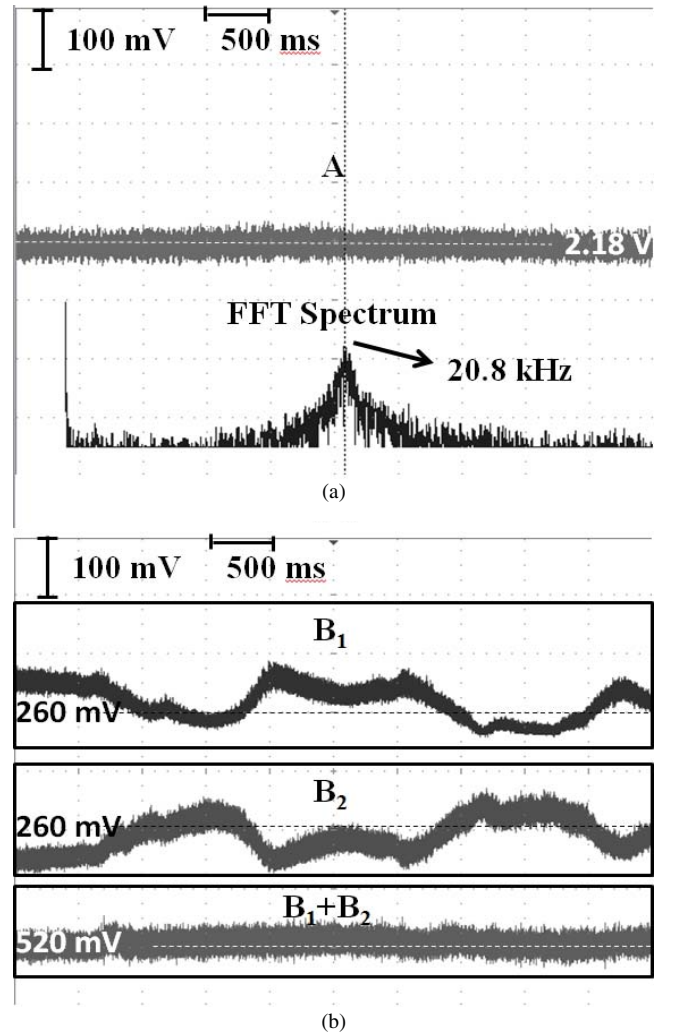


Fig. 3. Optical output from (a) output A and (b) B₁ and B₂, with FFT frequency distributions that have been measured and calculated using the built-in MATH function of the digital oscilloscope.

the pump power, laser cavity length, erbium concentration, cavity reflectivity and cavity loss. Fig. 3(b) shows the optical power from outputs B₁ and B₂ measured simultaneously using both input channels on the digital oscilloscope, at wavelengths of 1532.10 nm and 1532.90 nm respectively, at independent maximum levels of 260 mV. It is clearly demonstrated that the fluctuations of the optical output power at the two wavelengths are totally inverted with respect to each other, i.e. that the levels are substantially complementary.

Increasing the optical power level at one wavelength causes the optical power of the second wavelength to decrease by the same amount. To identify the inverted nature of the two outputs, a summation of both outputs was performed using the built-in MATH function of the digital oscilloscope. The result is to produce a steady output level similar to that of output A, but at a much lower power level (on average, a photo-detected level of 532 mV).

There are several reasons for the difference in the output power. One is the difference between the output power levels from the forward and backward directions of the fiber laser. Due to the fact that the fiber laser is not pumped to the

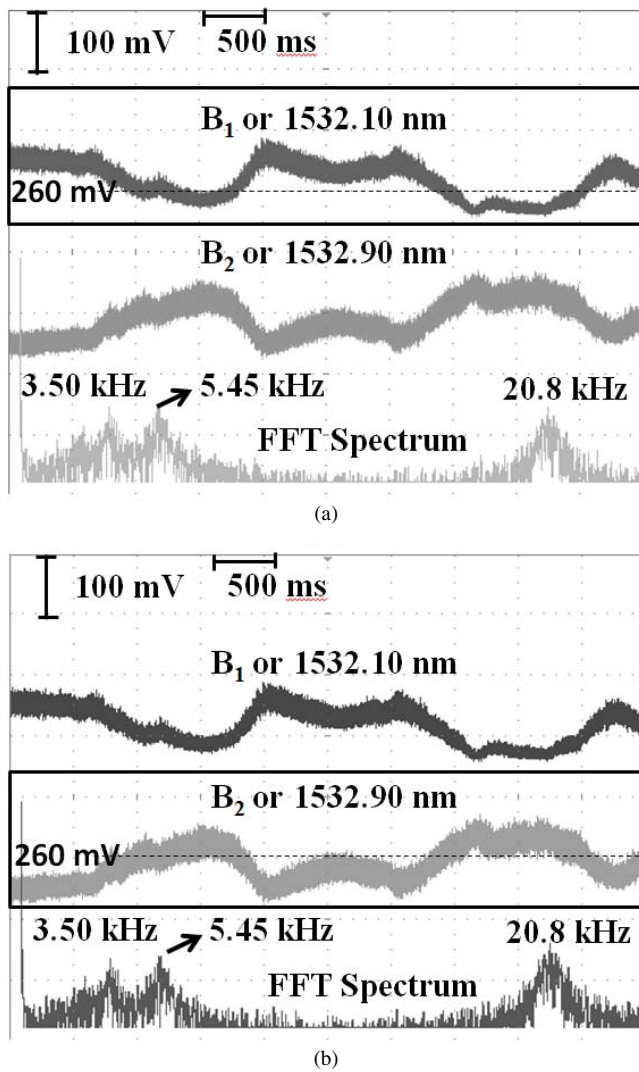


Fig. 4. Detected optical level from both outputs B_1 and B_2 , with calculated FFT frequency distributions for (a) output B_1 and (b) output B_2 .

population inversion condition throughout the length of the EDF (at the low pump power levels being used), reabsorption will happen towards the end of the EDF where there is less inversion population. A second reason could be the losses caused by the AWG, due to insertion and coupling losses. A further reason is the loss caused by the other 14 channels that are in the range from $70 \mu\text{W}$ up to $150 \mu\text{W}$; however these losses at the ASE level are less significant.

Analysis of the optical power fluctuation in the frequency domain has been performed by studying the FFT of the optical power fluctuation. Fig. 4(a) and 4(b) show the same optical output power level from output B_1 and output B_2 , measured using both channels of the digital oscilloscope simultaneously for a sampling period of 5 s. In the case of Fig. 4(a), the FFT spectrum taken is from the output of B_1 , with B_2 shown to indicate the opposite response of B_1 . Similarly, for Fig. 4(b), the FFT spectrum is shown for B_2 , with the B_1 trace as the comparison. From the two FFT spectra, it can be observed that there are three distinct peaks, at frequencies of 3.50 kHz, 5.45 kHz, and 20.8 kHz. The 20.8 kHz peak is contributed by the resonant frequency of the fibre laser system, as mentioned

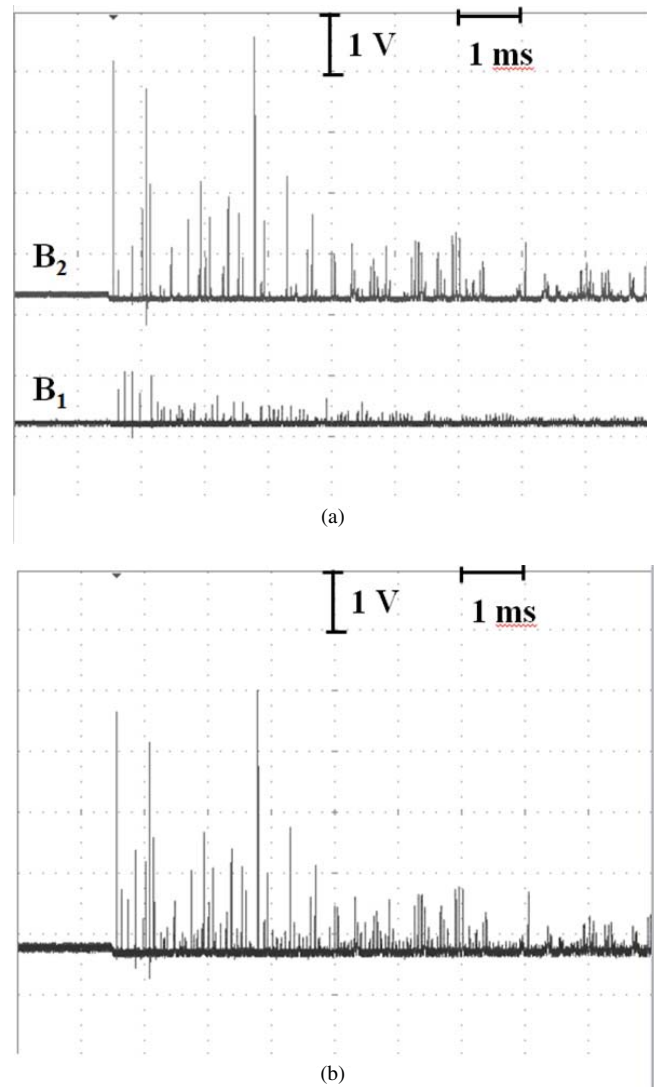


Fig. 5. Random spiking due to the transient effect from outputs (a) B_1 and B_2 and (b) summation of outputs B_1 and B_2 .

previously, and is observed on all of the optical outputs A, B_1 and B_2 . The other two peaks, at 3.50 kHz and 5.45 kHz, are contributed by the resonant frequency of each mode that oscillates at different wavelengths and can only be observed in outputs B_1 and B_2 . The existence of both resonant frequency peaks at both outputs indicates that they are correlated with each other. The FFT frequency distribution from outputs B_1 and B_2 are almost identical, with only slight differences in their amplitude that are not significant enough to merit further analysis. These frequencies of 3.5 kHz and 5.45 kHz can be understood as the mode competition frequency or how frequent of the dominant laser shifts from one wavelength to another. This phenomenon is more obvious when the laser is under a 'chaotic' state as in Fig. 5.

Observation of the mode competition behavior for the fibre laser under chaotic conditions has been made by introducing a small impact on the bench where the fibre laser is placed—and obtained by knocking using a metal ruler. The perturbation generated will cause the laser to undergo chaotic operating conditions and produce random spiking effects that

may be described as transients - and have been well explained in terms of the laser dynamics [10], [11]. Fig. 5(a) shows the spiking generated at both output B_1 and output B_2 , due to laser dynamic transient effects. For better visualization, outputs B_1 and B_2 were slightly offset, at a different amplitude level from the base level, in order to separate the two outputs clearly on the oscilloscope panel.

It is clear that, under chaotic operating conditions, lasing at 1532.90 nm from output B_2 dominates by producing major high energy spikes, as compared to B_1 . When the captured images of the two outputs are placed together, it can be observed that most of the spikes generated in B_1 fill up the empty gap between the spikes generated in B_2 . In other words, most of the time, under chaotic conditions only one mode at a time survives. The total output level from B_1 and B_2 together can be obtained by adding up the two outputs, as presented in Fig. 5(b). The domination of the pulsing effect is probably related to the stability and laser peak power. The domination of the lasing effect will switch alternatively between the two lasing wavelengths, causing the low frequency distribution in the FFT spectrum as given in Fig. 4.

Our earlier work [1], [2] has indicated that the relatively large acoustic modulation with frequencies below the resonance frequency of the laser system will trigger the laser transient and generates pulse trains that will carry the acoustic frequency information with embedded high frequency satellite pulses. However these high frequency satellite pulses contribute to the loud hissing noise when the signal is translated back into the acoustic waves. In this setup, the spiking phenomenon that takes place in each wavelength and causes a reduction in the spiking frequency of other wavelength. Reduction of these spiking frequencies will effectively reduce the number of satellite pulses and hence contribute to noise reduction when the acoustic modulation is under transient phenomenon. Thus the quality of sound reproduction for frequencies that fall within our listening region (below 20k Hz) is significantly improved when the output is taken from either output B_1 or B_2 .

In our previous study also, acoustic modulation was obtained on the basis of the dynamic behavior of the fiber laser in multimode operation, but without explicit consideration of the modal competition behavior. For detection of acoustic waves, the perturbation produced on the output optical power of the laser must be large enough to provide an observable impact on the gain or loss parameters of the laser system. If the perturbation is small, loss introduced on one mode will be compensated by the increased gain of another mode (or other modes), leading to unobservable small changes in the total output power, just as was observed for the mode competition shown in Fig. 3.

To observe the effect of these small perturbations on the oscillation of the two wavelengths, low amplitude acoustic waves at 500 Hz were generated near the fiber laser using a multimedia speaker connected to a personal computer. The amplitude of the acoustic waves was increased slowly until outputs B_1 and B_2 responded to the acoustic wave. Fig. 6 shows the optical outputs from B_1 and B_2 under modulation by 500 Hz acoustic waves at sound levels of: (a) 65.0 dBA

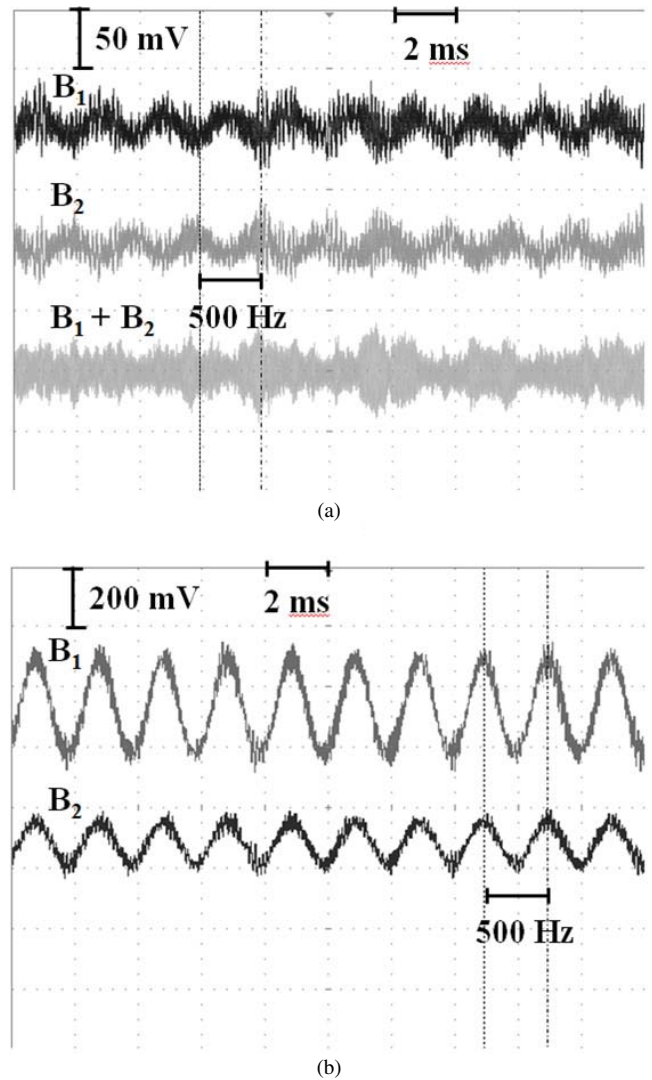


Fig. 6. Optical outputs from B_1 and B_2 for modulation by 500-Hz acoustic waves at amplitudes of (a) 65.0 dBA and (b) 88.3 dBA.

SPL (sound pressure level) (or equivalent to 68.5 dB SPL) and (b) 88.3 dBA SPL (or equivalent to 91.5 dB SPL) which are equivalent to 0.0514 N/m² and 0.752 N/m² respectively. In a more general form, 65.0 dBA SPL is close to the sound made by a vacuum cleaner operating at a distance of 1 m, while 88.3 dBA SPL is similar to sound of a diesel truck from 10 m away [12]. The larger the level of the sound pressure, the larger the pressure exerted onto the fibre, which in turn causes a large change in the refractive index of the fiber which in turn leads changes in the loss and gain of the fibre laser as described in [2].

Both optical outputs have a sinusoidal form at 500 Hz. The larger modulation amplitude shown in Fig. 6(b) is due to the larger acoustic wave amplitude. Another difference between Figs. 6(a) and 6(b) that can be observed is that, in Fig. 6(a), B_1 and B_2 are “out of-phase” by 180°, while they are “in-phase” in Fig. 6(b). We believe that the outputs from B_1 and B_2 are “out-of-phase” not because of delay or changes of path length that cause a relative phase shift between output B_1 and B_2 . Interaction of the acoustic waves with the fiber causes modulation of the modes oscillating in the fibre laser. However,

the acoustic modulation at this amplitude (65.0 dBA SPL) is far too weak to modulate the total gain and loss of the system. Hence, when one of the modes experiences changes in gain or loss, the other mode will experience an opposite effect to compensate for the changes in the system - and to maintain a stable lasing condition. Thus, when the outputs from B_1 and B_2 in Fig. 6(a) are summed, or the total output power from A is measured, the modulation effect on the laser is small. As the acoustic modulation increases, the sinusoidal amplitude of output B_1 and B_2 also increase. This will continue until at a certain stage whereby the output of B_1 and B_2 become "in-phase" as shown in Fig. 6(b). The transition from "out-of-phase" to "in-phase" happens when the acoustic waves is approximately 87 dBA. After the transition state, there is no observation of modulation amplitude suppression in both of the outputs of B_1 and B_2 . Above 88.0 dBA the acoustic amplitude is large enough to modulate the refractive index in the core along the fibre, causing fluctuations in the total gain and loss of the fibre laser and the outputs from B_1 and B_2 show "in-phase" modulation. Furthermore, it is obviously possible to observe the modulation pattern on the total output - either directly from output A or from the summation of B_1 and B_2 , as shown in Fig. 6(a).

Compared with acoustic modulation measurements performed on the total output power of a fluctuating multimode fiber laser, measurement of a single wavelength output from a dual-wavelength fiber laser has significantly reduced the sensing threshold of the acoustic wave SPL by the fibre laser, although the background noise remains high due, to the power fluctuations. The threshold sensing level has been reduced by more than 23 dB, as tested by modulating the fiber laser with a 500 Hz sound wave at 65.0 dBA SPL, together with a background noise level of 58.7 dBA SPL (mainly contributed by the cooling fan of experimental instruments) - without using an additional sensing fibre. This improvement by 23 dB was estimated from a comparison between the measured 88.3 dBA SPL required to trigger unstable dynamic behavior in the whole multiple longitudinal mode fibre laser (based on previous work [1], [2]) and the 65.0 dBA SPL that is sufficient to modulate a single wavelength output, without significantly affecting the system gain. Significant further increase of the acoustic wave SPL above 88.3 dBA, at 500 Hz, causes dynamic spiking behavior, in which a pulse-train with satellite pulses can be observed [2]. This 23 dB difference can be considered as providing an estimate of the dynamic range of the acoustic sensor, since the output is similar to the modulating wave, until chaotic dynamic behavior starts to be triggered.

We have observed that the dynamic range of the acoustic sensor is different at different frequencies and are currently studying this aspect in detail, with a view to a further publication. The sensitivity of the system to acoustic waves can be enhanced by increasing the total length of the laser cavity or the use of a thin cladding type fibre that allows for a more efficient of energy transfer into the core layer. The benefits of increased length will be investigated in future work, where the focus will be on the dual-wavelength mode competition that can occur in EDFLs due to acoustic wave interaction.

Application wise, the sensor can be used to pick-up human vocalizations, musical instruments, ultrasounds, and any other acoustic waves that fall within frequency range from 100 Hz up to 100 kHz as presented in previous work [1], [2] so long as it is above the sensing threshold. In this case, it is 65.0 dBA SPL for 500 Hz. Due to the poor acoustic impedance matching between air and fibre [13], the efficiency of sensing the sound wave is extremely low as compared to vibration. Hence the sensing of sound can only be done under a vibration free environment. An anti-vibration packaging is believed to be an important solution for this sensor.

IV. CONCLUSION

In conclusion, we have studied the power fluctuation of each lasing wavelength in a dual wavelength fibre laser. By observing the power level for each individual lasing wavelength, we have observed greater sensitivity to acoustic wave modulation, in comparison with the sensitivity of the total output power, since the laser system will always tend to reduce the induced system fluctuation by compensating the loss or gain changes for other wavelengths or modes in the laser system. With this observation, the sensing of the laser system to acoustic waves has been reduced by more than 23 dB - with possible further improvement being obtainable by optimization of the laser system.

REFERENCES

- [1] C. H. Pua, S. F. Norizan, S. W. Harun, and H. Ahmad, "Non-membrane optical microphone based on longitudinal modes competition," *Sensors Actuat. A, Phys.*, vol. 168, no. 2, pp. 281–285, 2011.
- [2] C. H. Pua, H. Ahmad, S. W. Harun, and R. M. D. L. Rue, "Direct airborne acoustic wave modulation of Fabry-Pérot fiber laser (FPFL) over 100 kHz of operating bandwidth," *Appl. Opt.*, vol. 51, no. 15, pp. 2772–2777, 2012.
- [3] X. P. Dong, L. Shenping, K. S. Chiang, M. N. Ng, and B. C. B. Chu, "Multiwavelength erbium-doped fibre laser based on a high-birefringence fibre loop mirror," *Electron. Lett.*, vol. 36, no. 19, pp. 1609–1610, 2000.
- [4] S. Xuewen, J. Shan, and H. Dexiu, "Fiber grating Sagnac loop and its multiwavelength-laser application," *IEEE Photon. Technol. Lett.*, vol. 12, no. 8, pp. 980–982, Aug. 2000.
- [5] C. Zhe, S. Hongzhi, M. Shaozhen, and N. K. Dutta, "Dual-wavelength mode-locked erbium-doped fiber ring laser using highly nonlinear fiber," *IEEE Photon. Technol. Lett.*, vol. 20, no. 24, pp. 2066–2068, Dec. 2008.
- [6] H. Ahmad, M. Z. Zulkifli, A. A. Latif, and S. W. Harun, "Tunable dual wavelength fiber laser incorporating AWG and optical channel selector by controlling the cavity loss," *Opt. Commun.*, vol. 282, no. 24, pp. 4771–4775, 2009.
- [7] P. J. Moore, Z. J. Chaboyer, and G. Das, "Tunable dual-wavelength fiber laser," *Opt. Fiber Technol.*, vol. 15, no. 4, pp. 377–379, 2009.
- [8] C. H. Yeh, C. W. Chow, F. Y. Shih, C. H. Wang, Y. F. Wu, and S. Chi, "Tunable dual-wavelength fiber laser using optical-injection Fabry-Pérot laser," *IEEE Photon. Technol. Lett.*, vol. 21, no. 24, pp. 125–127, Dec. 2009.
- [9] H. Xiaoying, D. N. Wang, and C. R. Liao, "Tunable and switchable dual-wavelength single-longitudinal-mode erbium-doped fiber lasers," *J. Lightw. Technol.*, vol. 29, no. 6, pp. 842–849, Mar. 2011.
- [10] Y. I. Khanin, *Fundamentals of Laser Dynamics*. Cambridge, U.K.: Cambridge International Science Publication, 2006.
- [11] T. Erneux and P. Glorieux, *Laser Dynamics*. New York: Cambridge Univ. Press, 2010.
- [12] E. Sengpiel. (2011, Jul. 4). *Decibel Table—SPL—Loudness Comparison Chart* [Online]. Available: <http://www.sengpielaudio.com/TableOfSoundPressureLevels.htm>
- [13] N. Bilaniuk, "Optical microphone transduction techniques," *Appl. Acoust.*, vol. 50, no. 1, pp. 35–63, 1997.

Chang Hong Pua was born in 1982. He received the B.Sc. and M.Sc. degrees in physics from the University of Malaya, Kuala Lumpur, Malaysia, in 2006 and 2009, respectively. His M.Sc. research was on the fabrication process of planar lightwave circuits. He is currently pursuing the Ph.D. degree with the Photonics Research Center, Physics Department, Faculty of Science, University of Malaya, with research on fiber-optic acoustic sensors.

His current research interests include fiber-optic sensors and their applications, high-power fiber lasers, and planar lightwave circuits.

Harith Ahmad received the B.Sc. (Hons.) degree from the University of Malaya, Kuala Lumpur, Malaysia, in 1979, and the M.Sc. degree in high-voltage technology and the Ph.D. degree in laser technology from the University of Wales, Cardiff, U.K., in 1980 and 1983, respectively.

He is currently a Professor with the Physics Department, University of Malaya. His initial research is on solid-state lasers and diode-pumped solid-state lasers. In 1995, he researched optical fiber devices, such as optical amplifiers, and planar waveguides. His current research interests include nonlinear optical effects in optical fibers and optical fiber sensors.

Sulaiman Wadi Harun received the B.E. degree in electrical and electronics system engineering from the Nagaoka University of Technology, Nagaoka, Japan, in 1996, and the M.Sc. and Ph.D. degrees in photonics from the University of Malaya, Kuala Lumpur, Malaysia, in 2001 and 2004, respectively.

He is currently a Full Professor with the Faculty of Engineering, University of Malaya. His current research interests include fiber-optic active and passive devices.

Richard M. De La Rue (F'03) joined Glasgow University, Glasgow, U.K., in 1971, as a Lecturer, and he became a Senior Lecturer in 1982, a Reader in 1985, and a Professor of optoelectronics in 1986. His research is focused on photonic-crystal and photonic-wire structures, waveguide microcavities, and metamaterials. His research in photonic crystals has evolved to cover compact lasers, planar microcavities, photonic-crystal LEDs, and synthetic and inverse opal structures. His research on metamaterials has particularly emphasized the use of semiconductor substrates and the impact of the choice of metallization.